INVESTIGATION OF THE FACTORS AFFECTING 2nd HARMONIC GENERATION IN BULK HIGH T_C SUPERCONDUCTORS

by

Eylem Gülce Çoker

Submitted to Graduate School of Natural and Applied Sciences

in Partial Fulfillment of the Requirements

for the Degree of Doctor of Philosophy in

Physics

Yeditepe University

2015

INVESTIGATION OF THE FACTORS AFFECTING 2nd HARMONIC GENERATION IN BULK HIGH T_C SUPERCONDUCTORS

APPROVED BY:

Assist. Prof. Dr. Ercüment Akat ……
(Thesis Supervisor)

Assoc. Prof. Dr. Uğur Topal ……
(Thesis Co-advisor)

Prof. Dr. Ahmet T. İnce ……

Prof. Dr. M. Hikmet Yükselici ……

Prof. Dr. Merih Serin ……

Prof. Dr. Şahin Aktaş ……

Assist. Prof. Dr. Vildan Üstoğlu Ünal ……

DATE OF APPROVAL : …./…./2015

To My Beloved Daughter & Son,
İlke Serra & Münip Mert ÇOKER…

ACKNOWLEDGEMENTS

I would like to express my deep and sincere appreciation to my Co-Adviser Assoc. Prof. Uğur Topal for his great patience, guidance and support which made this thesis possible.

Special thanks to Prof. Dr. Ahmet T. İNCE who encouraged me to do this thesis.

This thesis was supported by the 109T715 project which was in content of TÜBİTAK Research Projects Support Programme (TÜBİTAK-1001). I am grateful to the supporting agency for their aid and co-operation. I would also thank to TÜBİTAK-UME researchers, especially Magnetic Laboratory Group, for their help and effort.

I would like to thank to my adviser Assist. Prof. Dr. Ercüment Akat for his guidance and friendness for twenty years.

I would like to thank to my friends who encouraged and supported me in writing this thesis Assoc. Prof. Dr. İpek KARAASLAN and M.SC Fatma ALIKMA.

I would like to thank to my friend Hava CAN who encouraged and supported me in writing this thesis.

Finally, I would like to thank to my beloved family; my father Salih ÖZEN, my mother Nuran ÖZEN, my brother Erk ÖZEN and his wife Emily Stuart ÖZEN; my daughter İlke Serra ÇOKER, my son Münip Mert ÇOKER and their father Hasan Can ÇOKER for their patience and respect to my job.

ABSTRACT

INVESTIGATION OF THE FACTORS AFFECTING 2nd HARMONIC GENERATION IN BULK HIGH TC SUPERCONDUCTORS

The researches on granular high-T_C cuprates have shown that these materials make quite low flux entries possible through grain boundaries and show nonlinear magnetization which causes the generation of harmonics of excitation field. Especially, perfect linear dependence of second harmonic signal to applied DC fields, where the second harmonic signal is generated by co-application of AC and DC fields, has attracted interests to magnetic sensor technology.

The aim of this thesis was to inspect the factors affecting second harmonic signal, which could be done by developing a DC magnetometer with a sensitivity of the order of 10^{-9} T that uses polycrystalline superconductor as a sensor element. The key conclusion is that the field of 0.5 nT can be easily measured. In order to attain this result, many different parameters have been improved and the affects of those parameters on the sensor's sensitivity have been studied broadly. In order to study the affect of the inter-grain connectivity on the sensor's sensitivity, yttrium superconductor was doped with different elements, like boron, bismuth and zinc which, according to the literature, are known to either ascend or descend the inter-grain connectivity in this material. The superconducting properties and the performance as a sensor element for superconductors were studied by annealing at different temperatures and thus having a different crystalline structure. In order to get the maximum signal to noise (S/N) ratio, the environmental conditions have been optimized. The environmental noise was suppressed from the working frequency by active and passive band-pass filters. By optimizing the configuration of the superconducting sample and the coils the best sensor geometry has been found. Furthermore, the optimal excitation frequency and amplitude have been determined.

ÖZET

BÜTÜN YÜKSEK SICAKLIK SÜPERİLETKENLERİNDE İKİNCİ HARMONİK OLUŞUMUNU ETKİLEYEN FAKTÖRLER

Tanecikli yapı içeren yüksek sıcaklık süperiletkenlerini analiz etmeye yönelik yapılan araştırmalar bu malzemelerin tanecikler arası bölgelerine çok düşük manyetik akının dahi girebildiğini ve bu sebeple doğrusal olmayan bir mıknatıslanma gösterdiklerini ortaya çıkarmıştır. Doğrusal olmayan mıknatıslanma ise uyarma sinyalinin harmoniklerinin oluşmasına sebep olmaktadır. İkinci harmonik sinyalinin uygulanan doğru akımlı alana geniş aralıkta doğrusal bağımlılığı bu malzemelerden manyetik alan sensörü olarak da faydalanabilme düşüncesinin oluşmasına sebep olmuştur.

Tezde ikinci harmoniğe etkiyen faktörlerin araştırılabilmesi için, çok kristal süperiletkenlerin algılama nüvesi olarak kullanıldığı ve 10^{-9} T mertebelerinde doğru akımalan büyüklüklerinin ölçülebileceği manyetometre tasarımı hedeflenmiştir. Çalışma esnasında sensör hassasiyetine etkiyen parametrelerin iyileştirilmesi amaçlanmış, 0.5 nT doğru akım alanı ölçülmüştür.İtriyum süperiletkenlerine değişik iyonlar katkılanarak tanecikler arası bağların etkisi incelenmiştir. Aynı süperiletkenlerle farklı tavlama sıcaklıklarında çalışılarak sensor uygunluğu test edilmiştir. Sinyal/Gürültü (S/N) oranının en üst seviyede olabilmesi için çalışılmıştır. Çalışma frekansı dışındaki çevresel gürültülerin etkisinin azaltılabilmesi için pasif ve aktif bant geçişli filtreler kullanılmıştır. Bununla beraber süperiletken numune ve bobin konfigürasyonunun optimizasyonu yapılarak en uygun sensör geometrisi belirlenmiştir. Böylelikle uyarma frekansı ve genliği belirleme çalışmaları başarıyla tamamlanmıştır.

TABLE OF CONTENTS

LIST OF FIGURES

LIST OF TABLES

LIST OF SYMBOLS / ABBREVIATIONS

AC	Alternative Current
B	Inductive Magnetic Field
DC	Direct Current
H_C	Critical Magnetic Field
J_C	Critical Current Density
H_{C1}	Lower Critical Field
H_{C2}	Upper Critical Field
M	Magnetization
N	Demagnetisation Factor
H_{c1j}	Intergrain first critical field
J_{c1}	Intergrain first critical current density
H*	Minimum field required for penetration through the entire specimen
H_{DC}	DC Magnetic Field
H_{AC}	AC Magnetic Field
V_{2f}	Second Harmonic Signal
T_C	Critical Temperature
T	Temperature (Kelvin)
ξ	Coherence Length
μ	Magnetic Permeability
μ_0	Magnetic permeability in free space
λ	Penetration Depth
χ	Pinning Force
BCS	Bardeen-Cooper-Schrifer Theory
FC	Field- Cooled
HTS	High-Temperature Superconductor
SC	Superconductor

S/N	Signal to Noise Ratio
SQUID	The Superconducting Quantum Interference Device
YBCO	Yttrium-Barium-Copper-Oxide
ZFC	Zero-Field-Cooled

1. INTRODUCTION

There are several kinds of sensors used for the detection of objects that move or are at rest in the air, in water or under the ground. The type called "magnetic sensor" has some advantages over the others such as the optical, infrared or acoustic sensors and radars because of the greater ability of determining the location of the things. Besides, a magnetic sensor is more suitable to follow the moving objects. Since the signals emitted by the magnetic objects are not attenuated by the interfering medium it is reasonable to use magnetic sensors. Especially when they are used together with a source of low-frequency AC magnetic field, it becomes possible to detect a metallic target such as a ground mine, unexploded ammunitions, chemical, biological and nuclear waste [1].

There are also other areas where these sensors are used such as detection of naval mines and submarines, studies of geophysical anomalies, detection of underground water and petrolium sources [2,3]. Very low magnetic fields can be detected by using Superconducting-Quantum-Interference-Device (SQUID) that have a very high sensitivity allowing for the detection of magnetic fields in the range of 10^{-10} to 10^{-14} T ($1T = 10^4$ Gauss, the Earth's field is approximately 0.5 Gauss) or Fluxgate sensors that can be detect a magnetic field as low as on the order of 10^{-8}-10^{-9} T.

SQUID sensors, although having a high sensitivity, are less common than Fluxgate sensors because **i-** they require the use of liquid helium and **ii-** they detect not the absolute value of magnetic field but the magnetic field change.

As mentioned above the magnetic sensors can be used in critical applications in many different areas where the sensitivity is of high importance, from detection of ground mines (defense industry) to geophysical anomalies, detection of underground water and petrolium sources (geology) or even in medicine [1,3]. Therefore the sensor should have a vast range in the interval of 10^{-9}-10^{-4} T for applications in the navigation systems [4].

In our previous studies we have been able to design a magnetic sensor having a sensitivity of measuring DC fields as low as 1nT consisting of polycrystalline $YBa_2Cu_3O_7$ superconductors as sensing core [5,7]. The working principle of the sensor is based on the fact that very low magnetic fields can penetrate into ceramic superconductors through

poorly superconducting grain boundaries. If an AC magnetic field (H_{AC}) with amplitude greater than H_{c1j} (intergrain first critical field), a ceramic superconductor generates only higher odd harmonics. But if there is also a DC magnetic field H_{DC} superimposed on the AC field then the even harmonics appear in addition to the odd harmonics. To give sharp linear variations is an advantage of a sensor [8, 9] which can be obtained in case that $H_{DC}<<H_{AC}$. In this work we report the ways of sensing DC fields as low as 0.5 nT using polycrystalline Bi-2223 superconductors as sensing core (instead of Y-123) and analyze the performance.

One has to choose the most appropriate sensor for the vast range of magnetic applications such as archaeology, medicine, military, mineral exploration, space etc. as far as the sensitivity is concerned [4,25]. For example, applications in the navigation systems require the dynamic range of the sensor around 10^{-9}-10^{-4} T, while the investigation of local anomalies of Earth field requires a measurement capability in the range of 10^{-5}-10^{-3} T [4,25]. In order to measure magnetic field signals generated from the ionic current activity of heart muscle, the sensor should detect fields less than even 10^{-12} T.

The main technologies used for magnetic field sensing are search coils, fluxgate, nuclear precession, squid, Hall-effect, giant magnetic resistance, fibre optic and magneto-optic [10]. One must choose the more suitable case according to the type of application. Hall-effect sensors are to be suitable for analyzing Earth field analysis, squid magnetometers and search coils are good candidates for the analysis of the ionic current activity of heart muscles [11].

Magnetic sensors gradually become more and more sensitive (from micro tesla down to pico tesla) and are used in navigation systems and defence applications [12]. In the dynamic range of 10^{-8}T to 10^{-4}T) the most widely used sensors are fluxgate magnetometers [13,14]. There is one more method whose working principle is almost the same as the fluxgates, which uses polycrystalline high-Tc superconductors instead of ferromagnetic core. It works in this dynamic range with even less minimum detectable magnetic fields down to several nT [15,16]. The fluxgates are based on the periodical saturation of a soft ferromagnetic core driven by an AC field [11-13]. An external field (to be measured) can only affect the magnetization of the core until when the core saturates.

But since the core becomes unsaturated again after the decay of the magnetic field that causes the excitation and this field can vary the magnetization thereafter. Now the induced potential contains only the even harmonics of the applied frequency.

Polycrystalline type II superconductors magnetize nonlinearly when the core is subject to both an AC and a DC field [17-22]. Thus, the core is excited by an AC field and the even harmonics are generated due to the external DC magnetic field to be measured. It is also known from the studies that the even harmonic signal changes quite linearly and sharply with a DC field. We know that there are circulating currents in a superconductor which contribute in the intergranular and intragranular way whose sum causes the magnetization of a polycrystalline superconductor [23,26].

If the field is low it is the intergranular regions that predominate the magnetization of the sample, that is, the flux first enters the specimen through intergrain regions instead of the intragrain regions.

In order to make quite low flux entries possible and thereby to increase the DC field sensitivity the links between grains are required to be weak. Since the recent work in literature has shown that Zn doping reduces the inter-granular couplings [24] it can be expected that dc field sensitivity can be improved by Zn doping. In order to understand the contribution of the weak links to the second harmonic signal strength we synthesized the polycrystalline $YBa_2Cu_3O_7$ samples at different concentrations of Zn atoms [26].

In order to find out the role of weak links (such as to avoid demagnetization factor) synthesis conditions (such as, furnacing temperatures) and dimensions of the superconducting samples are maintained. In addition to magnetic measurements (such as M-T and the M-H) mechanical (hardness, elastic modulus) properties are also measured [26].

Type-II superconducting materials generate higher harmonic components of magnetization in case that they are placed in a magnetic field. But it is also known that only odd harmonics are generated in a pure ac field. However, if an AC field is applied together with a DC field then even harmonics are generated in addition to the odd harmonics [22]. At this point, it is interesting to notice that 2^{nd} harmonic voltage depends linearly on the applied DC field even if the magnitude of DC field is much smaller than that of the Earth

field [6,16]. Because of this type-II superconductors are good candidates for the measurement of ultra-low DC fields, as low as 10 nT [6,16]. It is necessary to satisfy some conditions to improve the sensitivity of a DC magnetic field sensor. Therefore the ways of detecting DC fields (on the order of nT) are studied, which is a significant process to detect the naval mines and submarines, to study the geophysical anomalies, to detect the underground water and petrolium sources. [2,3,6].

The following things are investigated: i- To find the optimal sensor geometry, sensors of various shapes and dimensions are measured. ii- To generate the 2^{nd} harmonics an AC and a DC magnetic field should be applied simultaneously and the total magnetic field should exceed a certain threshold value. According to the main principles of superconductivity the frequency of the AC field should have an effect on the noise level. Therefore, measurements should be done in a frequency range 20 - 200 kHz to determine the optimal frequency resulting in a minimal noise. iii- One of the most important parameters that influence the sensitivity of a sensor is the "signal to noise" ratio. By the same manner an electronic filter is also designed to reduce the total noise arising from various sources, such as; magnetic flux jumps in the superconductor, the Johnson noise in the pick-up coil and the inherent noise of the Lock-in amplifier and other circuit elements [6].

The working principle of the fluxgate magnetometers which have recently been used at a large scale as a field sensor is based on the transformer physics. The fluxgate sensor consists of a soft ferromagnetic material with nonlinear magnetization, one excitation coil creating an AC signal and one pick-up coil to get the induced potential. A periodical saturation by an AC field is required to generate odd harmonics of the fundamental signal. If a DC field is added then some even harmonics are observed in addition to the odd harmonics. Linear dependence of 2f signal (2^{nd} harmonic) on the DC field is a characteristic property of the core material. In this study superconducting ceramic compounds are used rather than ferromagnetic materials. Type II superconductors exhibit a nonlinear magnetization similar to the ferromagnetic materials. Since it was observed that the sensitivity of a sensor may be adjusted by controlling granular structure it was previously reported that the nature of links between grains of superconductive samples have an important role on the strength of 2f signal. Today it is known that due to the addition of boron the intergranular couplings weaken [27,28]. So it is decided to work on

the effects of boron doping on the DC field sensitivity of fluxgate like (but uses superconductive samples as sensing element) magnetometer. First, the polycrystalline $YBa_2Cu_3O_7$ samples were prepared at different concentrations of B atoms in order to investigate the contribution of the weak links to the 2^{nd} harmonic signal strength. Synthesis conditions (e.g. annealing temperature) and dimensions of the superconducting samples were kept the same to clarify the role of weak links (such as avoiding the demagnetization factor). Some mechanical (such as hardness, elastic modulus) and magnetic measurements (M-T and M-H) [27,28] are also carried out.

2. THE THEORY BEHIND THIS WORK

2.1. SUPERCONDUCTIVITY

In literature the general explanation for the superconductivity phenomenon is given as display zero resistance when the temperature was lowered below a certain characteristic temperature of the element. At this certain temperature which is called the critical temperature, T_C, the electric and magnetic properties of some materials such as lead, mercury and some oxides radically change and they become superconductors [53].

This phenomenon was discovered by Dutch physicist Heike Kammerling Onnes on April 8, 1911 in Leiden an about a hundred years ago. In 1933 Meissner Effect was discovered by Meissner and Ochsenfeld. During the 1950s, the phenomenological Ginzburg-Landau Theory (1950) and the microscopic BCS Theory (1957) were discovered [53].

This theory, which combined Landau's theory of second-order phase transitions with a Schrödinger-like wave equation, had great success in explaining the macroscopic properties of superconductors. In particular, Abrikosov showed that Ginzburg-Landau theory predicts the division of superconductors into the two categories now referred to as Type I and Type II. Abrikosov and Ginzburg were awarded the 2003 Nobel Prize for their work [53].

In 1986, it was discovered that some cuprate-perovskite ceramic materials have a critical temperature above 90 K (−183 °C). Such a high transition temperature is theoretically impossible for a conventional superconductor, leading the materials to be termed high-temperature superconductors [49, 53].

Today, superconductivity is an extremely active field of research which includes solving the original mechanism, creating new superconductors, and finding yet new applications. Superconductivity also enables spectacular feats of levitation [49,53].

2.2. SENSORS

The devices that measure a physical quantity and convert it to a signal which can be read by a user or a device are called “sensors”. The sensors that can measure very minute variations have a high sensitivity. Some of them may have advantages over others which are used for the same purpose. For example if the things under the surface have sufficient magnetic signals and since the magnetic signal is not attenuated by the medium the magnetic sensors may become more advantageous. The magnetic sensors may also show some functional differences depending on the type of sensing element. For instance in the fluxgate and squid magnetometers which are the mainly used sensors in low-field measurements a solenoid system and superconducting joints are used respectively. Fluxgate type of sensors can measure the magnitude of the field while SQUID type of sensors can detect the variations in the magnetic field. On the other hand fluxgate sensors can detect magnetic signals on the order of 10^{-8}-10^{-9} Tesla, whereas SQUID type of sensors can detect signals around 10^{-10}-10^{-14} Tesla (1 tesla = 10^4 Gauss and the Earth’s magnetic field is around 0.5 Gauss). Although the SQUID sensors may seem advantageous because of having a relatively high sensitivity for very low magnetic fields, their range of application is limited due to the necessity of using liquid helium and their reaction against the variation of the magnetic field. However, the studies on having a SQUID sensor that can be used by liquid nitrogen still continue.

There are several areas where it is necessary to detect very low magnetic fields. For instance, one can measure a magnetic field which is formed by the neural currents related with the physiological movements of the heart or brain by a sensor which can detect a magnetic field as low as 10^{-10} Tesla. Therefore the studies on improving the sensitivity of the magnetic sensors are continuing both scientifically and industrially. One can have more information through several references [29-41] about the fluxgate or SQUID type of sensors which are known to be the most sensitive magnetic sensors.

2.3. MAGNETIC SENSORS

The magnetic sensors are divided into two seperate parts; one of them is the vector magnetic sensors and the other is the scalar magnetic sensors. In the vector magnetometers there are several magnetometer types; Search-coil magnetometers, Fluxgate magnetometers, Superconductor magnetometers (SQUID sensors and Meissner effect used sensors), Hall effect sensors, Magnetoresistive magnetometers (AMR, GMR, MTJ, extraordinary and ballistic magnetoresistance), Spin-valve transistors, GMI, Magnetodiode, Magnetotransistor, Magnetostrictive magnetometers (fiber-optic magnetometer and magnetoelectric sensor), Magnetooptical sensors and MEMS based magnetometers. In the table below the best known magnetic sensors can be seen.

Table 2.1. The best known magnetic sensors [11].

10^{-5} G ⟶ 1G		
SQUIDS	FLUX-GATES	HALL EFFECT SENSOR
Measures field gradients, high sensitivity	Measures perturbations in the magnitude, medium sensitivity	Measures fields greater than Earth's magnetic field, low sensitivity
Brain function mapping, magnetic anomaly detection	Magnetic compass, traffic control	Magnetic memory readout, current measurement

As seen from the table, the SQUIDs are high sensitive, fluxgates medium sensitive and hall effect sensors are low sensitive sensors. The designed sensor for this thesis is medium sensitive and can be named as high temperature superconductor sensor. The working principle will be explained in detail in part 3.

2.4. MAGNETIC PROPERTIES OF THE SUPERCONDUCTORS

German physicists Meissner and Ochsenfeld observed in 1933 that a superconductor cooled inside a magnetic field excluded the magnetic flux (Figure 2. 1.) which is called the "Meissner effect". They also observed that the superconductivity of the sample deteriorates when it is subject to a magnetic field which is larger than a critical value BC and there occurs a phase transition (from superconducting to normal).

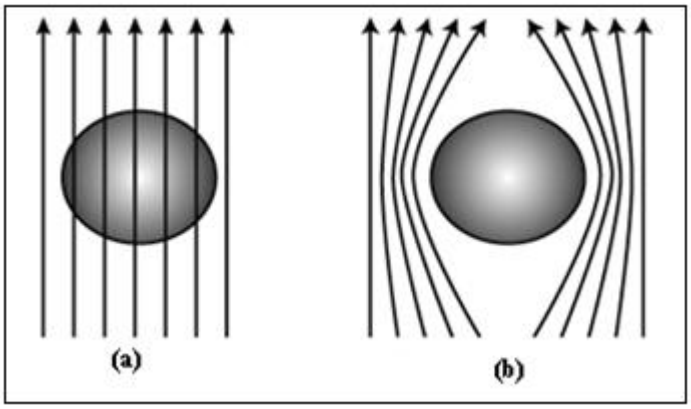

Figure 2.1. Field lines in (a) normal conducting state, (b) superconducting state. The magnetic field lines are excluded for $T < T_C$ [54].

It is also known that the value of the critical field depends on the temperature of the substance according to the empirical formula;

$$B_c(T) = B_c(0)\left[1 - \left(\frac{T}{T_c}\right)^2\right] \qquad [49] \quad (2.1)$$

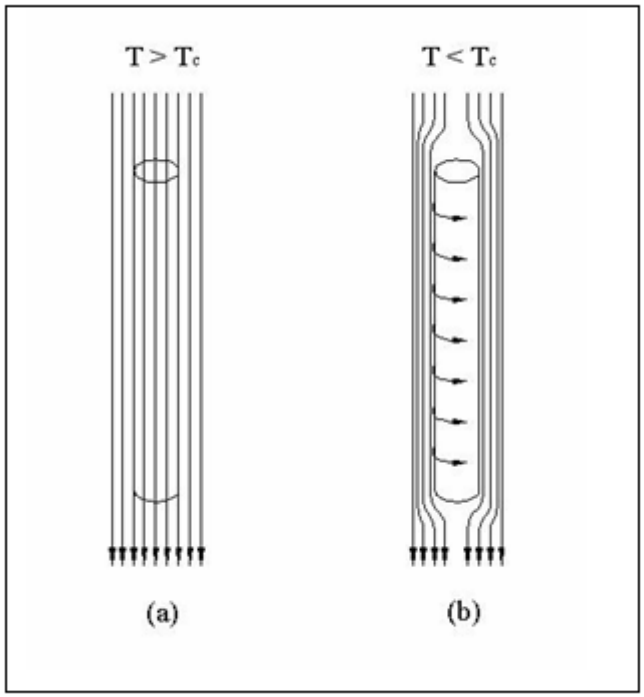

Figure 2.2. Meissnereffect: The magnetic field lines excluded for $T < T_C$ and the surface currents thereafter [49].

The magnetic field cannot penetrate the material because of the surface currents as shown in Figure 2.2. These surface currents exhibit an exponential decay towards the inside of the sample instead of ending completely within a very thin layer. Thus, the applied magnetic field shows an exponential decay from the surface towards the central part of the sample.

The magnetic field *B* decays according to the formula

$$B(x) = B_0 e^{-x/\lambda} \qquad [49](2.2)$$

where λ is the penetration depth. *B* (*x*) gives the value of the field at distance *x* from the surface and is schematically shown in Figure 2.3.

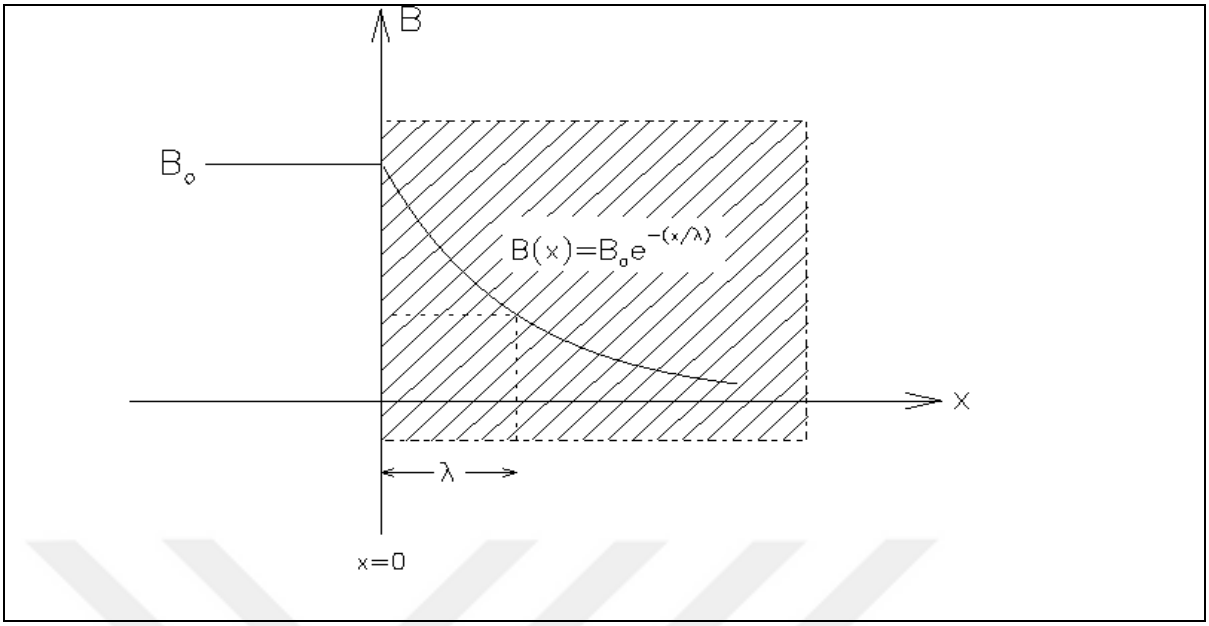

Figure 2.3. The exponential decay of the external magnetic field (B_o) from the surface [54].

The magnetic field is expelled totally from the superconducting material but it can exist within a very narrow region near the surface. The penetration depth varies as a function of temperature according to the formula;

$$\lambda(T) = \lambda_0[1 - \left(\frac{T}{T_c}\right)^2]^{-1/2} \qquad [49] (2.3)$$

where λ_o is the penetration depth at T = 0 K. As the temperature approaches T_C, λ approaches infinity and therefore the material becomes a normal conductor.

A superconducting material placed in an external magnetic field B is magnetized by M. The internal magnetic field B_{in} inside the specimen is the sum of B_{ext} and μ_oM:

$$\mathbf{B}_{in} = \mathbf{B}_{ext} + \mu_o\mathbf{M} \qquad [49] (2.4)$$

Since B_{in} = 0 for the superconducting phase the magnetization is

$$\boldsymbol{M} = -\frac{B}{\mu_0} = \chi\boldsymbol{B} \qquad [49](2.5)$$

where χ is the magnetic susceptibility.

Figure 2.4. shows the variation of the internal magnetic field B_{in} and the magnetization in superconductors of type I, as a function of the applied magnetic field when $T < T_C$.

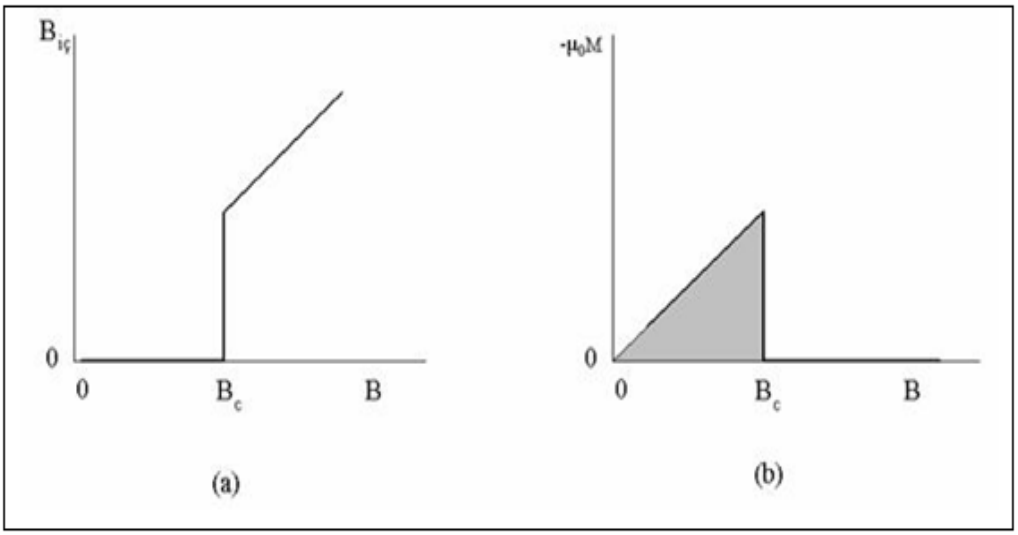

Figure 2.4.For the superconductors of type I the variation of (a) the internal magnetic field as a function of the external magnetic field, (b) the magnetization as a function of the external magnetic field [54].

In the superconductors of type II invented in 1950's there are two critical magnetic field values so called B_{C1} and B_{C2}. The material is in the superconducting state for a magnetic field $B<B_{C1}$ and Meissner effect is observable. If the external field is between B_{C1} and B_{C2} ($B_{C1}< B <B_{C2}$) then in the regions behaving as normal there are vortices. In this case the external field is said to penetrate partially. As the external field is increased and reaches B_{C2} the ratio of the normal regions increases and when $B =B_{C2}$ the material becomes totally normal (Figure 2.5.).

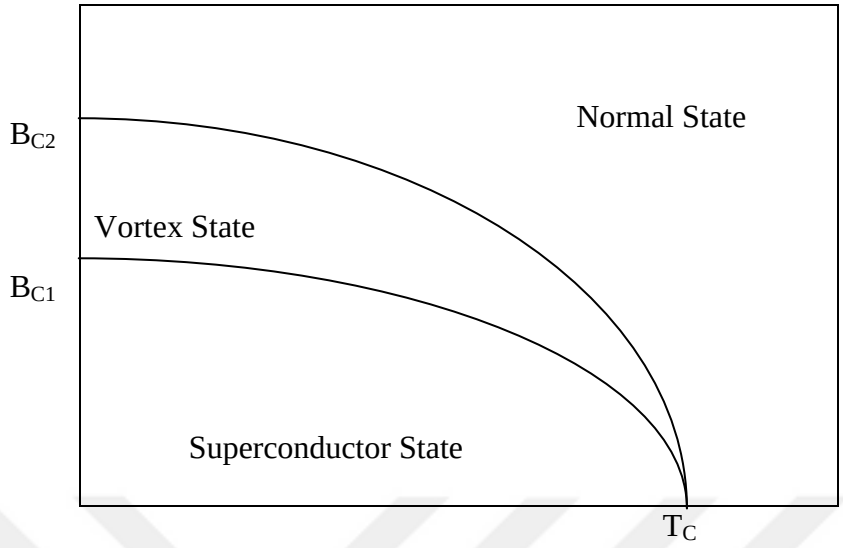

Figure 2.5. The phase diagramme for a superconductor of type II [54].

In the vortex state the external magnetic field penetrates the material partially as in the shape of cylindrical pipes. As the magnetic field and/or the temperature get higher and reach the critical values B_{C2} and T_C respectively, the relative ratio of these pipes in the cross-section will gradually increase and will totally span the material, thereby transforming the material to the normal state.

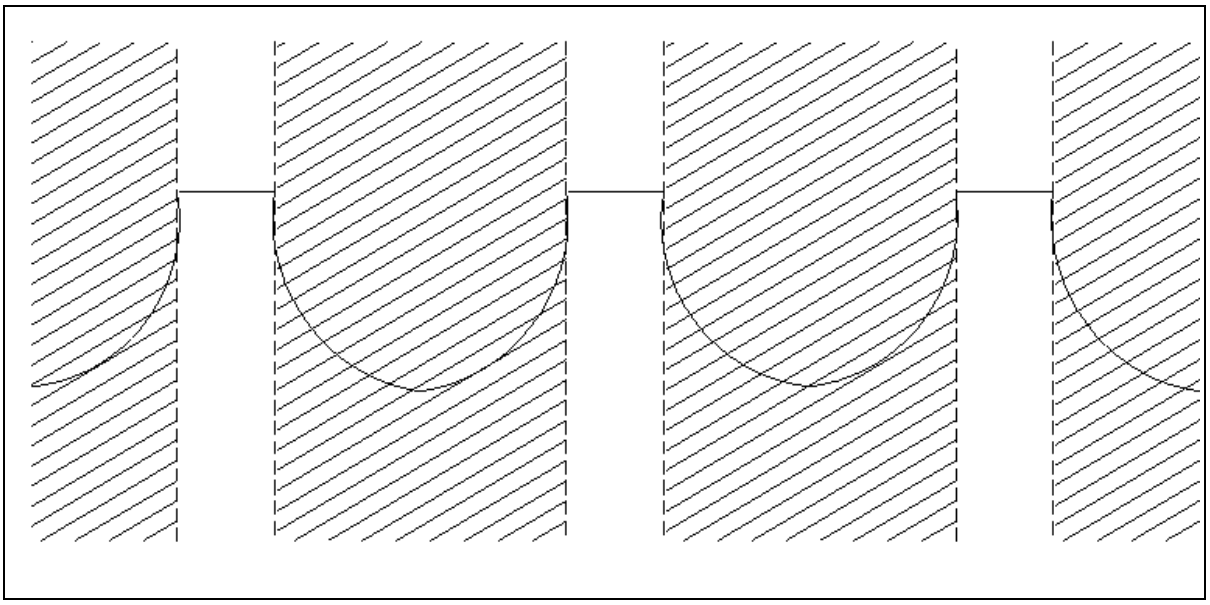

Figure 2.6. The vortices (white regions) and the penetration into superconducting regions for a superconductor of type II.

In Figure 2.6. the shaded parts represent the regions where the magnetic field cannot penetrate and the line shows the variation of the magnetic field within the material. The variations of the internal magnetic field (*B*) as a function of the applied magnetic field (*H*) for type I and type II superconductors are shown in Figure 2.7.

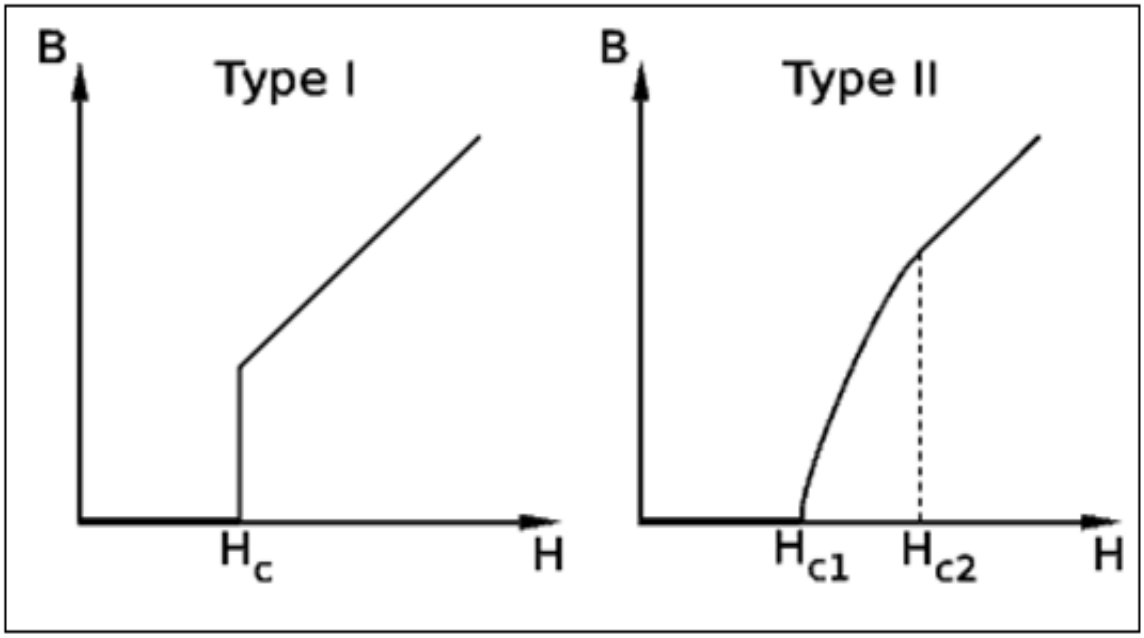

Figure 2.7. The variations of the internal magnetic field (B) as a function of the applied magnetic field (H) for type I and type II superconductors [54].

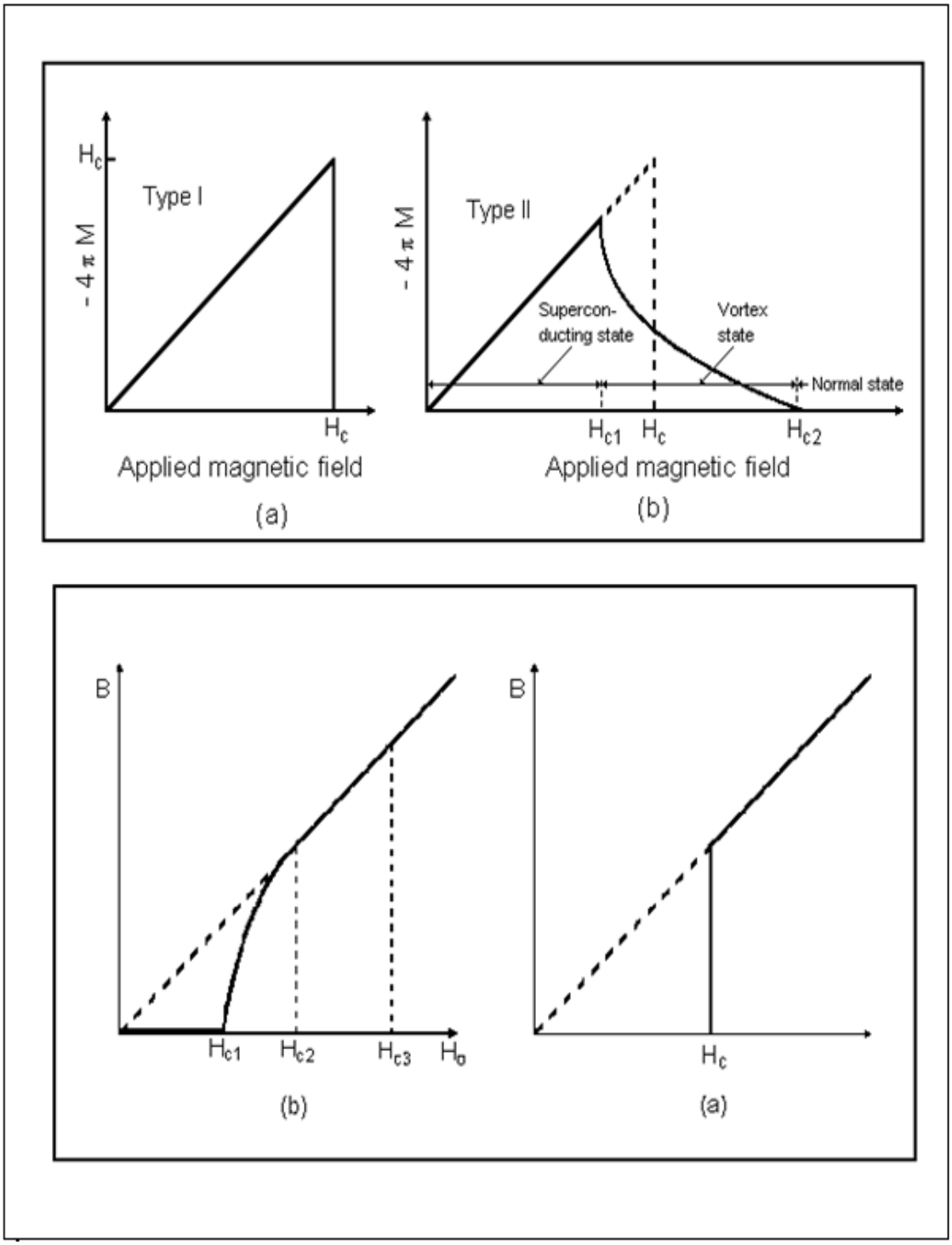

Figure 2.8. The variation of the magnetization as a function of the applied magnetic field (H) for type I and type II superconductors [54].

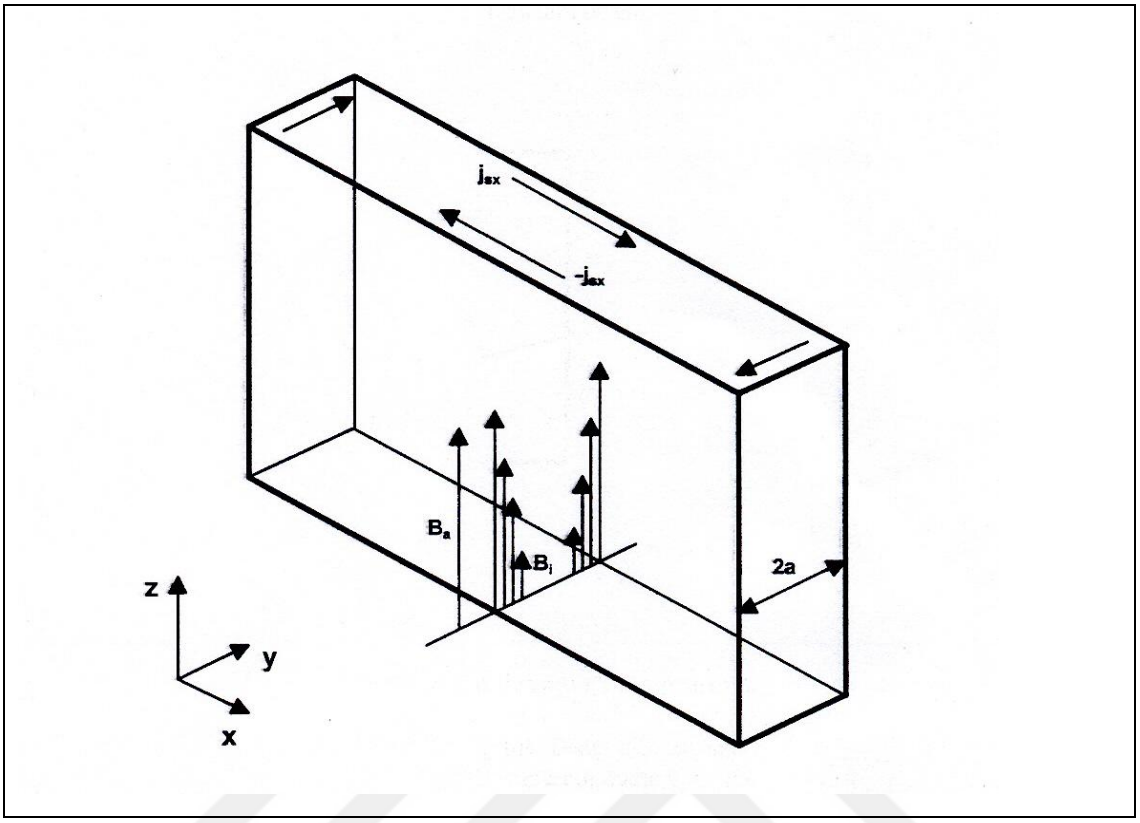

Figure 2.9. The distribution of the internal magnetic field (B) in a thin superconducting layer and the screening currents [14].

Figure 2.9. shows the distribution of the magnetic field B_a applied in the *z*-axis in a sample of thickness 2a. When the value of the magnetic field B_a exceeds B_{C1} the field begins to penetrate into the material from the surface. For fields not sufficiently high the screening currents near the central part of the slab and the internal field will be zero. In case that the internal field at the centre is different than zero the surface current density J_S is equal to the critical current density J_C. In the critical state model of Bean [17], the dependence of the current density J_C on the magnetic field is neglected. Maxwell's equation relating the internal magnetic field and the critical current density J_C is

$$\nabla \mathrm{x} \mathbf{B_i} = \mu_o \mathbf{J_c} \quad (\mu_o \text{free space permeability}) \qquad [49] \ (2.6)$$

For a successful explanation of the magnetization curves in the superconductors by the critical state model the distribution of the internal field against a changing external field should be given as shown in Figure 2.10. where the internal field decays towards the central part linearly with the distance. At the beginning (i.e. between 0 and *H**) the surface

currents that screen can make the internal field at the centre to be zero. For the case where the magnetic field is greater than H^* (= J_C x a) the current flows through the whole cross-section of the sample. Thus, there is a magnetic field in all parts of the sample. In the reverse process, that is, as the magnetic field drops from $2H^*$ down to zero the internal regions will be as shown in Figure 2.10. (b) the reverse magnetization occurring when the magnetic field is zero gives the residual current density trapped due to the pinning centres in the material. Although the critical current density is assumed to be independent of the field in the model of Beam, it *is* dependent on the field in real cases.

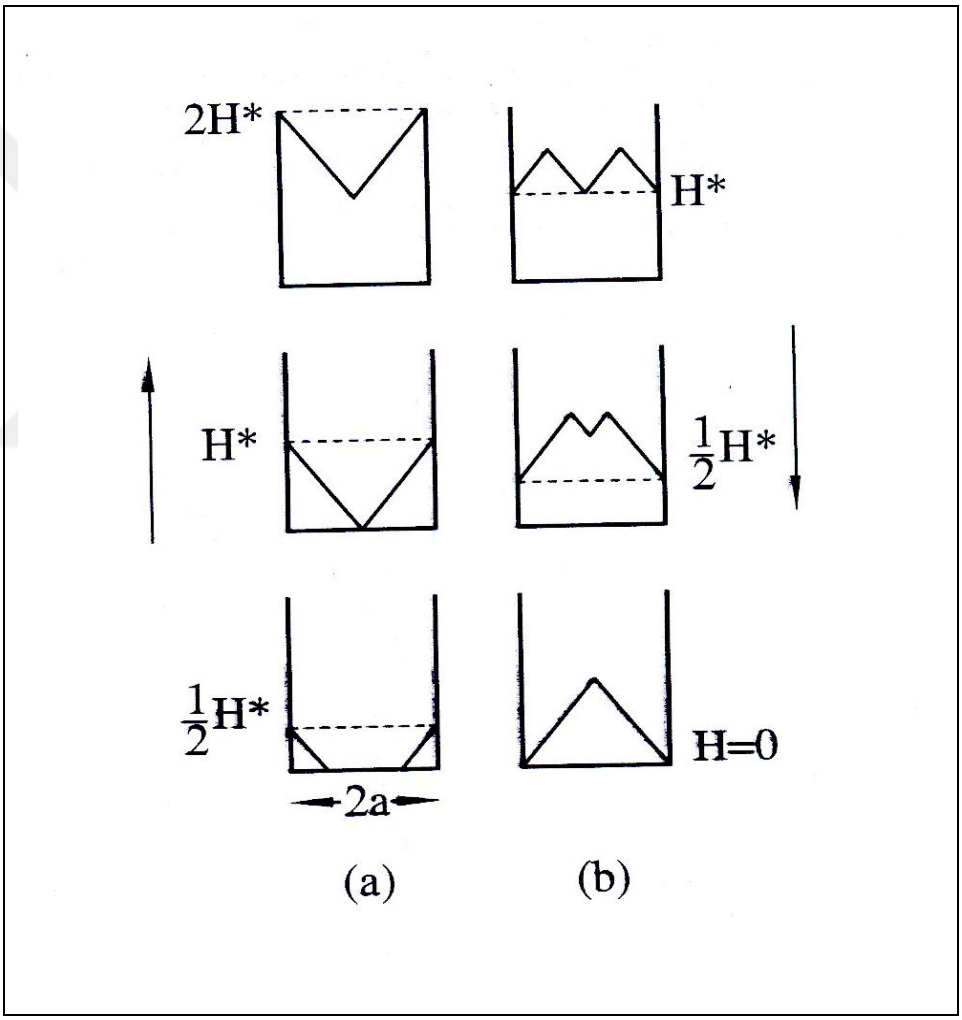

Figure 2.10. The distribution of the internal magnetic field (B) in an (a) increasing, (b) decreasing magnetic field [15].

2.5. THE NON-LINEAR MAGNETIC FLUX, CRITICAL STATE MODEL AND HARMONIC CASES IN HIGH TC SUPERCONDUCTORS

The effects of the AC or DC magnetic fields in high T_C superconductors are studied by a large number of researchers [45-52]. If an AC field (H_{AC}) of frequency f is larger than the first critical value H_{C1} the magnetic flux starts to penetrate a high T_C superconductor and the response of the superconductor is not linear because of the dependence of flux pinning on the magnetic field. As a result of this nonlinear behaviour observed in magnetization odd harmonics whose frequencies are $(2n+1)f$ occur. The application of a dc field in addition to an ac field causes even harmonics to occur. The harmonics are observed as long as the superconducting state is preserved.

It is first suggested by Bean that in case of applying an ac magnetic field odd harmonics in magnetization might occur in type II superconductors [17]. Bean explained this phenomenon by the critical state model, but not the formation of even harmonics observed in case that ac and dc fields are applied together. Several models have been suggested to explain this phenomenon observed in high T_C superconductors but no net result has been obtained [44,46-48]. The formation of odd and even harmonics is recently studied by L. Ji et al. and a solution is suggested [50]. They related the formation of even harmonics that can even be observed at very low fields to the strong dependence of the critical current on the field (whereas the critical current was supposed to be irrespective of the field in the Bean model). Having measured the harmonic power they suggested that the critical current passes from the Bean region to the Anderson-Kim region with an increasing magnetic field [51,52] (in this theory the critical current density J_C is inversely proportional to the magnetic field). The even harmonics that cannot be explained by Bean occur in the Anderson-Kim region.

2.6. FORMATION OF EVEN HARMONICS

L. Ji et al. suggested in the critical state model that the critical current does not have to be constant and independent of the field, instead, the critical current can depend on the local field [50]. When an AC field in the form of $x = 0.03H = H_{AC}\cos\omega t$ is applied to the

superconductor J_C will depend only on the $|H|$ and therefore the magnetization will be $M(\omega t) = -M(\omega t) + \pi$,considering that $|H|$ will be the same for ωt and $(\omega t + \pi)$. Thus, a symmetric magnetization curve is to be expected.

$M(\omega t)$ that can have this symmetry for

$$\sin(n\omega t) = (-1)^n \sin[n(\omega t + \pi)] \qquad [17](2.7)$$

and

$$\cos(n\omega t) = (-1)^n \cos[n(\omega t) + \pi] \qquad [17](2.8)$$

can explain the formation of odd harmonics.

Whereas in the case of applying a DC field in addition to an ac field, that is, a total field $H = H_{DC} + H_{AC}\cos(\omega t)$, J_C cannot be expected to be the same as the value at $H = H_{DC} + H_{AC}\cos(\omega t) + \pi$, because J_C depends on $|H|$. So in this case the symmetry will be broken. As a result the critical state model will enable the formation of even harmonics in the presence of $J_C(H)$ and a DC field.

L. Ji et al. have considered in the studies with conventional superconductors (superconducting alloys) that non observing even harmonics might originate from **i-** the independence of the critical field from the field, **ii-** the total field (AC and DC) being smaller than the first critical field H_{C1}. In the conventional superconductors H_{C1} has relatively high values. In the high T_C poly-crystalline superconductors the first critical value $x = 0.03H_{C1}$ of the field is around 1 Oe (Oersted). This value can even be less depending on the strength of the bonding between the particles. The smaller the strength of the bonding, the less will be $x = 0.03H_{C1}$. Therefore, it is more probable to observe odd and even harmonics in the high $x = 0.03T_C$ superconductors and at reasonable field values.

2.7. THE ANALYSIS FOR THE ANDERSON-KIM MODEL

In the model Anderson-Kim the critical current density is calculated by the magnetic flux pinning $\alpha = (1/c)J_C xH_{local}$ where alpha (α) is the pinning force per unit volume, *c* is the speed of light. To take α as constant simplifies the calculations and supplies good approximations for several systems. In this case the equation $J_C = c\alpha / H_{local}$ is obtained, which in turn causes a parabolic flux density profile as shown in Figure 2.11.

L. Ji et al. have applied the Anderson-Kim model on a plate of width *D* for the limiting cases of $H << H^*$ and $H >> H^*$ (H^* being the necessary magnitude for penetration until the centre of the plate) and obtained the magnetization curves of the material. The results can be summarized as follows (for the details see [50]): Numerical solutions are obtained for the magnetization profile for the cases where Δ^2 is greater or less than H^{*2}, assuming a magnetic field *H* varying between H_a and H_b ($H_a > H_b$) $\Delta^2 = \left[H_a^2 \operatorname{sgn}(H_a) - H_b^2 \operatorname{sgn}(H_b)\right]$ where $\operatorname{sgn}(x) = 1$ if $x > 0$ and $\operatorname{sgn}(x) = -1$ if $x < 0$. If the superconductor is inside the AC field ($H = H_{AC}\cos(\omega t)$ then $H_a = -H_b = H_0 = H_{AC}$. It is also shown that if $H_{AC} < H^*$ the harmonic signal is proportional with H_{AC}^3 / H^{*2} but if $H_{AC} > H^*$ no simple result is obtained. However, in this case it is shown that the harmonic signaşl formed is proportional with H^{*2} / H_{AC}.

Applying a DC field to the superconductor in addition to an AC field ($H = H_{DC} + H_{AC}\cos(\omega t)$ then $H_a = H_{DC} + H_{AC}$ and $H_b = H_{DC} - H_{AC}$ and besides this after delta squared $< 2H^{*2}$ is satisfied the magnitudes of the harmonic signals are calculated together with the signal variations as a function of the dc field (Figure 2.12.). In the region $H_{DC} < H_{AC}$ the harmonics other than $n = 2$ have shown a harmonically oscillating behaviour. On the other hand, in the region where the ratio H_{DC} / H_{AC} is very low the variation in the harmonic signal is very acute.

The graph for $n = 2$ was noticeable for our team and we prepared this project. In case that an appropriate value for H_{AC} is obtained such an acute response for the DC field gives an idea about the sensitivity of the superconducting sensor.

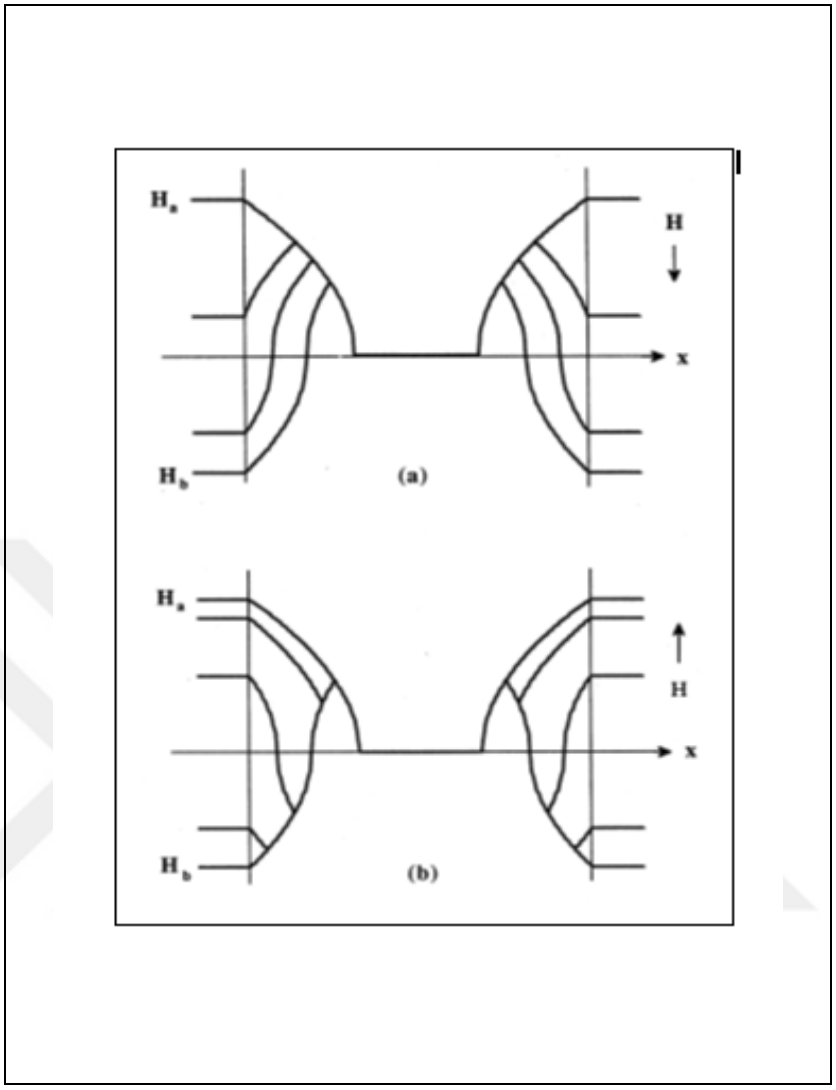

Figure 2.11. The profile for the infinitely long plate inside a magnetic field H. The field is changing between H_a and H_b ($H_a < 0 < H_b$), $|H_a| > |H_b|$, $H_a > H^*$. The applied field (a) decreases from H_a to H_b, (b) increases from H_b to H_a [50].

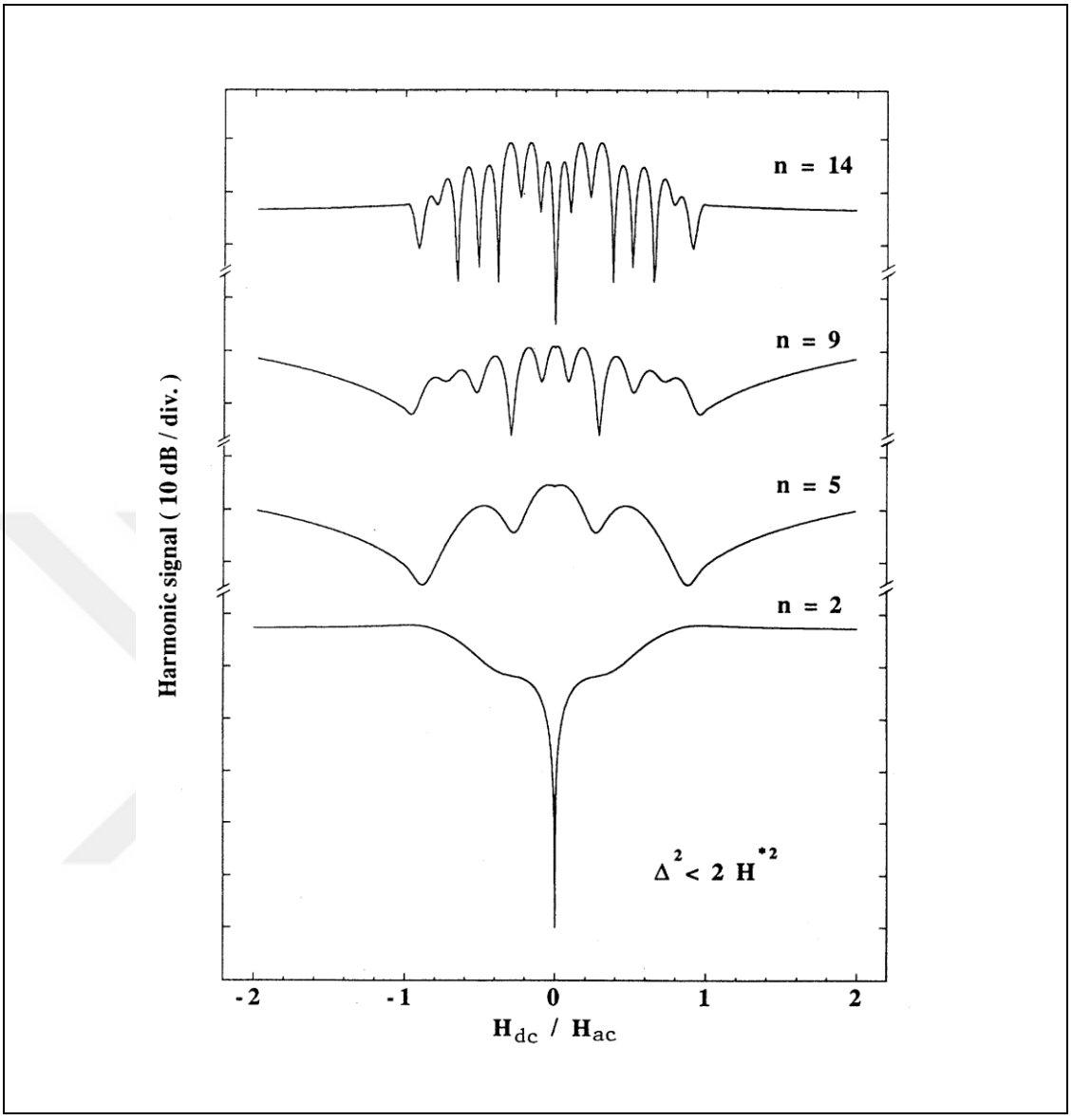

Figure 2.12. The variation of the harmonic signal calculated numerically by the Anderson-Kim model as a function of the dc field applied ($\Delta^2<2H^{*2}$) [50].

A similar study is conducted for the superconductor YBCO at 77 K and AC field of $H_{AC} = 2.3$ Oe by C. Jeffries et al. [42] and the behaviour in Figure 2.13. is obtained for the second harmonic. As can be seen from this study the 2nd harmonic exhibits an acute variation in the region -11 Oe and +100 Oe. It is understood from these observations that if the necessary conditions are satisfied (that is $\Delta^2 < 2H^{*2}$ and the ratio H_{DC} / H_{AC} is adjusted) a sensor which is very sensitive for the magnetic field can be developed. We

consider that as the exciting frequency is optimized (taken to be 52.5 kHz in this study) the degree of acuteness can be increased and this region can be made even narrower.

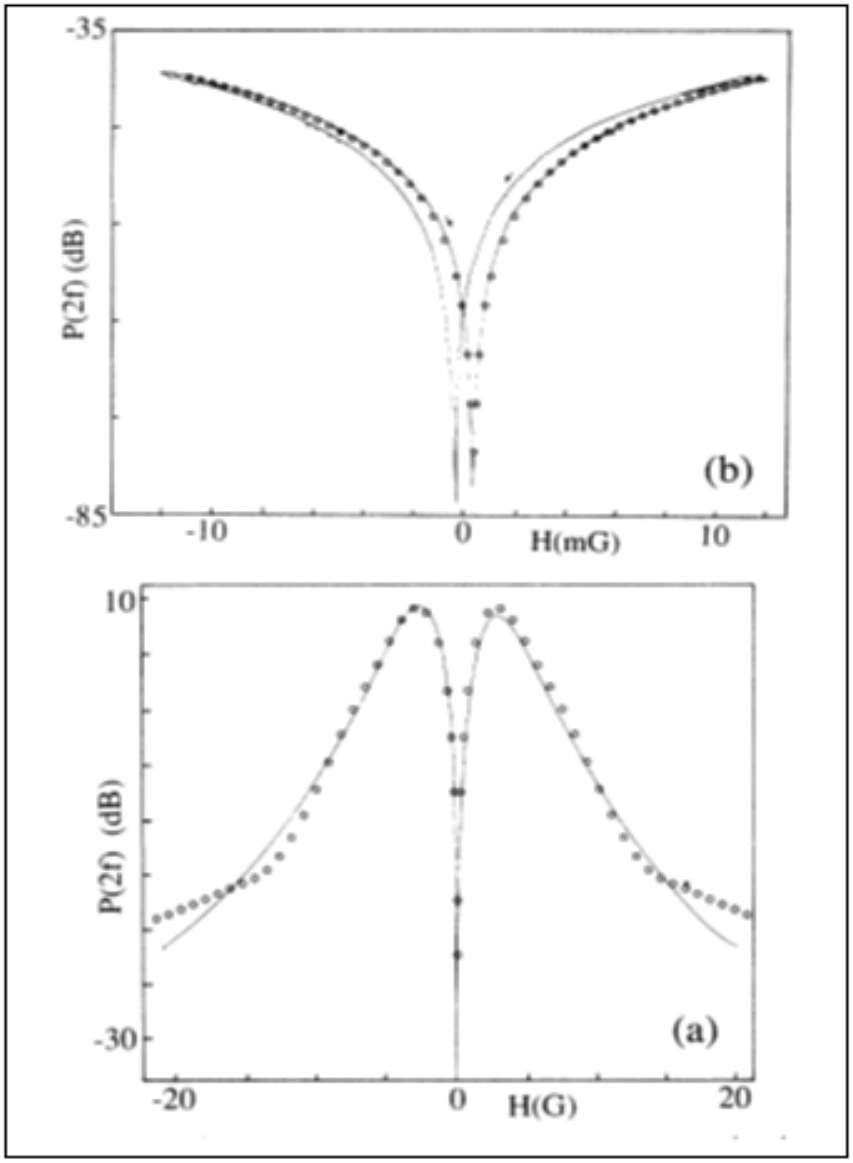

Figure 2.13. (a) The variation of the harmonic signal intensity with the DC field, (b) the graph widened around zero DC field [42]. ($H_{AC} = 2.3$G and $\omega = 52.5$ kHz) [50].

3. EXPERIMENTAL PROCEDURE

3.1. THE SYNTHESIS OF SUPERCONDUCTIVE MATERIALS

In this work, the superconductive elements which were used as sensing elementsin the magnetometer were synthesised by solid-state reaction method.The solid-state reaction method is the easiest and also the most common method in preparing the high-temperature superconductive samples.The critical temperature, grain growth and other types of properties of cuprate superconductors are directly related to the preparation methods of the samples.In solid-state reaction method homogeneous samples can be prepared.

3.2. THE EXPERIMENTAL SET-UP FOR YTTRIUM WITH BISMUTH

$Bi_{1.8}Pb_{0.35}Sr_{1.9}Ca_{2.1}Cu_3O_x$ (Bi-2223) ceramic superconductors, used as sensing elements, were prepared by the solid state reaction method. High purity powders (99.99 %) of Bi_2O_3, PbO, $SrCO_3$, CaO and CuO were weighed in the appropriate amounts and mixed well using an agate mortar. Then, the powder was pressed into pellets under pressure of 14000 N/cm^2. The pellets were calcined at different temperatures (700 ^oC, 750 ^oC, 800^oC, 820^oC, 820^oC and 850 ^oC) for 120 h with intermediate grinding, mixing and pelletizing after each 20 h. Finally, the pellets were oxygenated under oxygen flow (0.5 lt/min) by holding at 800 ^oC (8 h) and 450 ^oC (16 h). Final dimensions of the pellets were adjusted to diameter of 23 mm and thickness of 6 mm. At this stage superconductivity was tested by levitation experiments. Here, we must note that if the levitation is not observed, the annealing under oxygen must be repeated. The coil configurations used in experiments (the pick-up coil; for the detection of 2nd harmonic signal generated by superconducting specimen, and the excitation coil; for applying an AC magnetic field to the superconductor) were explained with details in [7, 25]. An electronic filter with high quality factor Q was used to eliminate signals other than $2f = 99.8\,\text{kHz}$ explained in detail in electronic filter design section [5,6]. The DC- field was applied by a calibrated solenoid with coil constant of 15.61 Oe/A, which is traceable to primary standards of dimensional and time & frequency over NMR tesla-meter. The tests were performed at liquid nitrogen

temperature and the test place was shielded from surrounding magnetic fields by using trio Mu-metal chambers. For electrical connections, well- screened cables were used. The M-T and the M-H measurements were done by using MPMS-5 SQUID magnetometer from Quantum Design [25].

3.3. THE PREPARATION OF YTTRIUM BY ZINC DOPING

The sensing elements of the magnetometer were prepared by the conventional solid state reaction method. $YBa_2Cu_{3-x}Zn_xO_{7-y}$ ($x = 0.00$, 0.01, 0.02, 0.03, 0.05, 0.1). High purity powders (99.99 %) of Y_2O_3, $BaCO_3$, CuO and ZnO were weighed in the appropriate amounts and mixed well using an agate mortar. Then, the powder was pressed into pellets under pressure of 14 000 N/cm^2. The pellets, containing different amounts of Zn given($x = 0.00$, 0.01, 0.02, 0.03, 0.05, 0.1) above, were calcined at 925^{o}C for 72 h with intermediate grinding, mixing and pelletizing after each 24 h. Here, it must be noted that all samples were furnaced at same atmospheric conditions in order to minimize the contribution of external factors and thus, to understand the effects of Zinc doping on second harmonic signal strength. Later, the samples were oxygenated under oxygen flow (0.5 lt/min) by holding at 900^{o}C (16 h) and 450^{o}C (24 h). Then, the samples were sandpapered to the same dimensions with diameter of 23 mm and thickness of 7 mm to avoid the possible variations coming from the demagnetization factor. The M-T and the M-H measurements were done by using MPMS-5 SQUID magnetometer from Quantum Design. Experimental set up for these second harmonic measurements were described with details in [5, 6, 26].

The coil configurations were determined for this experiment. The most appropriate one was used in all three experiments which can be seen in Figure 3.1. The pick-up coil, which was used for the detection of 2nd harmonic signal generated by superconducting specimen, has 2100 turns/cm (wire diameter is 100 μm). The driving coil, for applying an AC magnetic field to the superconductor, has 50 turns/cm (wire diameter is 200 μm) and the winding changes direction in the middle of the template. The pick-up coil was moved through the driving coil to minimize mutual inductance between these coils (i.e. mechanical compensation). We must note that the fiber glass was preferred as a template for the coils to minimize thermal expansion in liquid nitrogen [26].

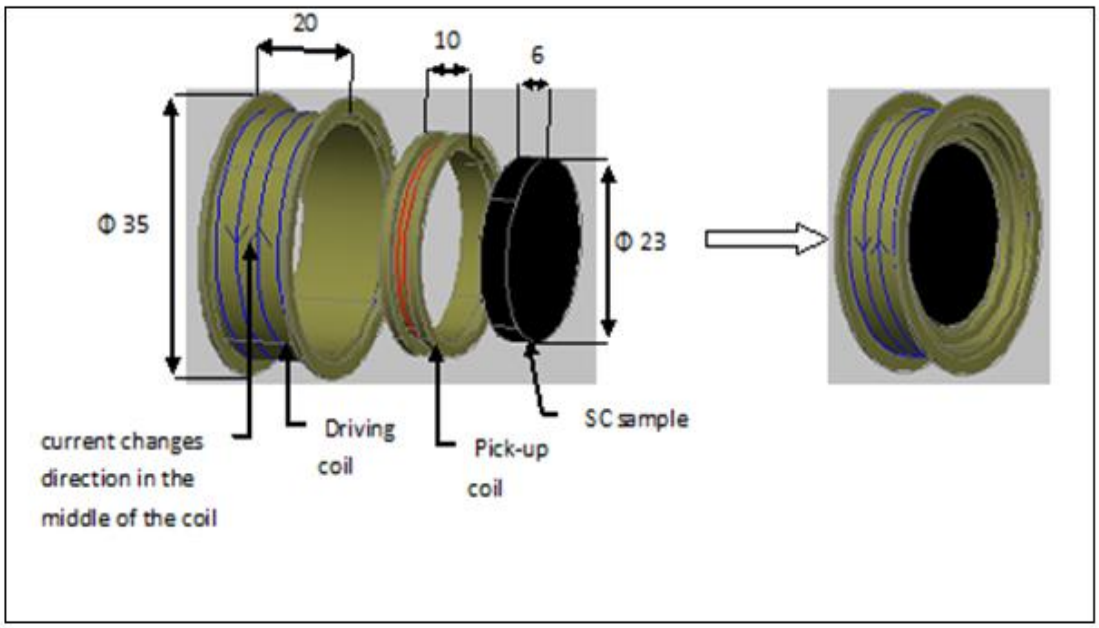

Figure 3.1. The coil design of the sensor [6,66].

An electronic filter with high quality factor Q was used to eliminate signals other than 2f=99.8 kHz (for details, [6]). The DC- field was applied by a calibrated solenoid with coil constant of 15.61 Oe/A, which is traceable to primary standards of dimensional and time&frequency over NMR teslameter. The tests were performed at liquid nitrogen temperature and the test place was shielded from surrounding magnetic fields by using trio Mu-metal chambers. For electrical connections, well- screened cables were preferred [26].

The indentation experiments were conducted with a Berkovich tip using the NH–2 Nanoindenter (manufactured by CETR) with load and displacement resolutions of ±0.1 μN and ±0.03 nm, respectively. Beforethe indentation experiments, the samples on the mounting stage were adjusted to prevent tilting in the z–axis. At least five-step load-unload indentation experiments were carried out at different locations of the samples as the nature of the samples was beingporous and heterogeneous. Loading steps were adjusted as 50, 100, 200, 300 and 400 mN [26].

3.4. BORON DOPING TO THE SYSTEM

$Y_{1-x}B_xBa_2Cu_3O_y$($x = 0.00$, 0.05, 0.1, 0.15) used as sensing elements were prepared by solid state reaction method. Appropriate amounts of Y_2O_3, $BaCuO_3$, B_2O_3 and CuO were weighed and well mixed using agate mortar. All chemicals were obtained at high purity (99.99 %) in powder form. The mixture was first calcinated at 920^0C for 20 hours. Then the mixed powder was pressed into pellets under pressure of 14 000 N/cm^2. After that, the pellets were placed into oven for 20 hours at 950^0C [28].
Finally the pellets were oxygenated under oxygen flow (0.5 L/min) by holding at 800^0C for 8 hours and 450^0C for 16 hours. Then the samples were sandpapered to the same dimensions of 23 mm in diameter and 7 mm in thickness [28].

The indentation experiments were conducted with a Berkovich tip using the NH-2 Nanoindenter (manufactured by CETR) with load and displacement resolutions of±0.1 μN and ±0.03 nm, respectively. Before the indentation experiments, the samples on the mounting stage were adjusted to prevent tilting in the z-axis. For a particular load at least five indentation tests were conducted on the sample surface to increase the reliability of the experimental results. The maximum load was changed at regular intervals, 100, 200, 300, 400 and 500 mN [28].

The M–T and the M–H measurements [28] were done by using MPMS-5 SQUID magnetometer from quantum design. Experimental set up for the second harmonic measurements were described in [55,56]. The electronics and the test conditions are explained in [55].

3.5. THE LEVITATION TESTS

After the preparation process all the superconductive samples were tested for levitation by immersing into liquid nitrogen. When the superconductive material is put into liquid nitrogen it gets colder and when it gets to the critical temperature it levitates. In this process many kinds of magnets with varying dimensions were used. The magnets were put onto the superconductive samples to see if they can levitate. If levitation has not occurred then the samples were re-oxygenated and the process was repeated. The samples were

synthesized and all the process was repeated from the beginning until the levitation was observed.

3.6. MAGNETIC MEASUREMENTS

The magnetization curves (M-H and M-T) were obtained for the superconductive samples by Quantum Design MPMS5 SQUID magnetometer at 77 K. As it is mentioned in literature if the magnetic field applied on the superconductive sample is bigger than the first critical field H_{c1} it begins to penetrate into the sample. In polycrystalline superconductors $H_{C1J} << H_{C1}$ thus the applied magnetic field begins to penetrate into the sample. The second harmonic signal can be composed if **i-** the total magnetic field ($H_{DC} + H_{AC}$) is greater than H_{C1J}, **ii-** DC field should be much smaller than AC field ($H_{DC} << H_{AC}$) and **iii-**the total magnetic field should be less than H^*. For this reason the values of H^* and H_{C1J} should be known. After the determination of those values the dynamic scale of the magnetometer can be defined by setting H_{DC} and H_{AC} values. The magnetic parameters (e.g. H^*, H_{C1J}) of the specially designed sensor, at its working temperature (77 K), obtained from M-H and M-T graphs. The measurements were done in slot geometry to minimize the geometric demagnetisation factor. The synthesized superconductor samples were cut accurately in slot geometry by a ceramic cutting machine. From the measurements of M-T (field-cooled-FC and zero-field-cooled-ZFC) the T_C, transition temperature for superconductivity and the pinning force for the samples were determined. The trapped magnetic flux was obtained from the difference in between FC and ZFC magnetisations from the M-T slopes. The trapped magnetic field gives explanation about the pinning force of the samples and therefore critical current density. The trapped magnetic flux in the sample ascends by the critical current density proportionally. The M-H measurements were done to calculate the H_{c1j} and H* parameters. After the process of ZFC, M-H loop obtained in between -1000 Oe-1000 Oe magnetic field. Since in polycrystalline high T_c superconductors the value of H_{c1j} is very low, the first magnetic field values were increased by **i-** between 0 – 30Oe, with step size 1 Oe (the lowest measurement capacity of SQUID), **ii-** between 30 – 100 Oe,with step size5 Oe. H_{c1j} defined as the first area deviated from the linearity of the first magnetization curve. H*

defined as the contact point of the first magnetization curve and the curve coming from the negative side of the M-H loop [63,64]. The critical current density J_C was calculated from M-H graphs by using Bean's Model [17].

$$J_C = \frac{20\Delta M}{a\left(1-\frac{a}{3b}\right)} \tag{3.1}$$

In this formula, *a* and *b* are the dimensions of the sample.

3.7. MEASUREMENTS OF THE HARMONIC SIGNAL

When a powerful enough sinusoidal AC magnetic field in the form of $H_{AC}\sin(\omega t)$ applied on a type II superconductor, magnetic response of the sample will not be linear.Thus the total magnetization of the superconductor can be expressed as follows

$$M = \sum_n [A_n \sin(n\omega t) + B_n \cos(n\omega t)] \tag{3.2}$$

In which A_n and B_n are respectively real (in-phase) and imaginary (out of phase) components are dependent on H_{AC} and H^*.

As is known from Faraday's law, the voltage measured on the sensor coil is proportional to the change in the magnetisation, effective area (*A*) and the number of turns (*N*) on the coil. In this case, the harmonics of the frequencies of the applied voltage components can be expressed as follows [65, 66]:

$$V_2 = \omega AN\left[A_n\left(H_{AC}, H^*\right)\sin(n\omega t) + B_n\left(H_{AC}, H^*\right)\cos(n\omega t)\right] \tag{3.3}$$

When just the AC field is present, single harmonics; when AC field coupled with DC field, both odd and even harmonics are simultaneouslyformed. The DC magnetic field dependency of the second harmonic signal is linear in the low magnetic field area. Since we aimed to improve the sensitivity of the superconductor sensor in low DC field, we limit

our trials in $0 < H_{DC} < 1$ Oe and $H_{C1J} < H_{AC} < H^*$ region (in this region high temperature cupratesuperconductors look suitable). In this case, the amplitude of the second harmonics signal is expected to be proportional to the $H_{DC}$and H_{3AC}/H^*. In other words, it can be defined as [65]

$$V_2 \approx \omega ANH_{DC}H_{AC}^3 / H^* \tag{3.4}$$

In our experiments three coils have been used. The first one is the excitation coil which has been employed to create the AC field ($H_{AC}\sin(\omega t)$) to be applied on the superconductor sample. The current applied to the coil has been generated by a SRS DS360 model ultralow distortion signal source which is capable of producing 0-200 kHz signal.

The second coil is the sensing unit (pick-up coil) which is used in detecting the second harmonic signal appearing on the superconductor sample. SR844 and SR830 model Lock-in amplifier detectors have been used in the sensing coil (APPENDIX A). The experimental DC field coil constant has been obtained from a third coil which has been calibrated earlier. The current on the DC coil has been obtained from Keithley 220 current source. To measure the AC current passing through the excitation coil, a 54642A model oscilloscope has been used. In order to measure the AC current, 1Ω manganese resistance has been placed in series with the excitation coil and the voltage readings have been made by an oscilloscope. By dividing the voltage to the resistance value, the AC current passing throught the coil has been measured. In order to reduce the noise all instruments have been covered with alumunium foil and grounded. Well insulated cables have been preferred to minimise environmental noises. All experiments have been carried out in the liquid nitrogen temperature of 77 K. To minimise the environmental factors, the sensor system and all experimental setup has been enclosed in a Mu-metal chamber. The schematics of the set-up are seen in Figure 3.2.

Since the 2*f* signal is approximately $V_2 \approx \omega ANH_{DC}H_{AC}^3 / H^*$ a proper working frequency and suitable AC field width has to be determined. To this end an optimal frequency-2nd harmonic signal and optimal AC field-2nd harmonic signal measurements have been carried

out and as a result of these measurements dependency of the DC field to the 2nd harmonic signal within thesuitable frequency and AC field amplitudes have been investigated.

During the DC field-2nd harmonic signal measurements a passive filter capable of filtering out 360 kHz and below as well as 1st harmonic signal intensity and environmental noise. Normally both *f* and 2*f* frequencies appear on the sensing coil. The value to be measured is the 2*f* frequency signal on the superconductor sample originated from the DC magnetic field. On a sensing coil that has not been properly compensated, the intensity of the *f* component in the total signal is much higher than the 2*f* component. Thus it is necessary to filter out the *f* component. To this end a passive filter working in 2*f* frequency (0.360-0.400 MHz) with a quality factor 10 and input and output impedences of 50 ohms has been designed (passive filter design, APPENDIX B, Figure B.1.).

Similarly, the DC field-2nd harmonic signal measurements a passive filter capable of filtering out 98 kHz and below, 1st harmonic signal intensity and environmental noise. (Active Filter design, APPENDIX B, Figure B.2.).

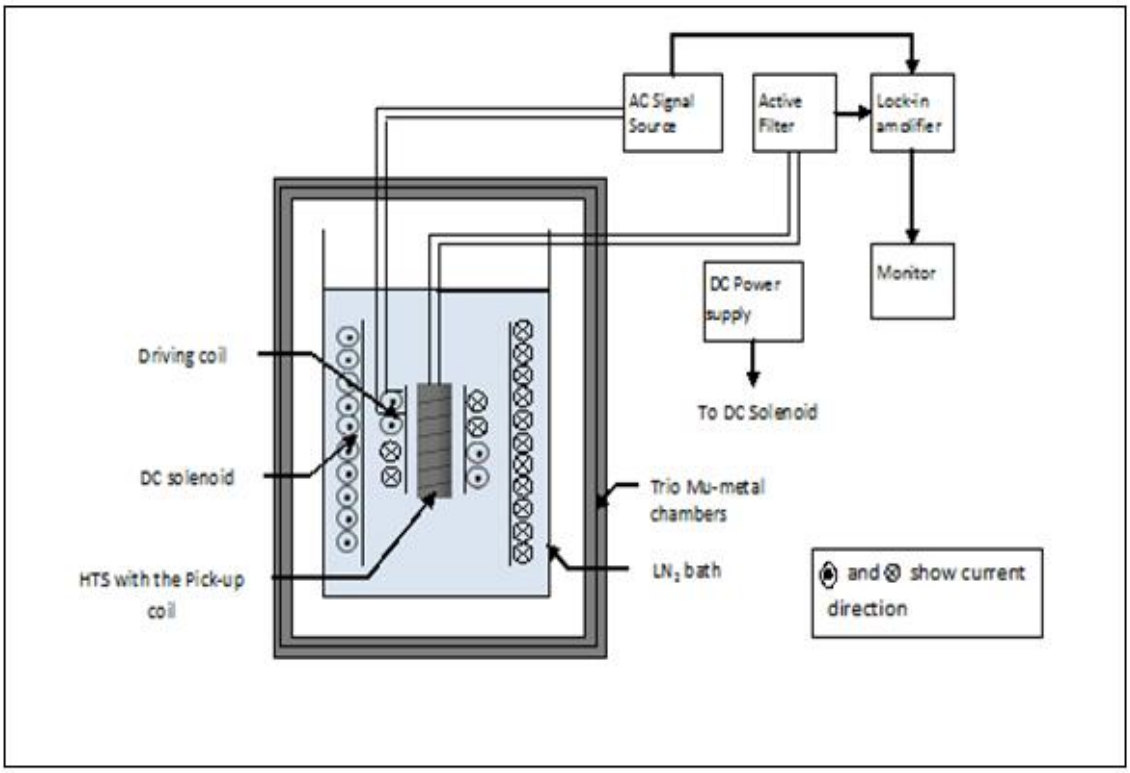

Figure 3.2. Shematic design of the system [66].

3.8 DESIGN OF THE COOLER

The compartment for the liquid nitrogen is formed by flat-based glass thermometer as shown below. It is better to keep the distance between the sensor and the sample as short as possible. The distance between the internal and external basesof the thermos is 15 mm. Since the base of the thermos is not covered with silver in order not to affect the sensitivity of the sensor for the magnetic field from below, the time of holding the liquid nitrogen is shortened from 36 to 24 hours which is still sufficient for the measurements.

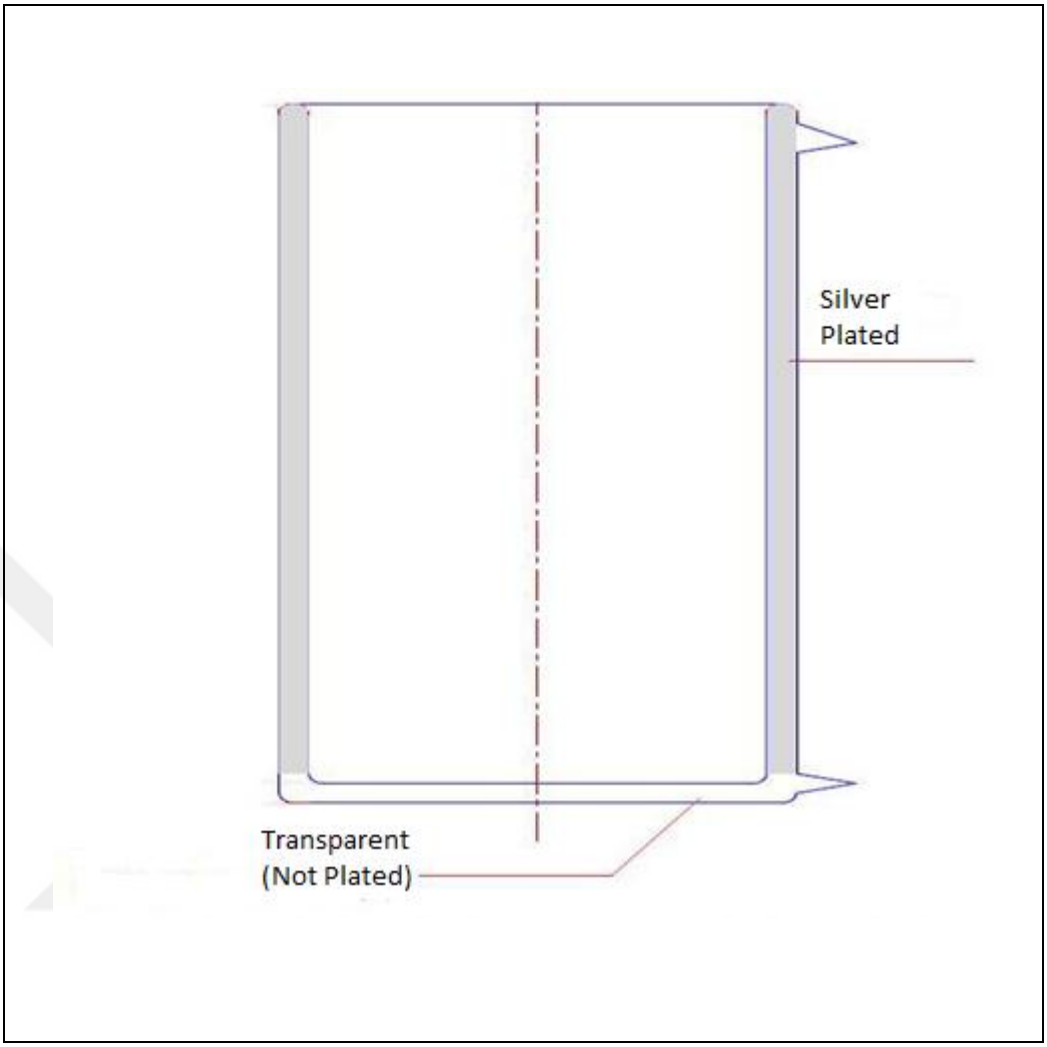

Figure 3.3. The cooler system.

However, since the thermos is quite brittle it is not possible to use it directly in measurements. Therefore, a plastic case is designed to put it in. The glass thermos is fixed in the plastic case by bracelets made of styrophore and a rod is screwed to the upper lid of thethickness 10 mm of diameter M16. The rod extends down to the bottom of the thermos and its height can be adjusted according to the size of the sensor.

The cables emerging from the sensor are carried by insulations of teflon and are soldered to connector which is mounted on the lid. The resistance of connector between the terminals is measured tobe larger than 10 TΩ.

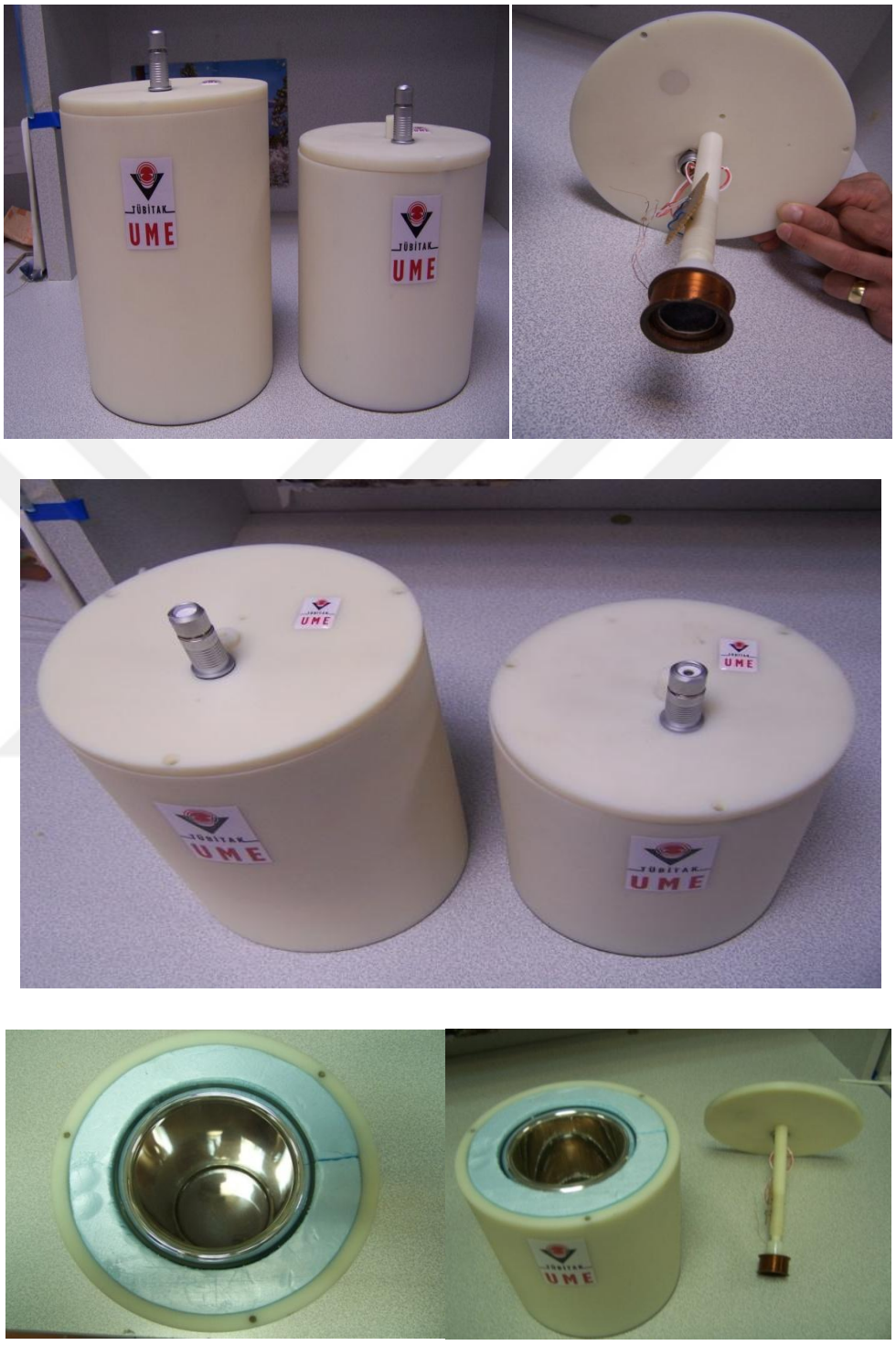

Figure 3.4. Different photos for the cooler system.

4. RESULTS AND DISCUSSIONS

4.1. BISMUTH SAMPLES

4.1.1. Magnetic Measurements

The M-T and the M-H curves of Bi-2223 superconductor are shown in Figure 4.1. The M-T data were collected at zero-field-cooled (zfc) and field-cooled (fc) modes in order to get an idea about the concentration of the trapped field and proportionally, about pinning force of studied superconductors. Here, we must note that a low pinning force is desired to release the movement of vortices. The transition to superconducting state T_C (on) starts at 107 K, which is in well agreement with the T_C (on) values known for Bi-2223 phase. The second phase transition seen at 70 K corresponds to the lower T_c phases of Bi-based superconductors, such as; Bi-2212. The large transition width indicates the presence of weak couplings between grains of the studied specimen [57,58]. It was estimated from the zfc curve that superconducting volume fraction at sensor working temperature of 77 K is 33 %. The trapped field at 77 K was also estimated as 44 % by taking the difference of magnetization data obtained by zfc and fc curves. It must be noticed that the trapped field varies between 70 % and 80 % of applied field for the Y-123 superconductors [7,25]. It means the applied field comes in and out to the Bi-2223 specimen more easily compared to the Y-123 one. It was verified before that the H_{c1j} (first critical field of grain boundaries) and the H^* (minimum field required for penetration through the entire specimen) parameters have a special role on the working performance and dynamical range of the sensor [5-7,25]. The H_{C1J} and H^* parameters were determined from the M-H curves to be less than 1 Oe and 110 Oe, respectively. The H_{C1J} is much lower than that of Y-123 (~10 Oe). However, the H* is a little bit larger than Y-123 (85 Oe-95 Oe). The critical current density J_C was derived from the M-H loops by using Bean model and found to be 145 A/cm^2 [17]. We must note that it varies between 550 A/cm^2 and 700 A/cm^2 for the Y-123 samples [7,25]. If we assume the formula $V_2 \approx \omega H_{DC} H^3{}_{AC} AN / J_C$ (where A is the

effective area and *N* is the number of turns of the detection coil) derived for the 2nd harmonic signal strength to be correct, then the Bi-2223 specimens as a core element must reveal higher the signal strength compared to the Y-123 one since the J_C of Bi-2223 is much smaller than Y-123 [59,60]. Comparison of the data published in [7,25] with the further part of the text has shown that there is no direct relationship between the J_C values and the 2nd harmonic signal intensity V_2. We investigated the dependence of the 2f signal on the frequency of AC field up to 200 kHz and expected the linear dependency from the formula given above. However, as it is seen from the Figure 4.2.(a) that the signal intensity first jumps to a maximum at 50 kHz and then decreases sharply. The relationship between the signal intensity and H_{AC} are also contrary to the formula and the experimental data in [59] (see Figure 4.2.(b)). While a saturation on the signal intensity is observed when $H_{AC} >> H^*$ in [59], we see such a saturation at values much smaller than the H*. Here, we must note that there is no such saturation in Y-123 samples [7,25]. On the other hand, from these measurements it is clear that optimal frequency of the excitation field is 50 kHz and optimal H_{AC} amplitude is somewhere between 10 Oe and 16 Oe for the present cores. The signal intensity vs. DC field curves is shown in Figure 4.3 for the excitation field frequency of 50 kHz and the amplitudes of 15.8 Oe and 27.5 Oe. As expected the data obtained at $H_{AC} = 15.8$ Oe is less noisy compared to the 27.5 Oe. The data in Figure 4.3. (a-b) and (c-d) were taken with the field steps of 0.5 nT and 2 nT, respectively. As seen it is possible to sense the 0.5 nT DC fields in case of $H_{AC} = 15.8$. In order to determine the dynamical range of the sensor the experiments were carried out in large range of DC fields (Figure 4.3.(e-h)). The deflection from the linearity was accepted to be the upper limit of the sensor and shown in Figure 4.3.(g) and 4.3.(h) with the arrows. The higher AC field amplitude results in the higher upper limit, but there is no excessive difference with the lower AC field amplitudes [25].

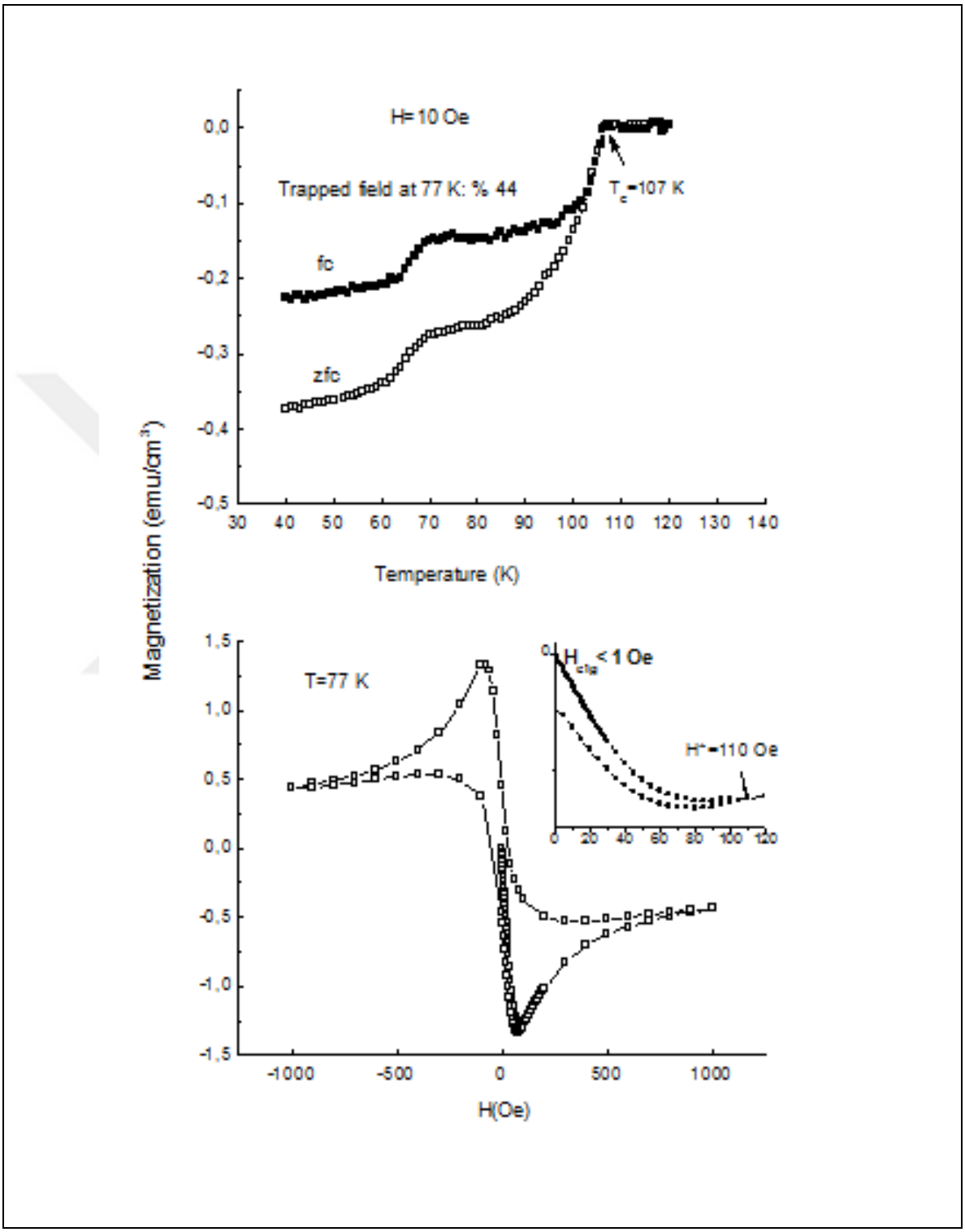

Figure 4.1. M-T and M-H curves of Bi-2223 superconducting samples [25].

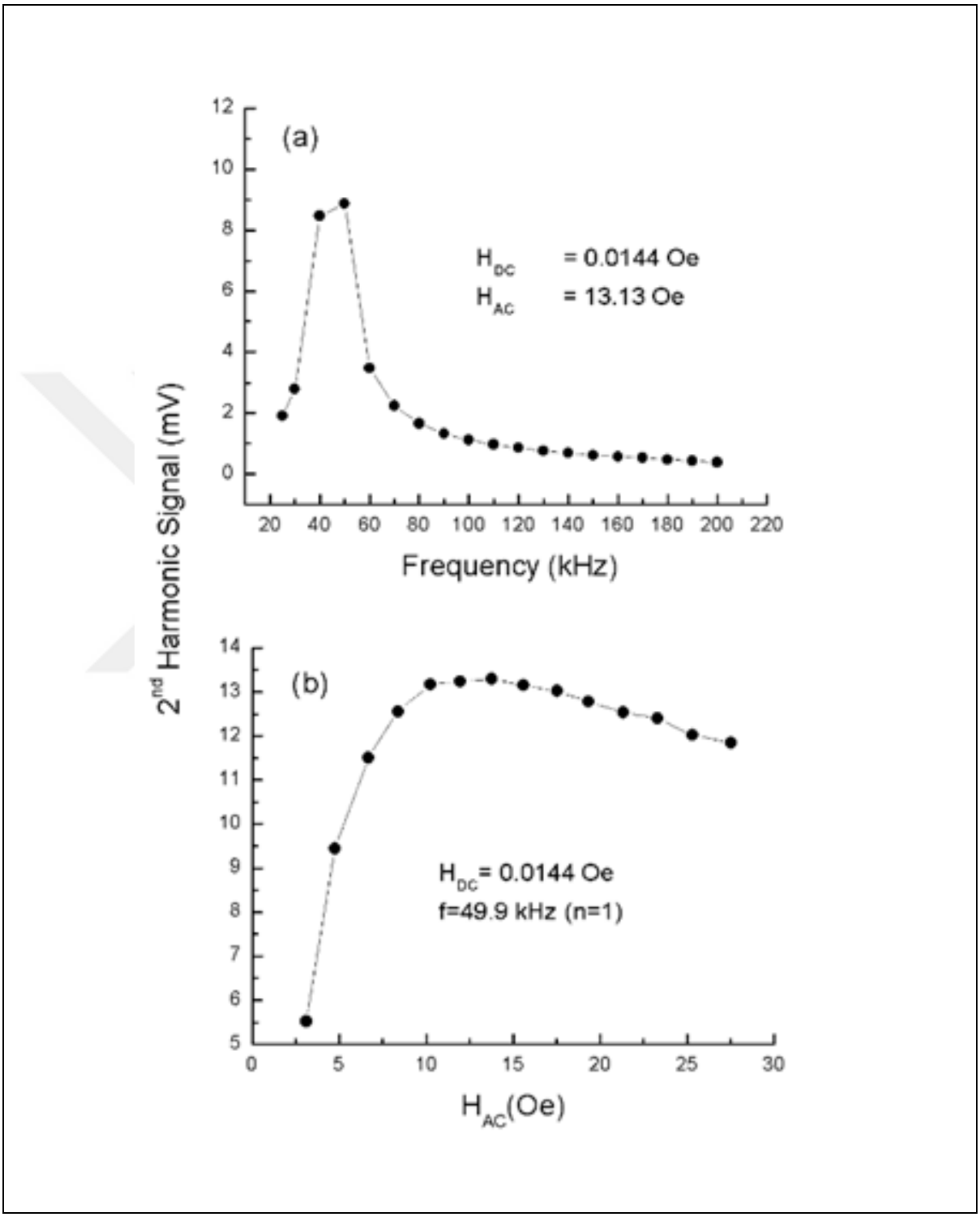

Figure 4.2. Obedience of the 2nd harmonic signal on driving field frequency and amplitude [25].

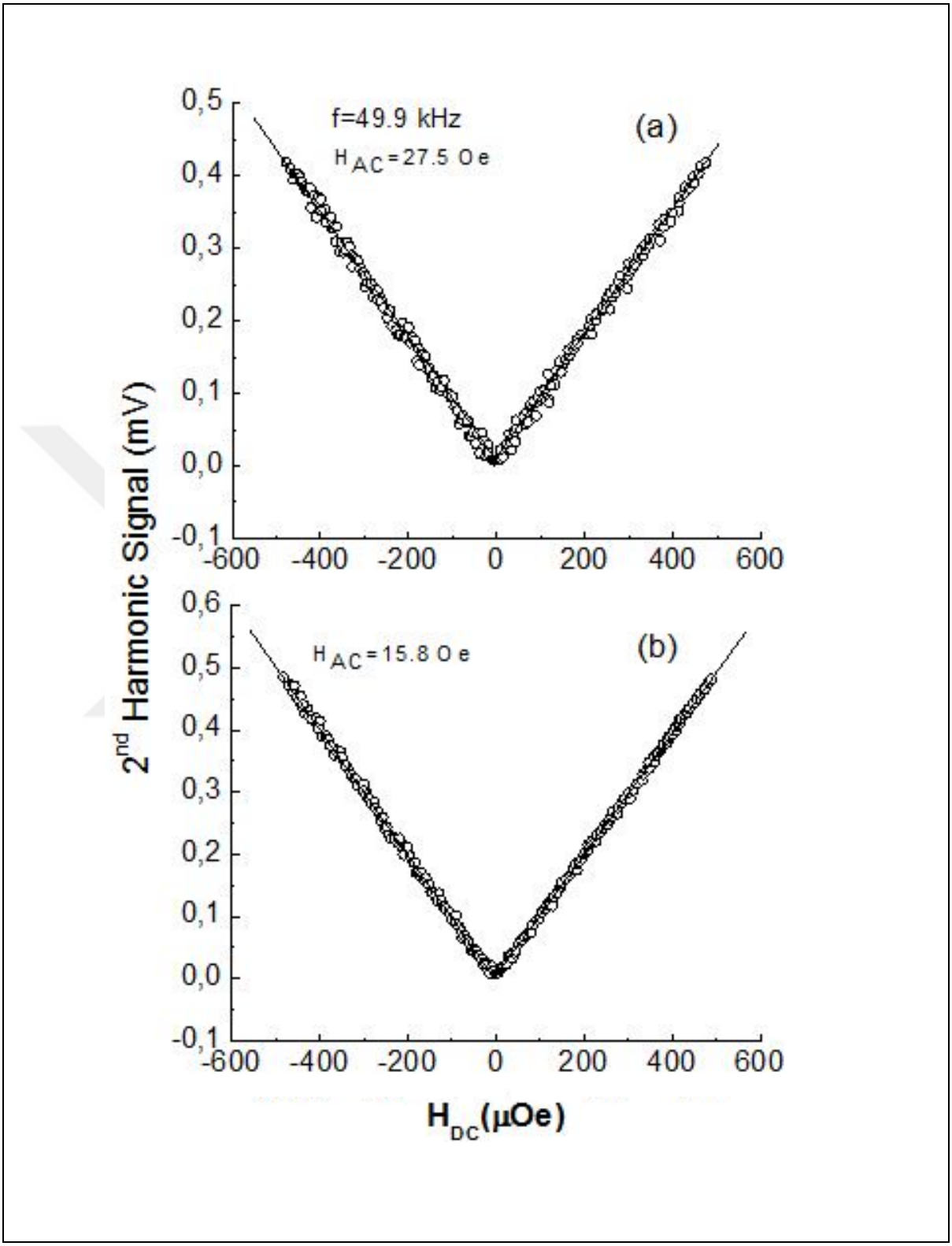

Figure 4.3. (a) and (b)Variation of the 2nd harmonic amplitude (V_{2f}) for the Bi-2223 specimen as afunction of applied DC field at 77 K [25].

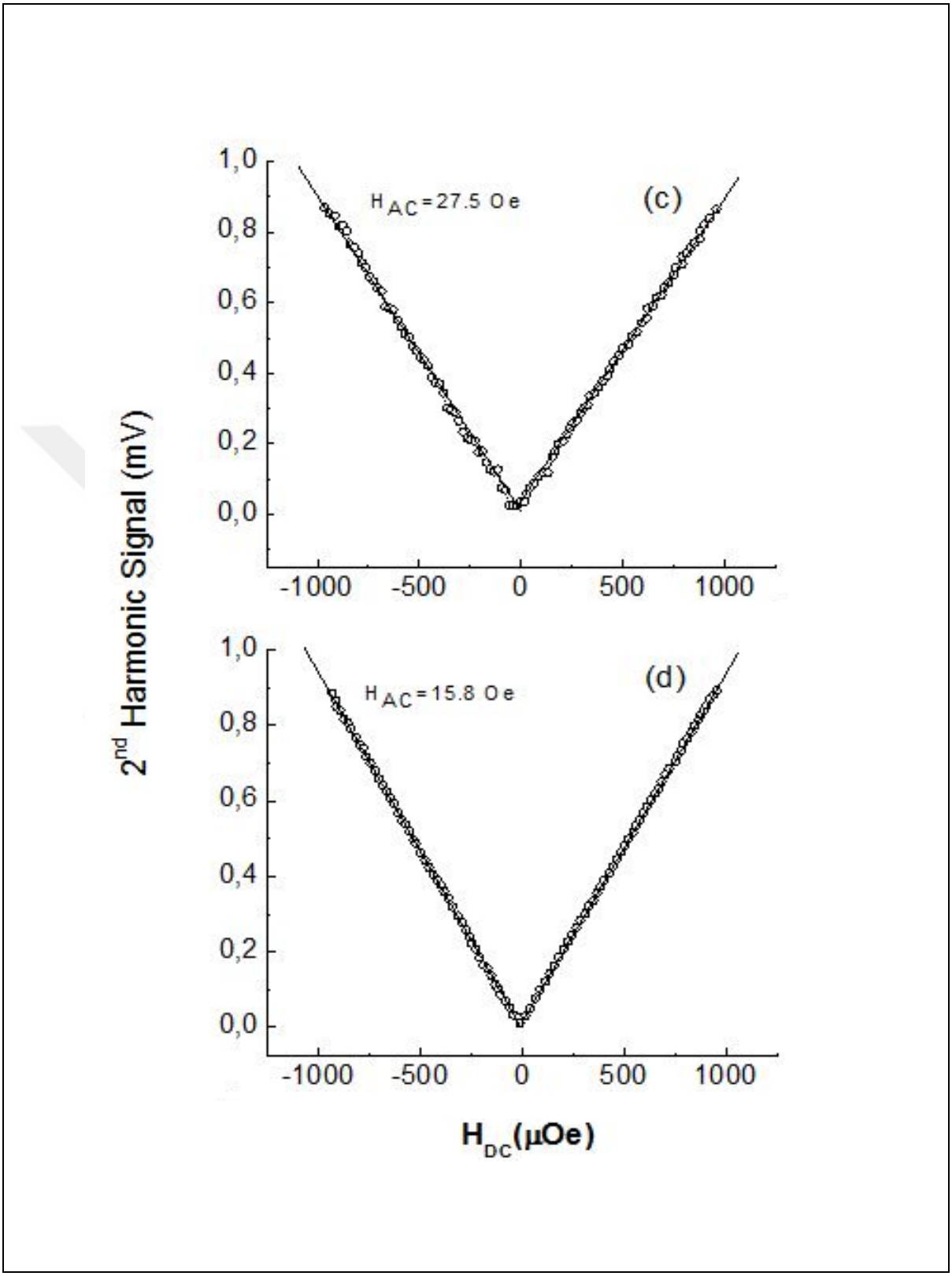

Figure 4.3. (c) and (d)Variation of the 2nd harmonic amplitude (V_{2f}) for the Bi-2223 specimen as a function of applied DC field at 77 K [25].

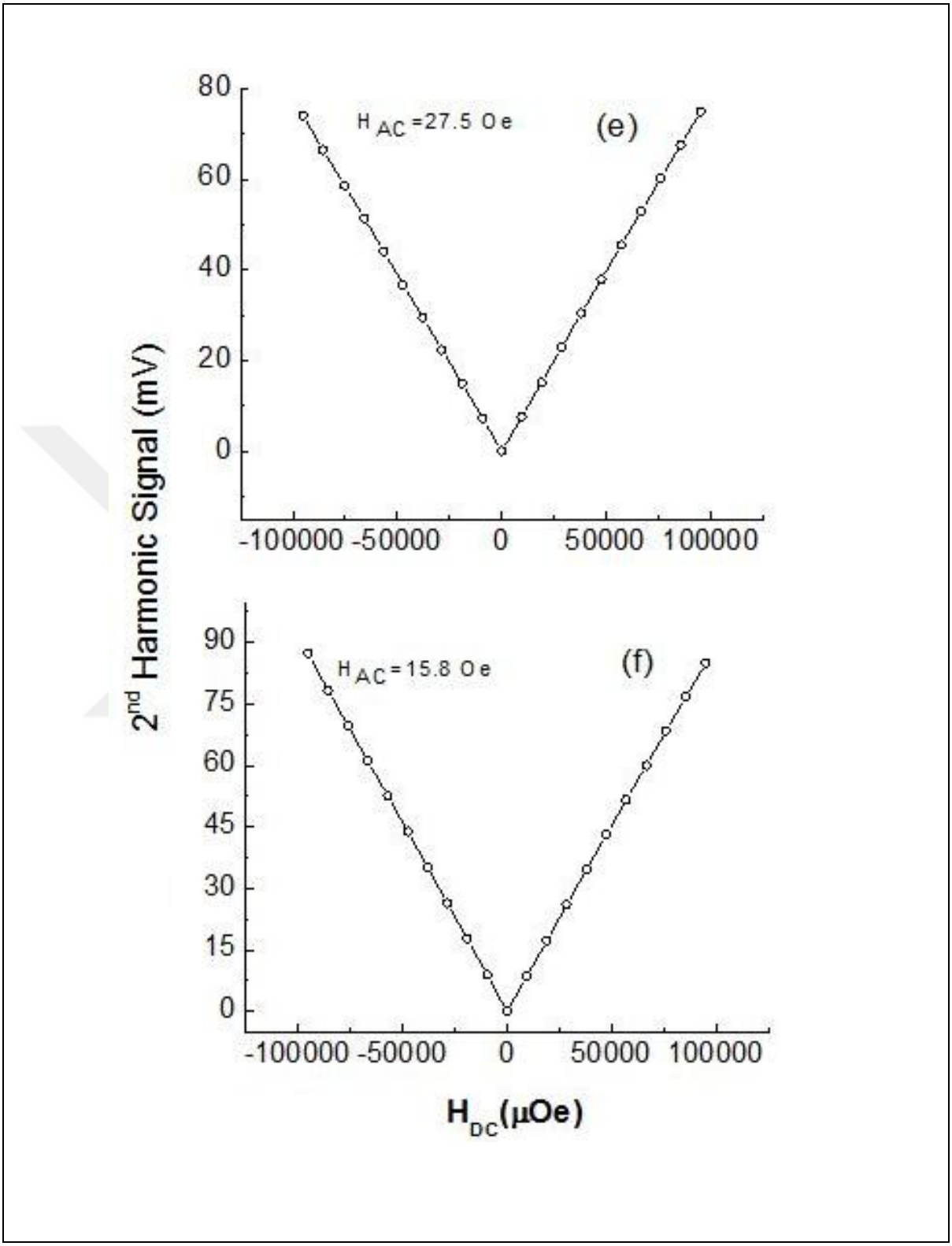

Figure 4.3. (e) and (f)Variation of the 2nd harmonic amplitude (V_{2f}) for the Bi-2223 specimen as afunction of applied DC field at 77 K [25].

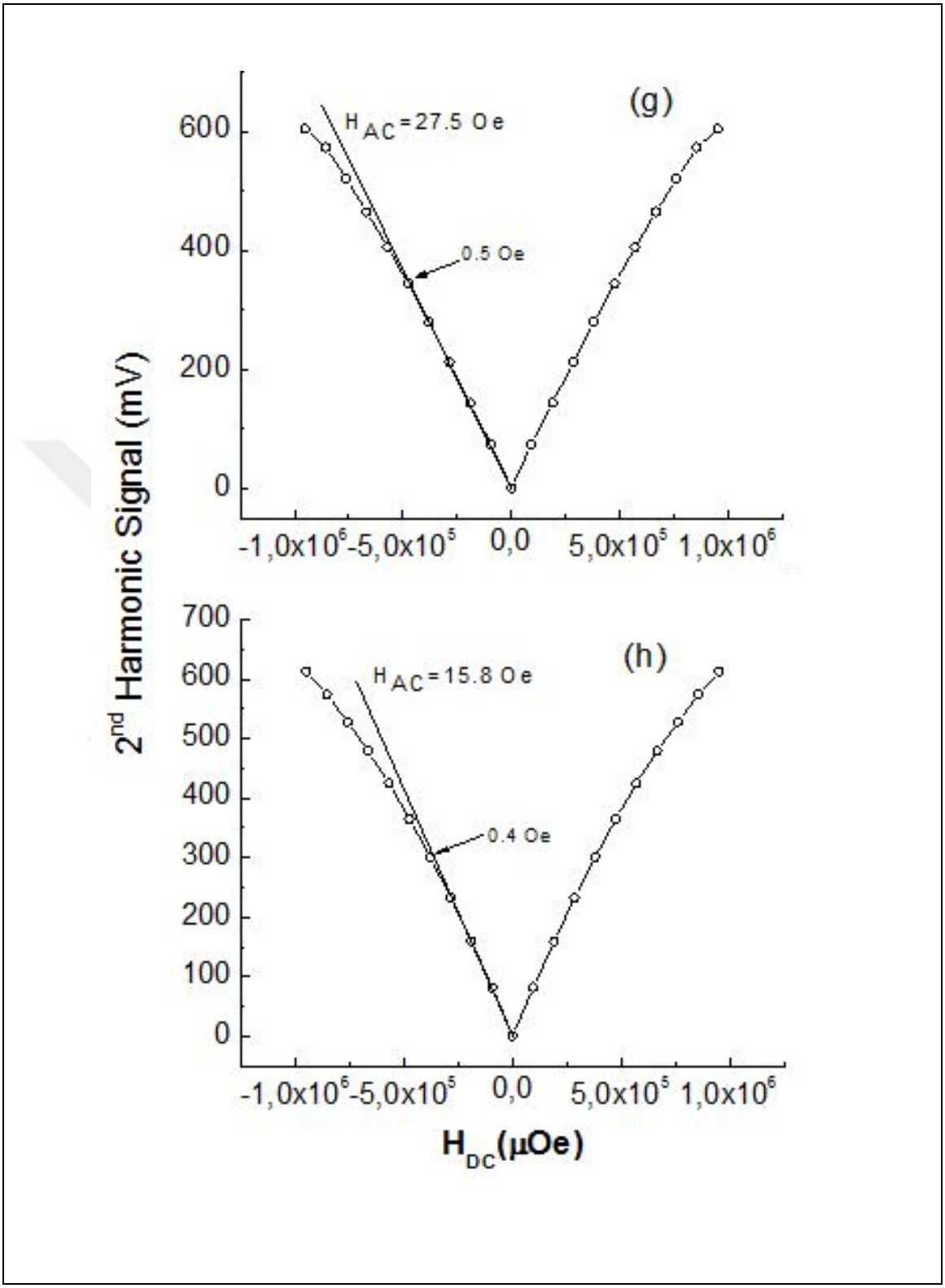

Figure 4.3. (g) and (h)Variation of the 2nd harmonic amplitude (V_{2f}) for the Bi-2223 specimen as afunction of applied DC field at 77 K [25].

In this particular part of this thesis, DC field sensing performance of polycrystalline Bi-2223 superconductors were analyzed by comparing the data with Y-123 superconductors and the theoretical models in literature. It was observed that the intensity of sensor signal (2^{nd} harmonic signal) is quite dependent on the superconducting properties of the core (H_{c1j}, H*, T_C, the trapped field, etc.) and not possible to make a general formula valid for all types of the superconducting cores. Instead, the optimal working conditions must be designated. The most important output of this study is sensing DC fields as low as 0.5 nT without requirement of any special electronics. It means the sensitivity can be further improved although it challenges to its competitors (like the fluxgates) even in the present form [25].

4.2. ZINC SAMPLES

4.2.1. Magnetic Measurements

The M-T and the M-H curves of Y-123 compounds as a function of Zn content are shown in Figures 4.4. and 4.5., respectively. It is seen that the superconducting transition temperature T_C (on) decreases significantly as the zinc concentration increases, which is in well agreement with the data published in [24] and attributed to the substitution of Zn atoms for Cu atoms in the CuO_2 planes. For $x = 0.05$, the T_C (on) decreases down to 70 K. The M-T data also reveal that the transition width increases with the increase of Zn content. Since large transition width indicates the presence of weak couplings between grains of ceramic superconductors (SC) [57,58], it will be correct to state that the strength of the links between grains becomes weaker with Zn addition, which also confirms the results of Ref. [24,26] and our mechanical measurements. As known the trapped field, which is the field remaining in SC specimen after the removal of the applied field, gives us information about the strength of the pinning force and proportional magnitude of the critical current density J_C. The trapped field at working temperature of 77 K was also determined from the M-T curves and found to be decreasing as Zn content increases. For instance, while the trapped field is ~4.0 % of applied field for Zn content of $x = 0.03$, it is determined to be 67.4 % for the undoped sample [26].

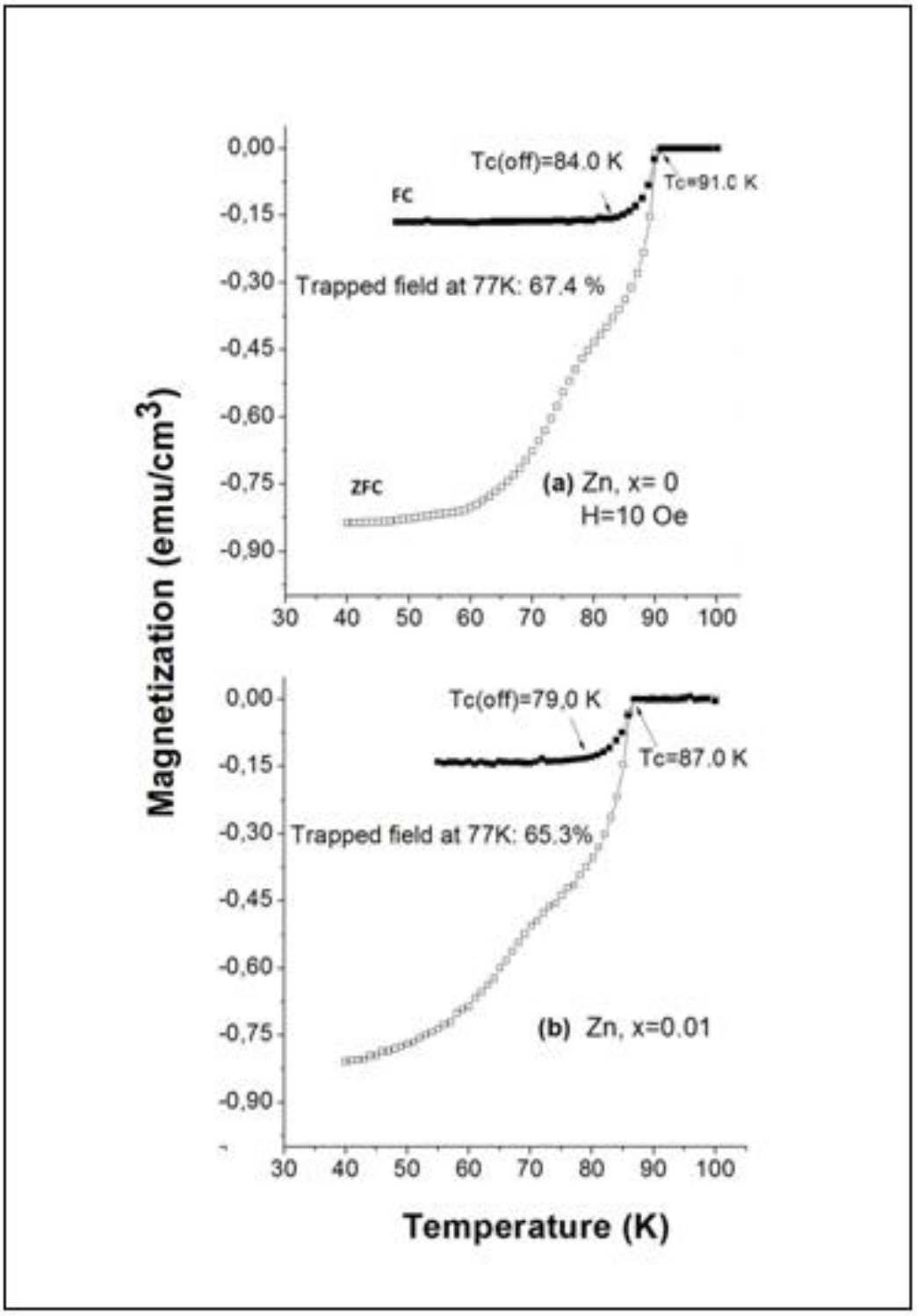

Figure 4.4. The M-T curves of the Zinc samples (a & b) [26].

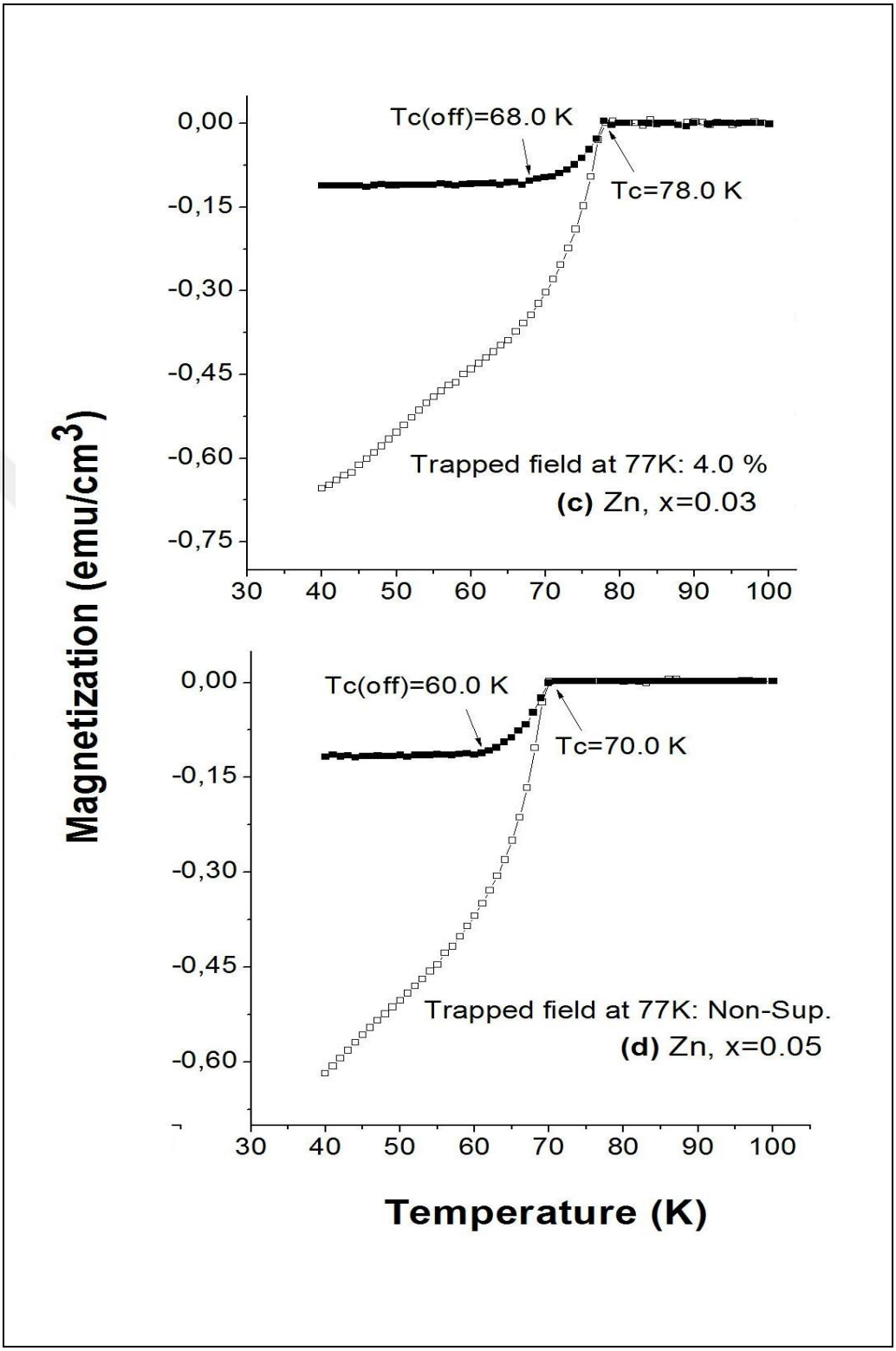

Figure 4.4. The M-T curves of the Zinc samples (c & d) [26].

The M-H curves at 77 K reveal that magnetic moment corresponding to superconductivity is apparent until the zinc concentration of $x = 0.03$, above which ferromagnetic like magnetization becomes visible and dominates the superconductivity. Here, we must note that the amplitude of the second harmonic signal is expressed to be $V_2 \sim \omega H_{DC} H^3_{AC} AN/J_c$ (where A is the effective area and N is the number of turns of the detection coil) [59, 61]. In this formula, the parameters other than the critical current density J_c, such as excitation frequency ω and excitation field amplitude H_{AC}, are not related to properties of the studied samples. However, the J_C is a characteristic parameter of the superconducting specimen and, as is well known, takes lower values for the granular samples having weakly coupled grains. With this reason, the Jc values were derived from the M-H loops by using the well known Bean model [17] and determined to be 290 A/cm^2, 220 A/cm^2 and 7 A/cm^2 at zero field for the undoped, $x = 0.01$ and $x = 0.03$, respectively. As is seen, the J_C decreases as the zinc concentration increases. This may also be ascribed to the weakening of the links between grains [26].

The reason of M-H measurements was also to extract some crucial parameters (H_{c1J}, H*, H_{DC}/H_{AC}) required for the determination of region where 2nd harmonic signal changes linearly with the DC-field, which is necessary for feasibility of the sensor. The insets of Figure 4.5. show the expanded 4th quadrant of the loops to determine intergrain first critical field H_{c1J} (i.e. the flux starts to penetrate SC specimen through grain boundaries above this field) and the minimum field required for penetration through the entire specimen H*. Magnetic field corresponding to first deviation from the linearity in initial magnetization curve was accepted to be H_{c1J}. Crossing point of initial magnetization curve with the M-H loop at fourth quadrant belongs to H*. With this approach, the H_{c1J} and H* are seen as decreasing sharply with the increase of Zn content. The H_{c1J} decreases from 8 Oe to less than 1 Oe in case the SC sample is doped with Zn of $x = 0.03$. Similarly, the H* falls to 5 Oe (from 65 Oe for the undoped one) with the same concentration of zinc [26].

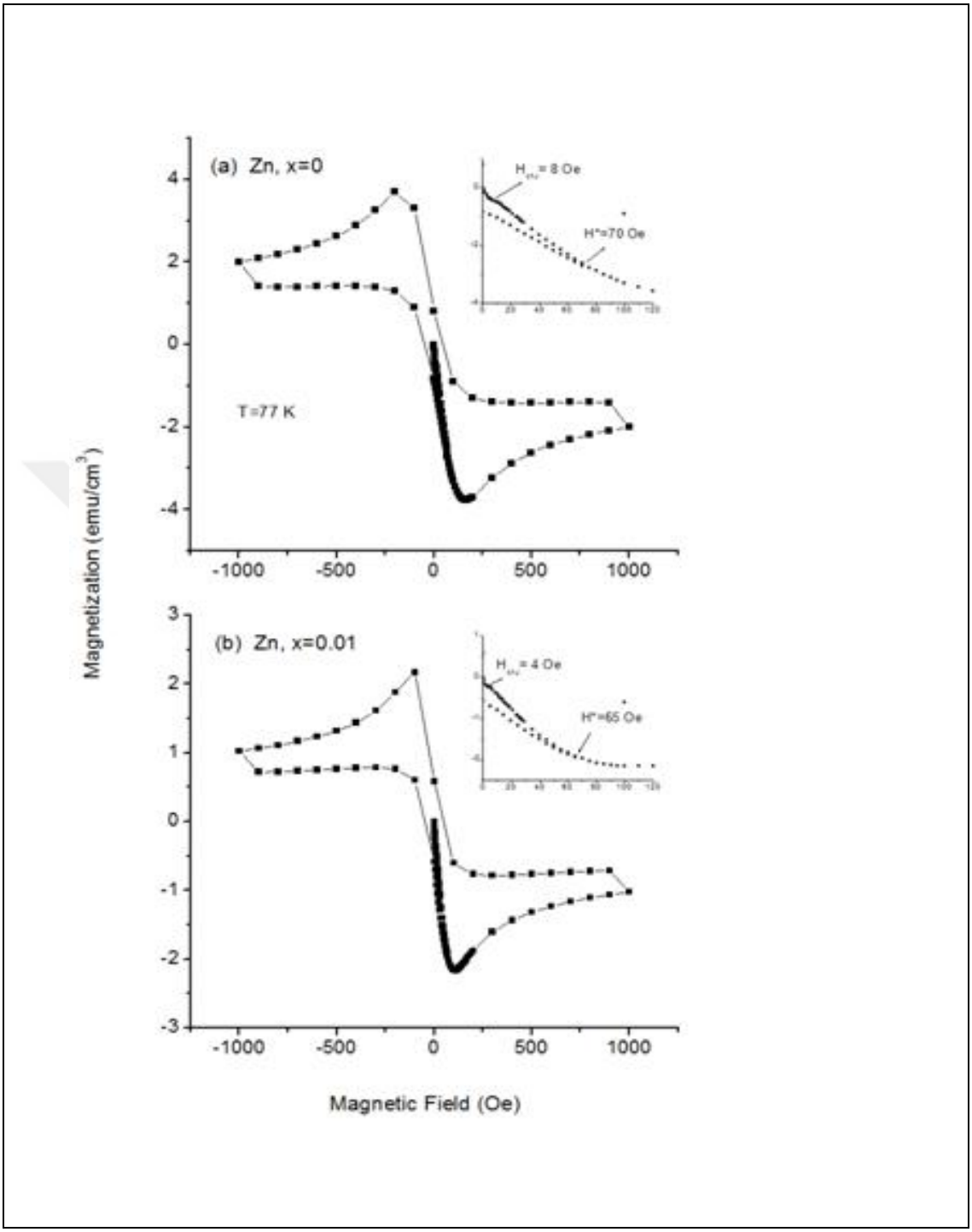

Figure 4.5. The M-H loops of the Zinc samples (a & b) [26].

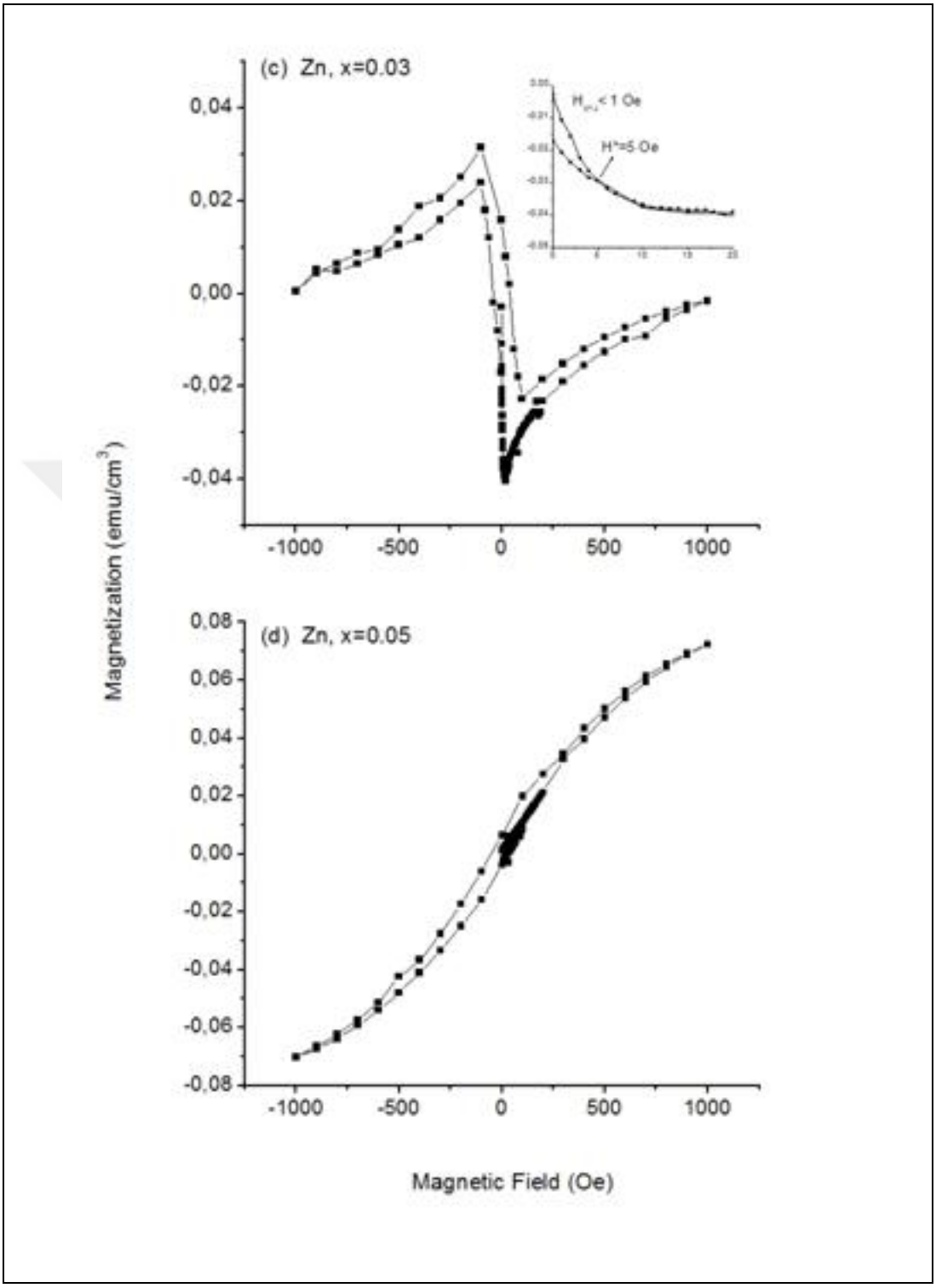

Figure 4.5. The M-H loops of the Zinc samples (c & d) [26].

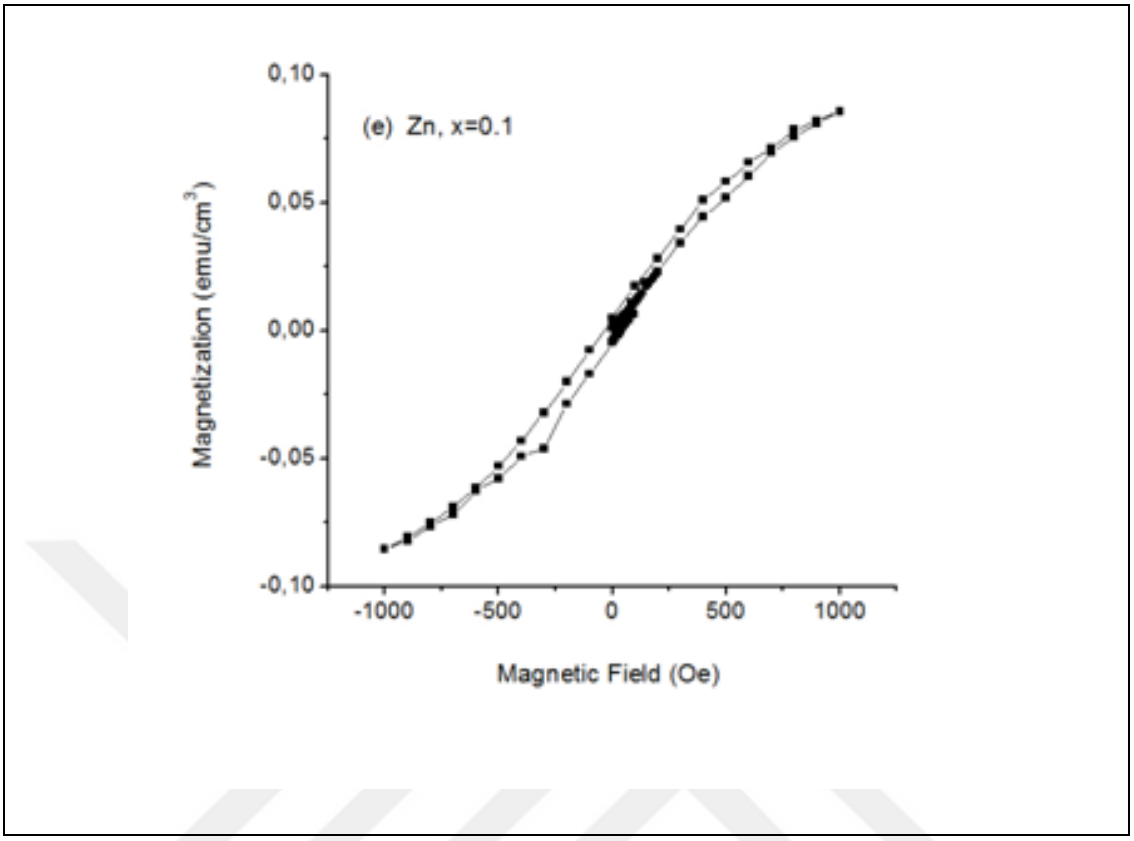

Figure 4.5. The M-H loops of the Zinc samples (e) [26].

4.2.2. The 2nd Harmonic Measurements

As mentioned before, the magnitude of the harmonic signal is expected to be linearly proportional to the frequency ω and H^3_{AC}/H^* if the amplitude of the AC field H_{AC} is larger than H_{c1J} (where $H^* \sim J_c$). On the other hand, some studies in literature have shown that there are optimal values for both of the parameters since, as is known in electronics, such optimal values show variations depending on the coil design [26, 62]. In order to define optimal frequency, a sinusoidal signal was driven to excitation coil by using an ultra low distortion function generator up to a frequency of 200 kHz. The signal amplitude H_{AC} was kept constant at 13.13 Oe. A DC-field of 0.0144 Oe, which is required for the generation of second harmonic signal, was applied by a calibrated solenoid and the signal induced on detection coil at frequency of 2*f* was monitored by a lock-in amplifier. Figure 4.6.(a) shows the 2nd harmonic signal vs. frequency curve of $YBa_2Cu_3O_7$ superconductors with different amounts of Zn atoms. Here, we must note that the measurements were carried out at liquid

nitrogen temperature. It is seen that the optimal frequency changes depending on the studied sample since all measurements were realized under the same conditions. While it is at 50 kHz for the undoped and $x = 0.01$, it is at 40 kHz for $x = 0.02$ and 0.03. It is also interesting that the signal amplitude initially showsslight increment with Zn doping for $x = 0.01$, but then decreases sharply above this concentration. Optimal AC-field analysis were done at a frequency of 49.9 kHz with AC field amplitude between 2.9 Oe and 27.5 Oe (maximum applicable field) and are shown in Figure 4.6.(b). As it is seen, the signal strength increases proportionally with an AC field amplitude except for the sample doped with Zn atoms of $x = 0.03$, on which optimal AC field amplitude was determined to be 10.2 Oe [26].

Figure 4.7. shows the variation of the second harmonic signal amplitude as a function of DC-field at 77 K and for different scales. The data were gathered for AC fields with amplitudes of 16.2 and 27.3Oe and at a frequency of 49.9 kHz ($n = 1$). The strength of the 2nd harmonic signal is larger for higher AC field amplitudes, but not changes linearly with H^3_{AC} as stated in the second harmonic formula given above. Besides, the experiments realized in high amplitude of AC-field reveal better sensitivity to DC-field (see Figures 4.7.(a) and 4.7.(b)). These experiments have shown that the highest signal strength was observed in the Zn-doped sample with $x = 0.01$. However, further increase of Zn concentration adversely affect the signal strength, which takes values more than one-tenth of the sample with $x = 0.01$ for the sample with $x = 0.03$. The data of the Zn-doped sample with $x = 0.01$ seem also less noisy, especially at high AC fields, compared to the others. Experiments with DC-field steps of 0.5 nT(Figures 4.7.(a)-(b)) and 2 nT (Figures 4.7.(c)-(d)) reveal that 2 nT can be detected by using the sample with Zn content of $x = 0.01$ [26].

Similar to our experimental results seen on H_{AC} dependence of V_2, the J_c dependence of 2nd harmonic signal also departs from the proposed relation of $V_2 \sim \omega H_{DC} H_{3AC} AN/J_c$. If we accept that this formula is correct, then the sample with low J_c (it is the Zn-doped sample with $x = 0.03$ in the present case) must result in higher signal strength. As a result, it seems to be incorrect to make such a generalization [26].

To determine the dynamic range of the sensor, the experiments were also realized at large DC-field intervals (Figures 4.7.(e)-(h)). The deviation from the linearity was accepted to

be the upper limit of the sensor (marked with arrows in the Figure 4.7.). The upper limits are 0.38 Oe, 0.57 Oe, 0.91 Oe and 1.06 Oe for the $x = 0.01$, the undoped, $x = 0.02$ and $x = 0.03$, respectively. The maximum values of the H_{DC}/H_{AC} ratios, above which the nonlinearity on DC-field dependence of 2nd harmonic signal is observed, were determined to be 0.014, 0.021, 0.033 and 0.038 for the same order of the samples. As it is seen, the most sensitive one to DC fields has a smaller the upper limit. So, it provides us with the opportunity to choose the desired dynamical range depending on our usage purpose. Besides, the transfer functions (dV/dB) were determined to be 7590 V/T, 5940 V/T, 3450 V/T and 350 V/T for the $x = 0.01$, the undoped, $x = 0.02$ and $x = 0.03$, respectively. It means that much lower DC fields can be detected if the noises coming from the external factors, such as; the coil, the core geometry and the main line, are suppressed [26].

In this work, the effect of weak links between the grains of YBaCuO ceramics on the strength of 2nd harmonic signal was examined. Contrary to the expectations of literature, there is no direct relationship between the signal strength and the weak links. Experiments carried out on a series of Zn-doped YBaCuO samples, where the J_C values were observed to be decreasing with the increase of zinc concentration, have shown that the highest 2*f* signal corresponds to at least the Zn-doped sample ($YBa_2Cu_{2.99}Zn_{0.01}O_{7-y}$). The 2 nT DC-field could be detected by using this SC specimen as the sensing core. On the other hand, the upper limit takes lower values compared to the less sensitive one [26].

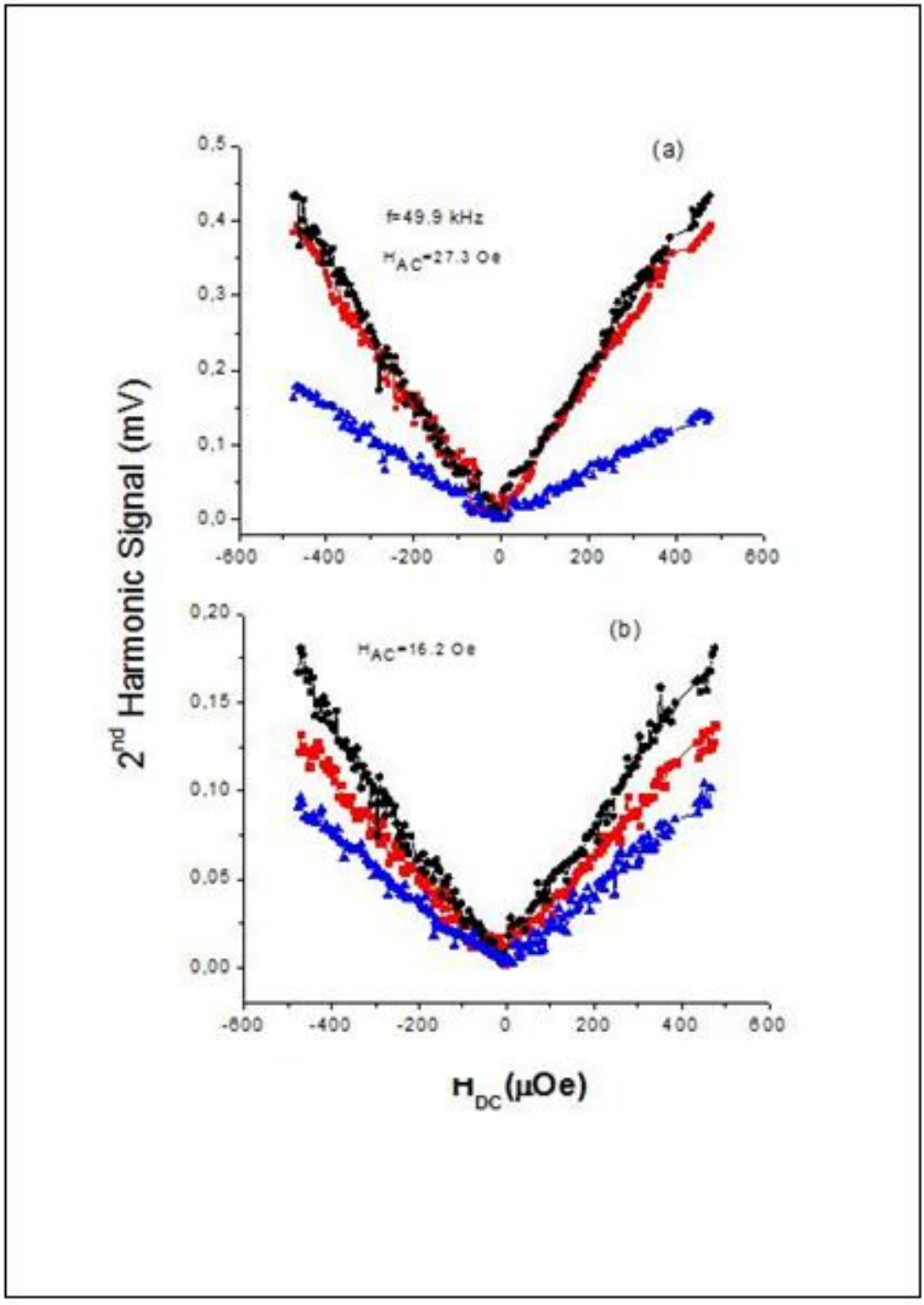

Figure 4.7. 2nd Harmonic Signal to DC Field (a & b) [26].

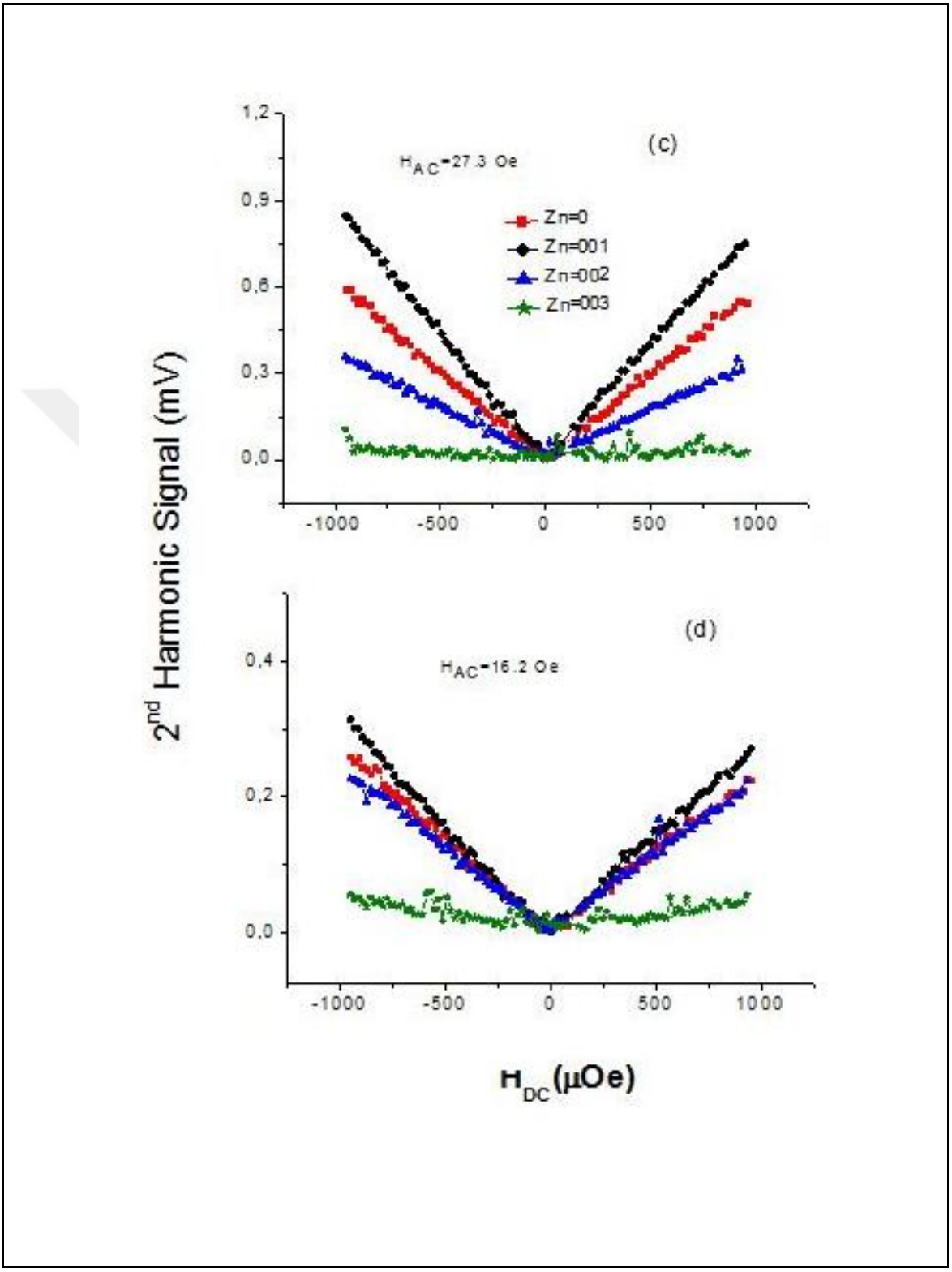

Figure 4.7. 2nd Harmonic Signal to DC Field (c & d) [26].

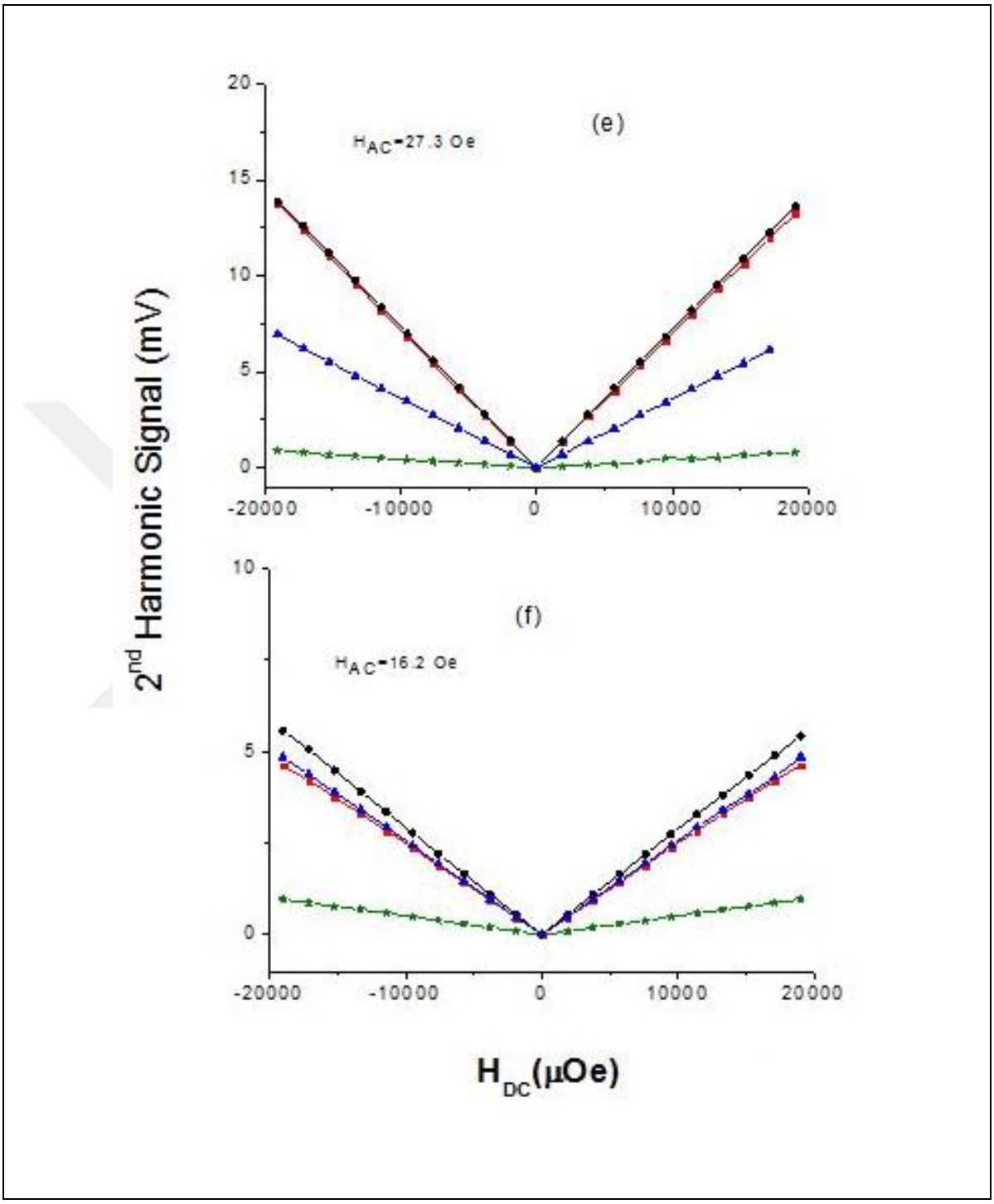

Figure 4.7. 2nd Harmonic Signal to DC Field (e & f) [26].

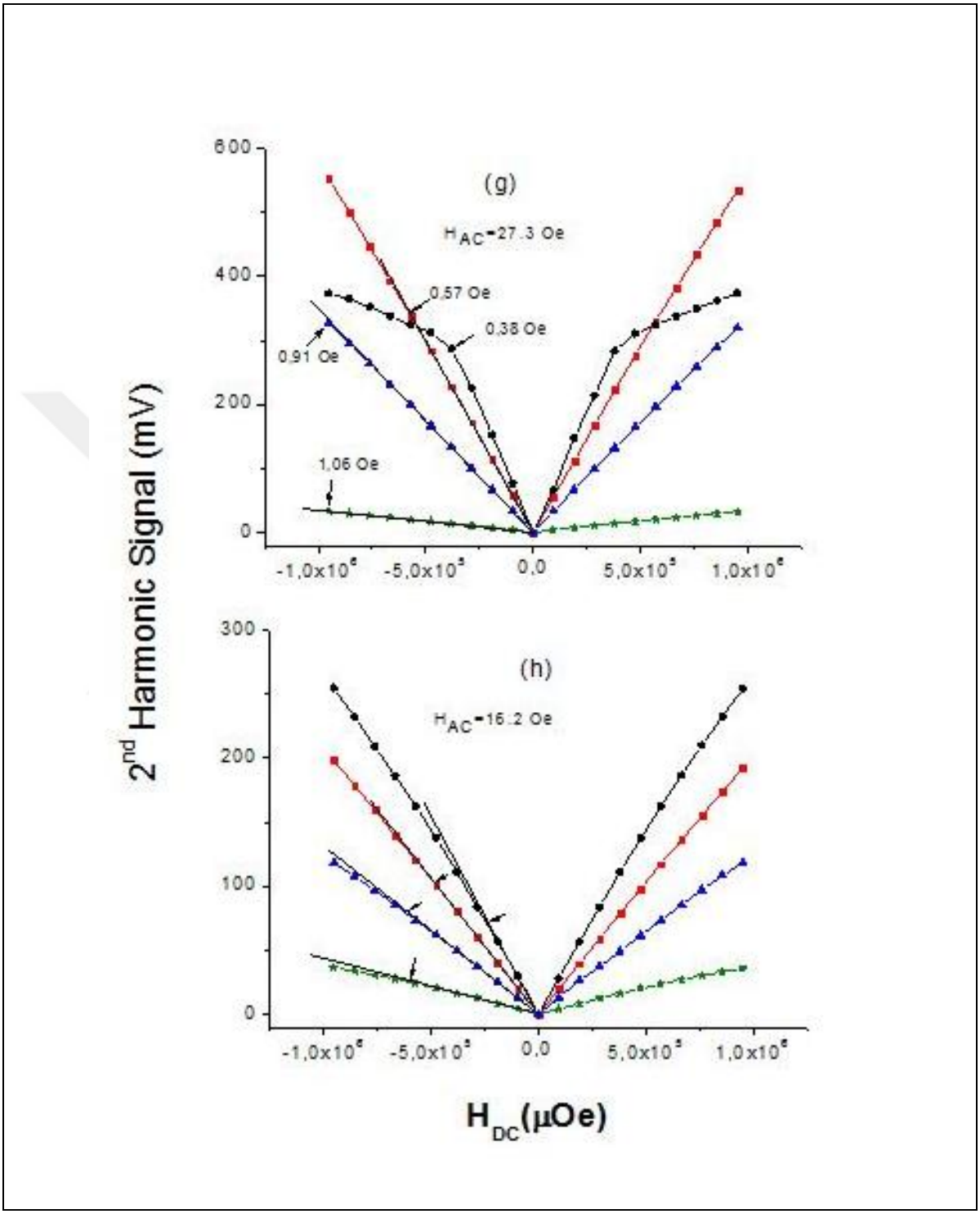

Figure 4.7. 2nd Harmonic Signal to DC Field (g & h) [26].

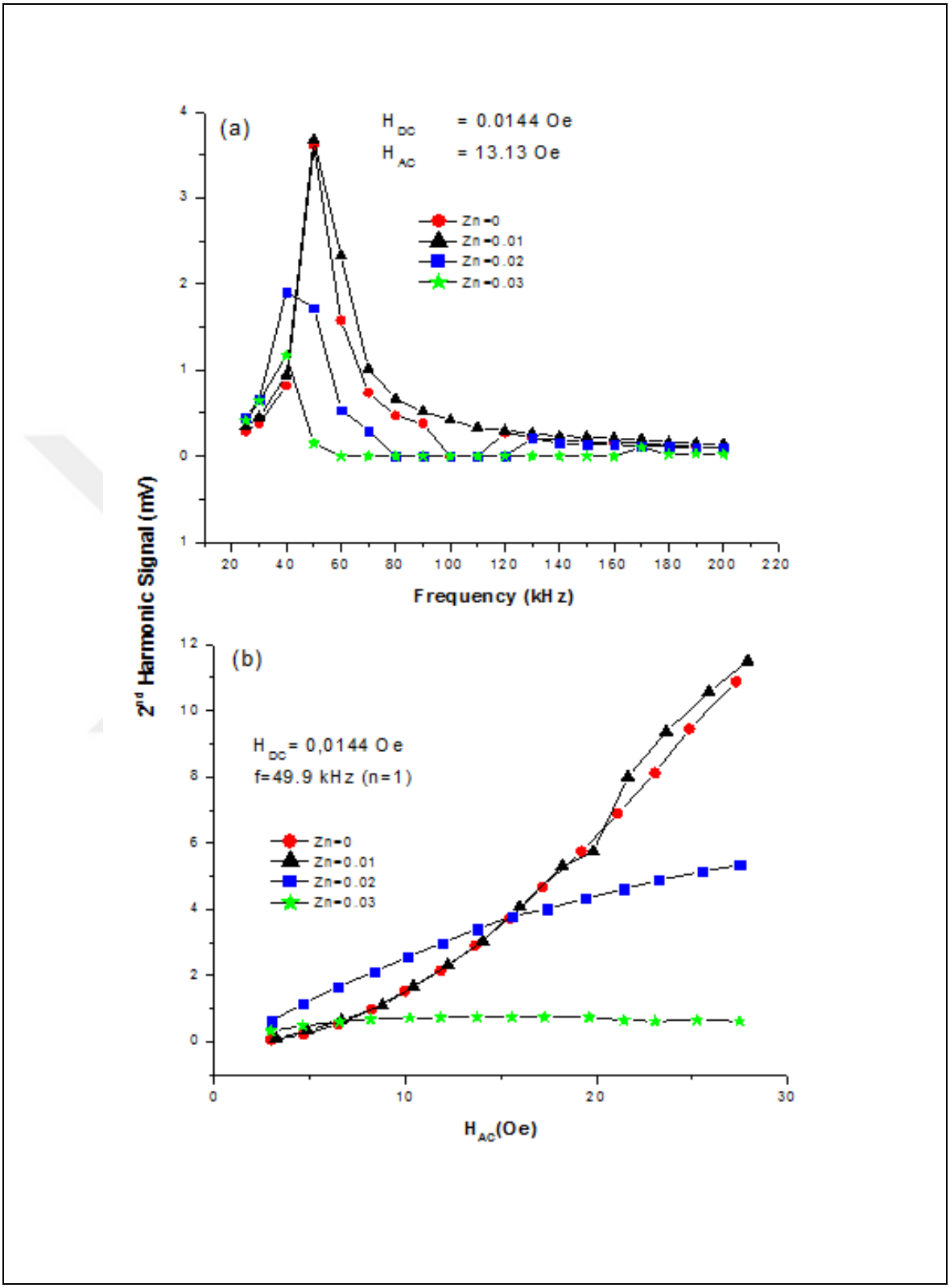

Figure 4.8. Optimal frequency and optimal H_{AC} graphs [26].

4.3. BORON SAMPLES

4.3.1. Mechanical Measurements

Figure 4.9. (a) and (b) shows the indentation hardness (H) and reduced modulus (Er) of the samples obtained under different loads. Both E_r and H values are nearly constant with increasing applied load, which means that the mechanical properties are independent from applied loads. As it is seen from the figures that, firstly, the H and E_r values of undoped sample dramatically increase with the minor doping levels ($x = 0.05$ and 0.1) and then decrease with increasing doping level. The increase in hardness with increasing doping level was attributed to solid-solution hardening, while the reduction of hardness was ascribed in terms of decrease in the packing forces between superconducting grains. Moreover, a possible phase transformation by B doping can be another reason for this behaviour. YBCO undergoes a structure phase transition from orthorhombic to tetragonal between the doping level of 0.33 and 0.50. Accordingly, the dramatic increase in H and E observed in this study can be related to phase transformation [28].

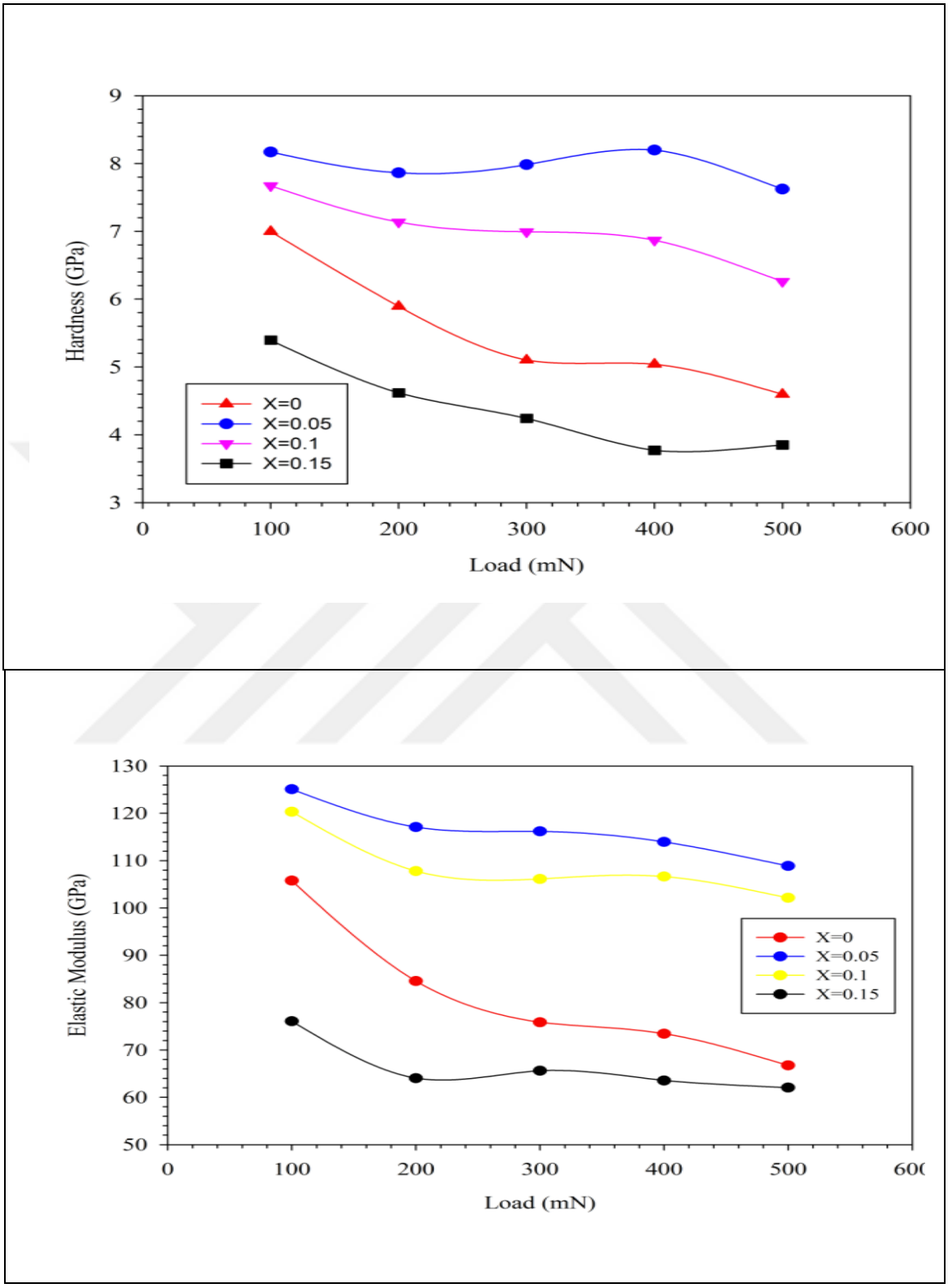

Figure 4.9. (a) Typical load-unloading curves for B doped and undoped polycrystalline YBaCuO samples, (b) Variations of the hardness and elastic modulus with the applied load for B doped and undoped polycrystalline YBaCuO samples [28].

4.3.2. Magnetic Measurements

The difference between values of the ZFC and the FC curves at certain temperatures (i.e. ΔM at 77 K) is proportional to the trapped field or the pinning force of the studied samples. If the difference is large it indicates a high pinning force and a high critical current density [28].

The M-T curves of Y-123 samples with the addition of boron concentration are shown in Figure 4.10. ΔM values at 77 K were determined to be 0.28, 0.33, 0.24 and 0.21 emu / cm^3 for $x = 0$, 0.05, 0.1 and 0.15 respectively. Therefore, the highest J_C and the greater grain coupling will be seen on the sample doped with 0.05 wt% B_2O_3. According to the figure, the transition widths determined to be 17, 25, 29, 20 K for $x = 0.0$, 0.05, 0.1, 0.15 wt% B_2O_3 doped samples respectively. As is known from literature, the transition width is inversely proportional to J_c, which means that if the transition width is large then J_c is small. As a result, the large transition width shows weak links. Therefore, for our results we can say that the transition width gets larger with the addition of B_2O_3, suggesting the presence of weak links between grains of ceramic superconductors (SC) [7,28], which will state that the strength of the links gets weaker [41].

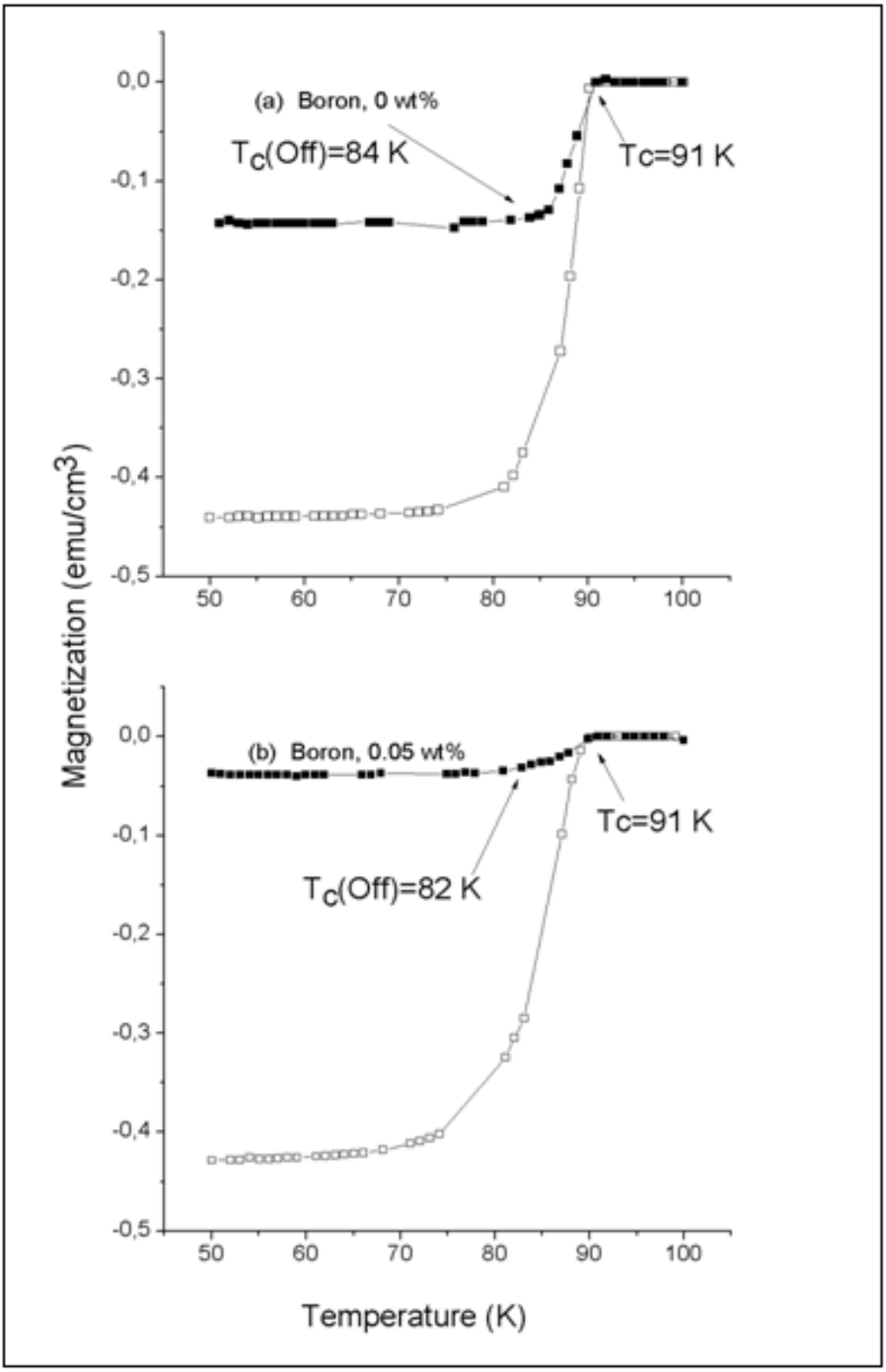

Figure 4.10. (a & b) The M-T curves of Y-123 compounds as a function of B content [28].

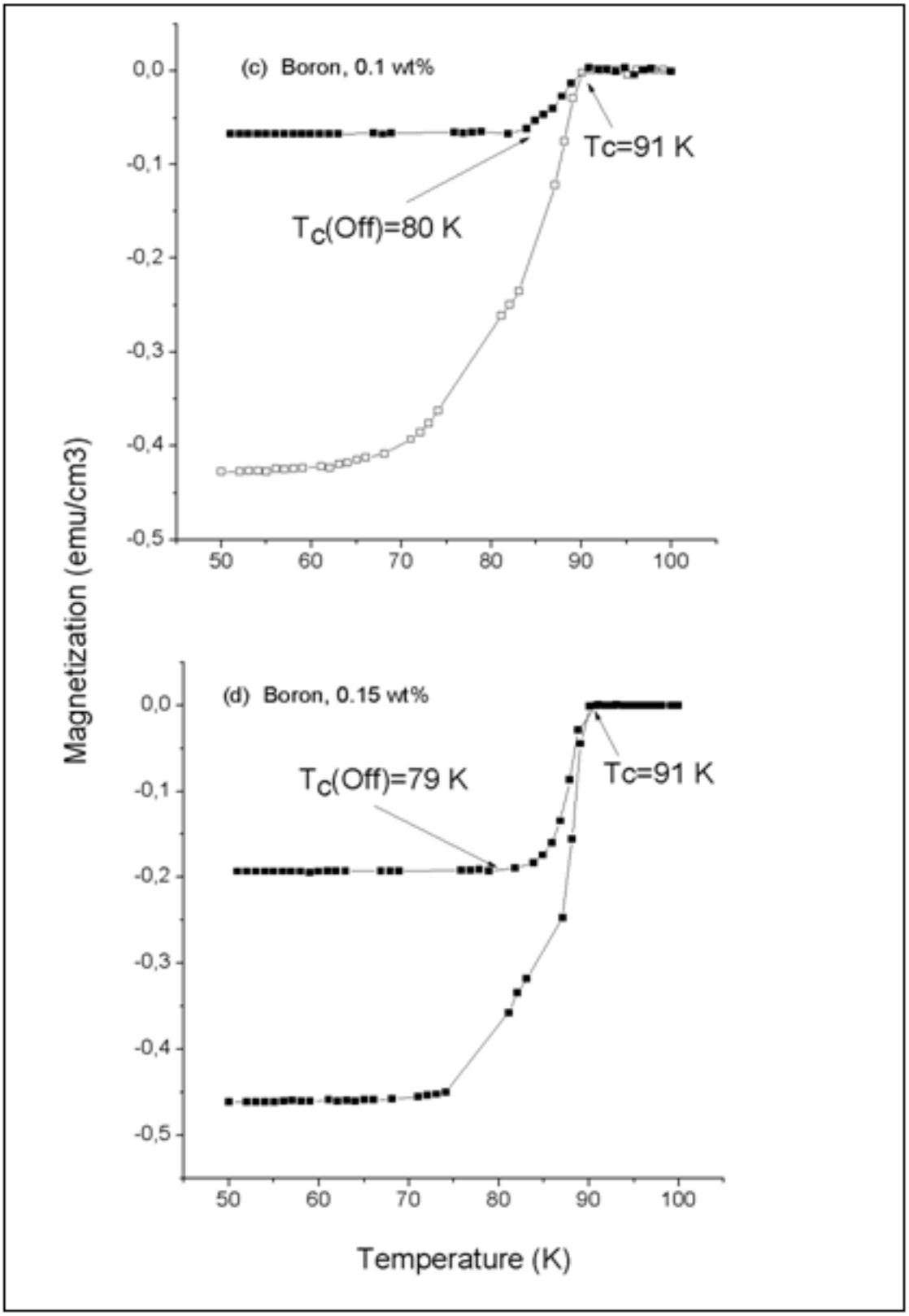

Figure 4.10. (c & d) The M-T curves of Y-123 compounds as a function of B content [28].

As is seen in Figure 4.11, the H_{c1J} and the H* values in our samples decrease with increase of boron concentration. The H* values decrease down to 50 Oe for the B doped sample with $x = 0.1$ and $x = 0.15$. Using these values and adjusting the amplitudes of H_{DC} and H_{AC}, the dynamical range of magnetometer can be controlled depending on the application area. From literature the strength of the 2nd harmonic signal is inversely proportional to the critical current density, Jc($V_2 \propto 1/J_C$) asserted by most authors [24]. The J_C values were derived from the M–H loops by using the Bean model [17] to check its relation with the 2nd harmonic signal. The values obtained at 77 K in A/cm^2 unit are, 650, 400, 360, and 545 for the samples with x: 0.00, 0.05, 0.1 and 0.15 respectively. These data show that Jc values decrease with an increase in B concentration. Consequently, the highest second harmonic signal is expected for the B doped sample with $x = 0.15$. On the other hand, the highest signal was observed for the sample with $x = 0.1$ [28].

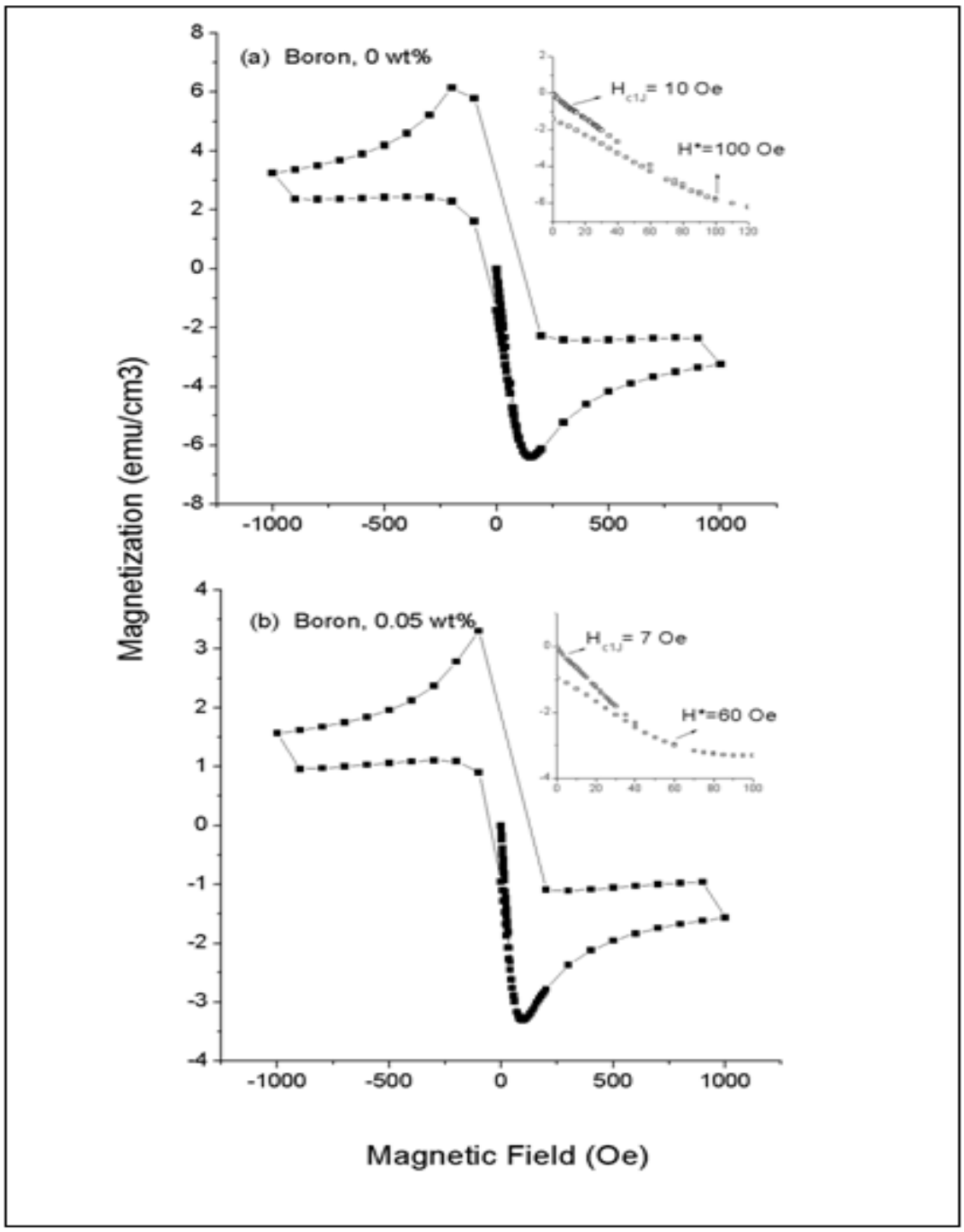

Figure 4.11. (a & b) The M-H curves of Y-123 compounds as a function of B content at 77 K with maximum field of 1000 Oe. Insets: The magnification of the 4th quadrant of the loops [28].

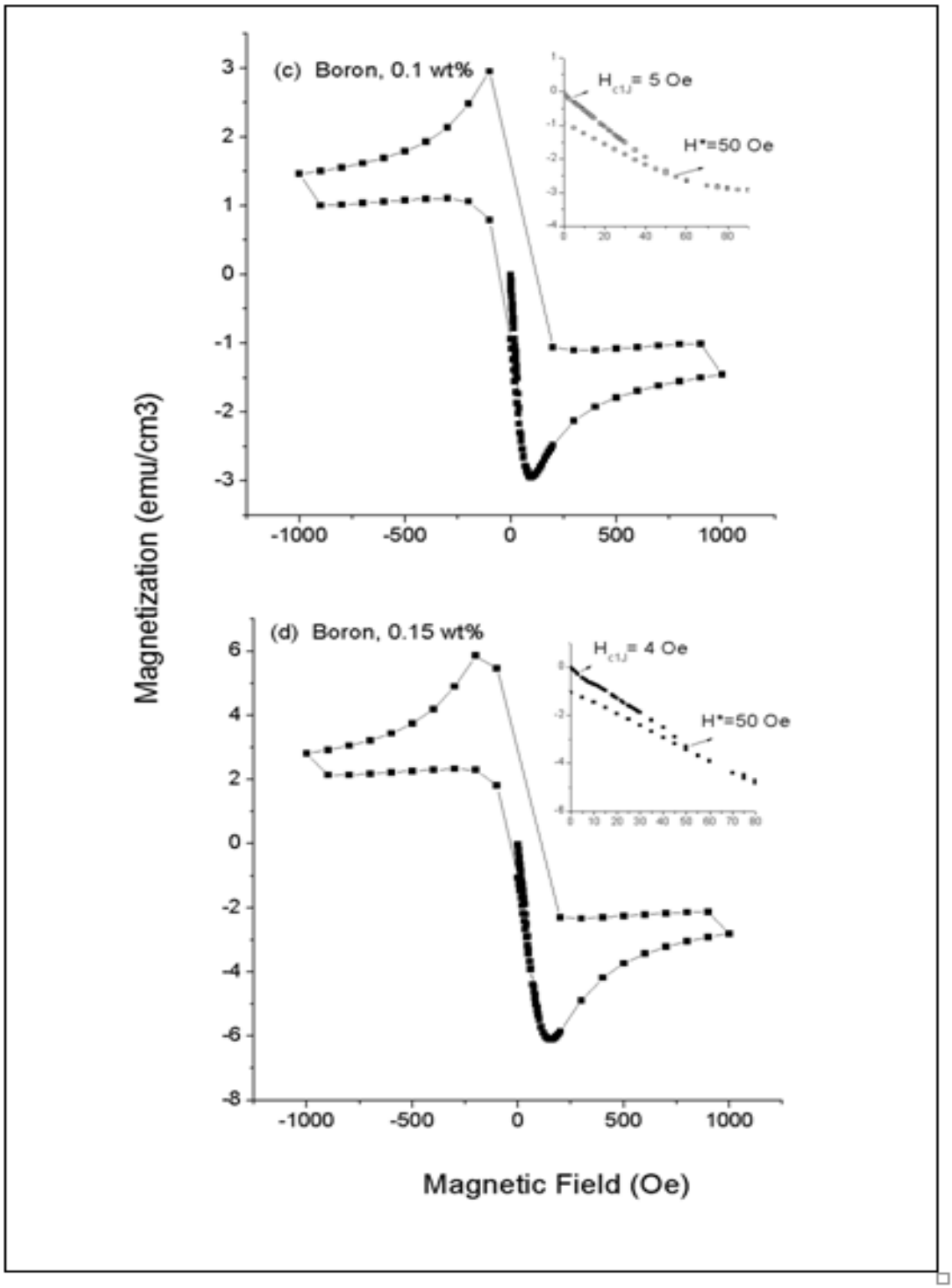

Figure 4.11. (c & d) The M-H curves of Y-123 compounds as a function of B content at 77 K with maximum field of 1000 Oe. Insets: The magnification of the 4th quadrant of the loops [28].

The optimal frequency and optimal H_{AC} were calculated from the computer measurements. The graphs related to those measurements are given in Figures 4.12. (a) and (b). According to the graphs the optimal frequency is 76 kHz and the optimal amplitude is 36 Oe rms.

Besides, the transfer functions (dV/dB) of the sensors were determined from the slope of linear fit data. Those are 3300, 7400, 9600 and 4100 V/T for the samples $x = 0.00$, 0.05, 0.1 and 0.15 wt% B_2O_3 respectively. The J_C dependence of 2nd harmonic signal is in good aggreement with the recommended relation of $V_2 \sim \omega H_{DC} H^3_{AC} AN/J_c$. For instance, the B-doped sample with lowest J_C ($x = 0.1$ in present case) has the highest $2f$ signal. Similarly the sample with the highest J_C ($x = 0$) has the lowest $2f$ signal [28].

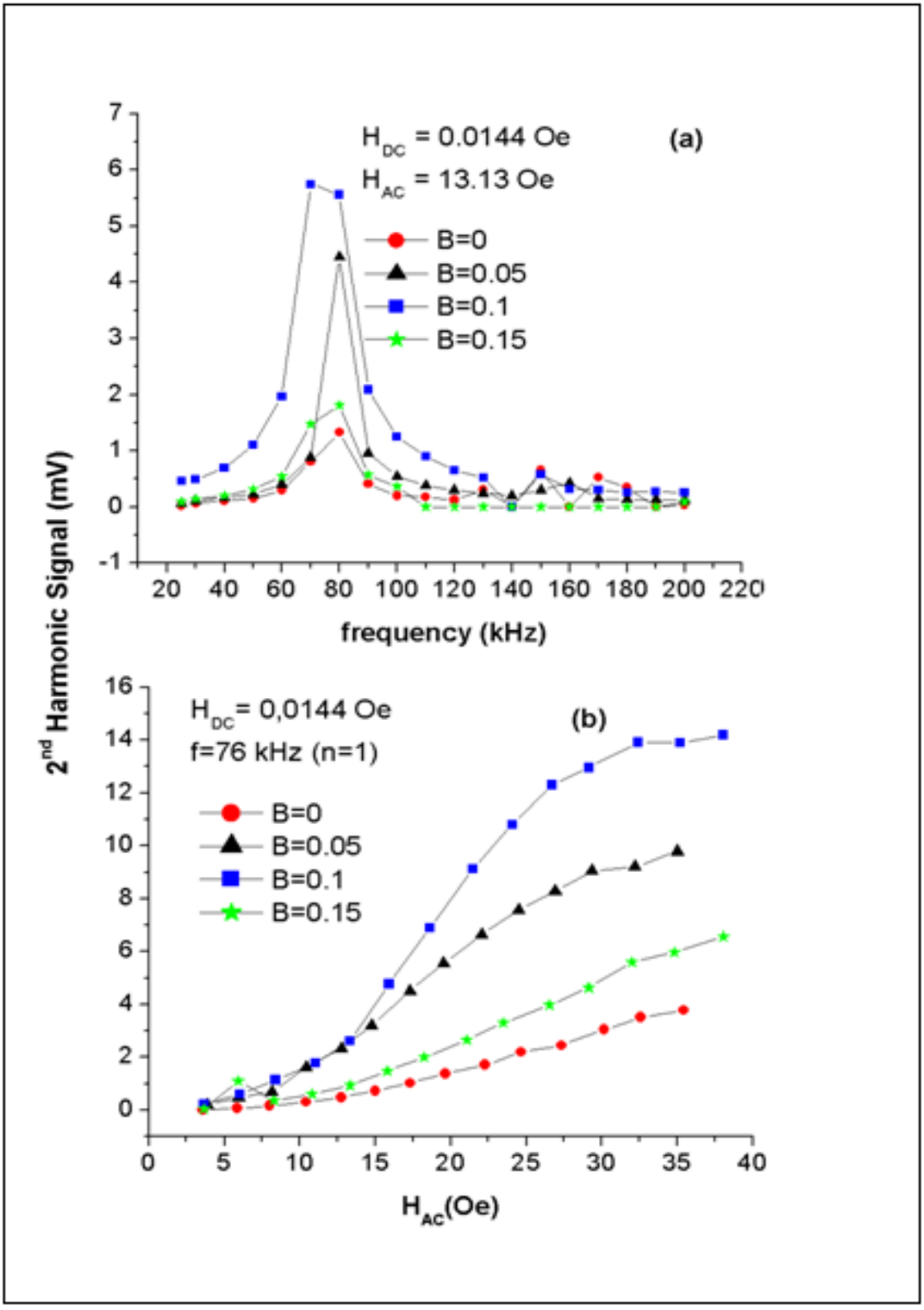

Figure 4.12. (a) & (b) Optimal Frequency and Optimal H_{AC} Graphs [28].

We have also determined the upper limit of present sensors from the experiments done at large DC interval (Figure 4.13.). The deviation from the linearity was accepted to be the upper limit of the sensor. The upper limits are 0.49, 0.48, 0.47 and 0.75 Oe for the samples $x = 0.00$, 0.05, 0.1 and 0.15 wt% B_2O_3 respectively. As seen all these values are almost larger than that of the Earth's field. So, these sensors may be used for long term Earth field analyses, like magnetotelluric applications.

As a result this thesis shows that boron addition has a role in getting transition width larger which is inversely proportional to J_c and that means grains between SC will get weaker (weak links occur). Secondly, for this thesis it can be said that the second harmonic signal increases till 0.15 wt% B_2O_3 after these data begin to get lower because the J_c gets higher [28].

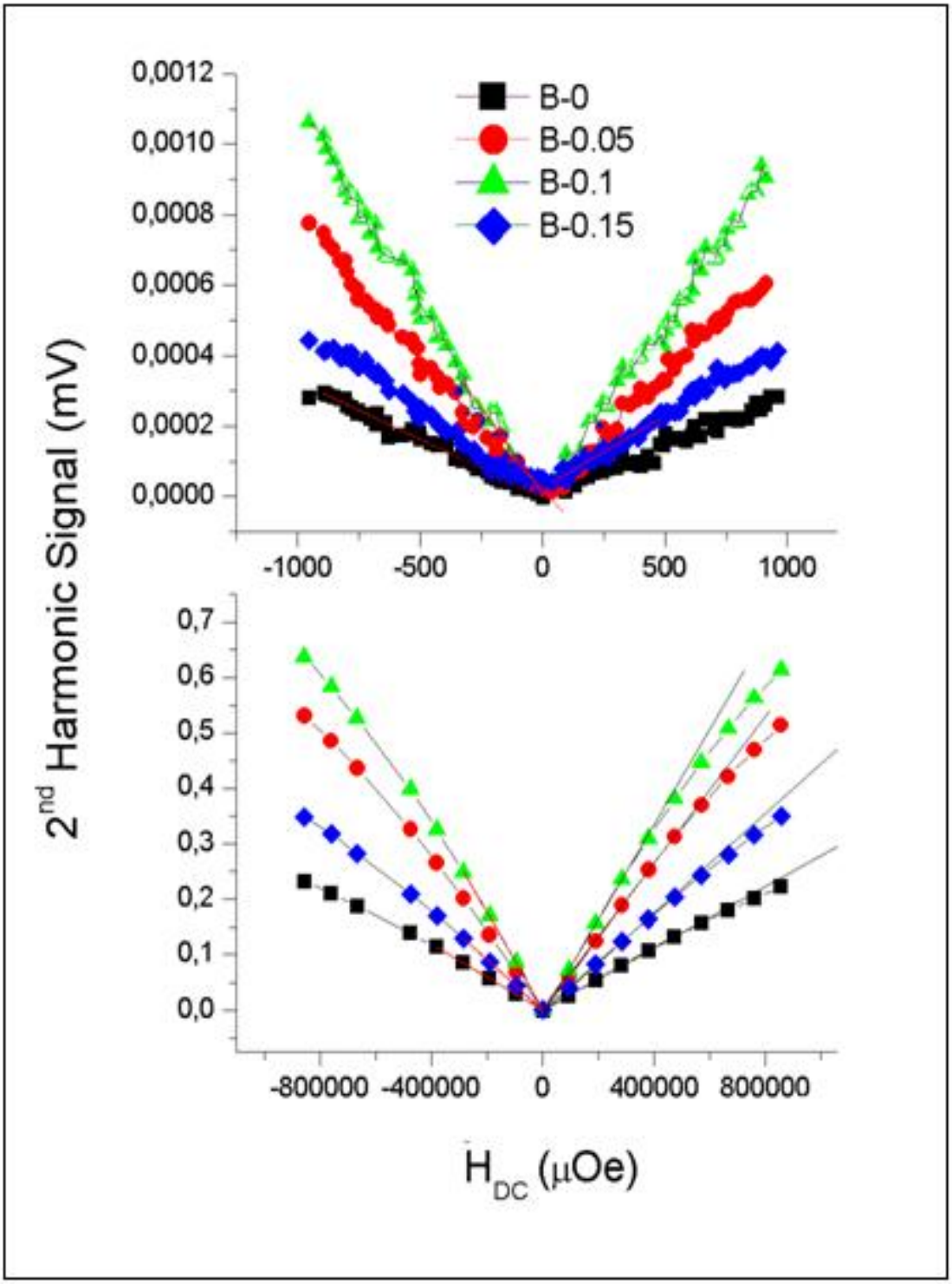

Figure 4.13. (a) Variation of the 2nd harmonic signal on YBCO pellets as a function of the applied DC field [28].

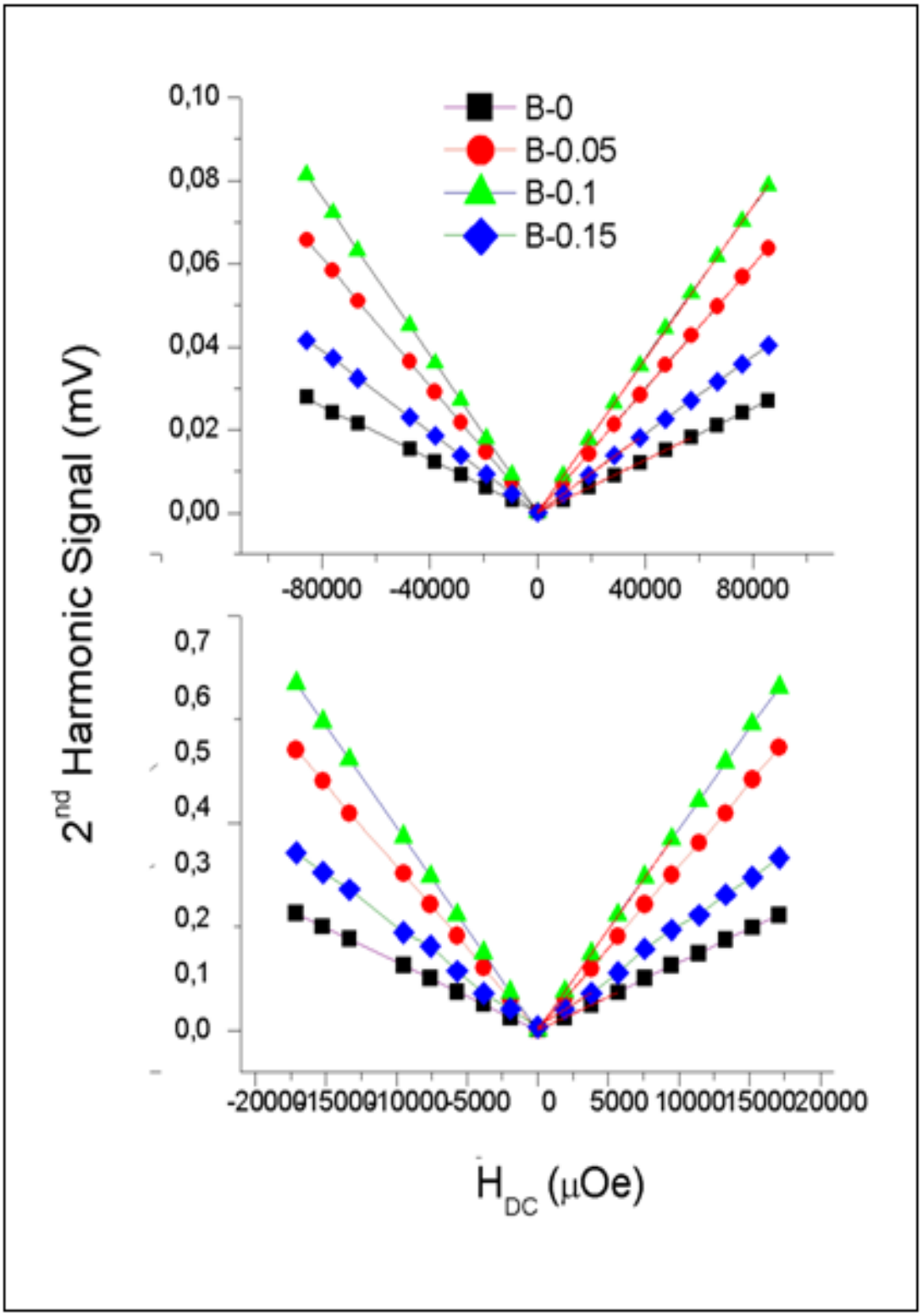

Figure 4.13. (b) Variation of the 2nd harmonic signal on YBCO pellets as a function of the applied DC field [28].

5. CONCLUSION

In this thesis, DC field sensing performance of three different samples (polycristalline Bi-2223, zinc and boron) were analyzed experimentally. The obtained data was compared with Y-123 superconductors and the theoretical models in the literature. In this part conclusions of the experiments will be given for three different samples.

The aim was to increase the sensitivity of the second harmonic signal, which is generated by a bulk Y-123 superconductor, with respect to an applied DC field by finding optimal pick-up and driving coil configurations, superconducting sample dimensions and optimal driving field frequency. It was found that the second harmonic signal changes with the DC field quite linearly in all measurement points (−0.11 Oe and 0.11 Oe). A 2 nT DC field could be detected by using a special coil system (Coil 26) described in the text. The optimal driving field frequency was 49.9 kHz (n = 1) with the amplitude of 28 Oe.

Bismuth studies show that the intensity of second harmonic signal was dependent on the superconducting properties of the core such as (H_{C1J}, H*, T_C and the trapped field). Therefore, a valid general formula could not be developed for all types of superconducting cores. Hence, the optimal operating conditions have been designated in the thesis. Obtaining as low as 0,5 nT without using any special electronics is the most important output of bismuth studies. In the current form this level competes with flux gates and there is a big potential for sensitivities to be further improved.

In this work, the effect of weak links between the grains of YBaCuO ceramics on the strength of 2nd harmonic signal was examined. Contrary to the expectations of literature, there is no direct relationship between the signal strength and the weak links. Experiments carried out on a series of Zn-doped YBaCuO samples, where the J_C values were observed to be decreasing with the increase of zinc concentration, have shown that the highest 2*f* signal corresponds to at least the Zn-doped sample ($YBa_2Cu_{2.99}Zn_{0.01}O_{7-y}$). The 2 nT DC-field could be detected by using this SC specimen as the sensing core. On the other hand, the upper limit takes lower values compared to the less sensitive one.

Experiments carried out for zinc doped YBCO samples showed no direct relationship between the signal strength and weak links as oppose to the literature. It was seen that Jc values decreased when zinc concentration increased. It was shown that the highest 2f

signal corresponded to the least zinc doped sample. When using as the sensing core the superconducting specimen yielded 2 nT DC field. However the upper limit of this specimen was lower than that of last sensitive one.

The H_{c1J} and the H* values in our samples decrease with increase of boron concentration. Using these values and adjusting the amplitudes of H_{DC} and H_{AC}, the dynamical range of magnetometer can be controlled depending on the application area. From literature the strength of the 2nd harmonic signal is inversely proportional to the critical current density, Jc($V_2 \propto 1/J_C$) asserted by most authors. The J_C values were derived from the M–H loops by using the Bean model to check its relation with the 2nd harmonic signal. The data show that Jc values decrease with an increase in B concentration. Consequently, the highest second harmonic signal is expected for the B doped sample with $x = 0.15$. On the other hand, the highest signal was observed for the sample with $x = 0.1$.

Boron studies showed that weak links occurred and the addition of B_2O_3 was inversely proportional to J_C . It was observed that the second harmonic signal increased until B_2O_3 content was 0,15 wt% percent. After that value it began to decrease since J_C increased.

REFERENCES

1. J. C. Peterson, R. Arredondo, T.Chao, G. L.Friedman, C. LaBaw, B. Lam P. L. Moynihan and J.Tupman. Sensor Technology Assessment for Ordnance and Explosive Waste Detection and Location. *Jet Propulsion Laboratory Sensor Technology Assessment for Ordnance and Explosive Waste Detection and Location JPL Report D-11367 Revision B*, 1994.
2. T.R. Clem. Progress in magnetic sensor technology for sea mine detection in Detection and Remediation Technologies for Mines and Minelike Targets II. *The International Society for Optical Engineering*, 3079:408-417, 1997.
3. D.C. Summey and G.J. KeKelis. Fused airborne sensor technology in Detection and Remediation Technologies for Mines and Minelike Targets. *The International Society for Optical Engineering*, 2765: 226-230, 1996.
4. M. D. Michelena. Small magnetic sensors for space applications. *Sensors*, 9: 2271-2288, 2009.
5. U.Topal, F. Alikma, and C. Birlikseven. Low DC magnetic field detection using ceramic superconductors. *Journal of Superconductivity and Novel Magnetism*, 25 : 931-934, 2011.
6. F. Alikma, C. Birlikseven, G. Gulmez, E.Turhan, E.G. Coker and U. Topal. Improving the sensitivity of superconductor based DC magnetometer. *Journal of Superconductivity and Novel Magnetism*, 25 :2539-2545, 2012.
7. U. Topal, F. Alikma, C. Birlikseven, U. Uzun and U. Kölemen. Measurements of ultra-low DC fields by High-Tc superconducting cores: the effect of calcinations temperature. *Journal of Alloys & Compounds*, 530 : 91-96, 2012.
8. L. Ji, R.H. Sohn, G.C. Spalding, C.J. Lobb and M. Tinkham. Critical state model for harmonic generation in high-temperature superconductors. *Physical Review B*, 40:10936-10945, 1989.
9. T.K. Dey, M.K. Chattopadhyay and S.K. Ghatak. Magnetic field sensor based on second harmonic response of polycrystalline YBCO pellets. *Sensors & Actuators B*, 55 :222-226, 1999.

10. L.Rovati and S.Cattini. Zero-Field Readout Electronics for Planar Fluxgate Sensors without Compensation Coil. *IEEE Transactions on Industrial Electronics,* 59:571-578, 2012.
11. J. Lenz and A.S. Edelstein. Magnetic Sensors and Their Applications. *IEEE Sensors Journal,* 6:631-649, 2006.
12. J.Lei, L. Chong and Y. Zhou. Fabrication and characterization of a new MEMS fluxgate sensor with nanocrystalline magnetic core. *Measurement Journal,* 45:535-540, 2011.
13. P. Ripka. Review of fluxgate sensors. *Sensors & Actuators A,* 33:129-141, 1992.
14. F. Kaluza, A. Gruger and H. Gruger. New and future applications of fluxgate sensors. *Sensors & Actuators A,* 106:48-51, 2003.
15. J.C. Gallop, S. Lilleyman, C.D. Langham, W.J. Radcliffe and M. Stewart. A Novel HTS Magnetometer, exploiting the low jc of bulk YBCO. *Magnetics, IEEE Transactions on,* 25:896-898, 1989.
16. T.K. Dey, M.K. Chattopadhyay and S.K. Ghatak. Magnetic field sensor based on second harmonic response of polycrystallineYBCO pellets. *Sensors & Actuators B: Chemical,* 55:222-226, 1999.
17. C.P. Bean. Magnetization of High-Field Superconductors. *Reviews of Modern Physics,* 36: 31, 1964.
18. C.D. Jeffries, Q.H. Lam, Y. Kim, C.M. Kim, A. Zettl and M.P. Klein. Nonlinear electrodynamics in the granular superconductor $\underline{YBa_2Cu_3O_7}$: Experiments and interpretation. *Physical Review B,* 39: 11526, 1989.
19. A. Shaulov and D. Dorman. Investigation of harmonic generation in the alternating magnetic response of superconducting Y-Ba-Cu-O.*Applied Physics Letters,* 53:2680-2682, 1988.
20. J. Mannhart, D. G. Schlom, J. G. Bednorz, and K. A. Müller. Influence of electric fields on pinning in $YBa_2Cu_3O_{7-\delta}$ films. *Physics Review Letters,* 67:2099, 1991.
21. T. Xia and D. Stroud. Nonlinear electrodynamics and nonresonant microwave absorption in ceramic superconductors. *Physical Review B,* 39: 4792, 1989.
22. H.K. Niculescu and P.J. Gielisse. High Sensitivity Sensor for Direct Measurement of Flux Density. *Applied Superconductivity,* 1: 1681-1689, 1993.

23. J.R.Buckley, N.Khare, G.B. Donaldson, A.Cochran and Z. Hui. Use of bulk high-T_c magnetometer for non destructive evaluation. *Magnetics, IEEE Transactions on Magnetics*, 27: 3051-3054, 1991.
24. N.P. Liyanawaduge, S.K. Singh, A. Kumar, V.P.S. Awana and H. Kishan. Superconducting and Magnetic Properties of Zn-doped YBa2Cu3O7−*δ Journal of Superconductivity and Novel Magnetism*, 24:1599-1605, 2011.
25. U. Topal, F. Alıkma and E. Gulce Coker. Measuring DC Fields as Low as 0.5 nT by Using Bi-2223 Polycrystalline Superconductors. *Journal of Superconductivity and Novel Magnetism*, 26:1831–1835, 2013.
26. U. Topal, E. Gulce Coker, F. Alıkma, U. Kolemen and O. Uzun. The Role of Weak Links and Zn-Doping on Magnetic Parameters of High-*Tc* Superconductors. *Journal of Superconductivity and Novel Magnetism,* 27: 133–141, 2014.
27. U.Topal and H.Ozkan. Effects of B_2O_3 addition on the properties of melt-processed $YBa_2Cu_3O_{7-\delta}$. *IOP Science: Superconductor Science and Technology*, 18: 82-85, 2005.
28. E.Gülce Çoker, U. Kölemen and U. Topal. Physical and Mechanical Properties of B2O3 doped YBaCuO Superconductors: Applicability as a Low DC Magnetometer. *Journal of Superconductivity and Novel Magnetism*, 28:513-518, 2015.
29. H.U. Auster, K.H. Glassmeier, W. Magnes, O. Aydogar, D. Constantinescu, D. Fischer, K.H. Fornacon, E. Georgescu, P. Harvey, O. Hillenmaier, R. Kroth, M. Ludlam, Y. Narita, K. Okrafka, F. Plaschke, I. Richter, H. Schwarzi, B. Stoll, A. Valavanoglu and M. Wiedemann. The THEMIS fluxgate magnetometer. *Space Science Reviews*, 141:235-264, 2008.
30. W. Magnes, M. Oberst, A.Valavanoglu, H. Hauer, C.Hagen, I. Jernej, H. Neubauer, W. Baumjohann, D. Pierce, J. Means and P. Falkner. Highly integrated front-end electronics for spaceborne fluxgate sensors. *IOP Science: Measurement Science and Technology*, 19:115801, 2008.
31. Y.Y. Reutov. A Sensitive Fluxgate Magnetometer. *Russian Journal of Nondestructive Testing*, 44:386-390, 2008.

32. L. Gang, Y. Huiping, B. Yanzheng, Z. Zebing. Space fluxgate magnetometer with high precision. *Journal of Huazhong University of Science and Technology (Natural Science Edition)*, 33:61-63, 2005.

33. P. M. Drljača, P. Kejik, F. Vincent, D. Piguet, F. Gueissaz and R. S. Popović. Single core fully integrated CMOS micro-fluxgate magnetometer. *Sensors and Actuators, A*: *Physical*, 110:236-241, 2004.

34. M. Vopálenský, P.Ripka and A.Platil. Precise Magnetic Sensors. *Sensors and Actuators, A:Physical* 106:38-42, 2003.

35. J.M.G. Merayo, J.R. Petersen, O.V. Nielsen, F. Primdahl and P. Brauer. A portable single axis magnetic gradiometer. *Sensors and Actuators, A:Physical* 93:185-196, 2001.

36. C. Granata, A. Vettoliere and M. Russo. Integrated dc SQUID Magnetometers in Multichannel Systems for Biomagnetic Imaging. EUROCON 2007- *The International Conference on Computer as a Tool*, art. no. 4400594:556-563, 2007.

37. T. Reich, P. Febvre, T. Ortlepp, F. H. Uhlmann, J. Kunert, R. Stolz and H.G.Meyer. Experimental study of a hybrid single flux quantum digital superconducting quantum interference device magnetometer. *Journal of Applied Physics*, 104:024509, 2008.

38. Y. Seki and A. Kandori. Two-dimensional gradiometer. *Japanese Journal of Applied Physics, Part 1: Regular Papers and Short Notes and Review Papers*, 46:3397-3401, 2007.

39. R. Cantor, D. Drung, M. Peters, H. J. Scheer and H. Koch. Integrated DC SQUID magnetometer with simplified read-out. *Superconductor Science and Technology*, 3:108-112, 1990.

40. J. Beyer and D. Drung. A SQUID series array dc current sensor. *Superconductor Science and Technology*, 21:095012, 2008.

41. http://en.wikipedia.org/wiki/Magnetometer [retrieved 24 April 2015].

42. C. Jeffries, Q.H. Lam, Y. Kim, L.C. Bourne and A. Zettl. Symmetry breaking and nonlinear electrodynamics in the ceramic superconductor $YBa_2Cu_3O_7$. *Physical Review B,* 37: 9840, 1988.

43. K.H. Mueller, J.C. MacFarlane and R. Driver.Nonlinear magnetic flux response in high temperature superconductors. *Physica C: Superconductivity and its Applications,* 158:366-370, 1989.

44. M. Gershenson. High Temperature Superconductive Flux Gate Magnetometer. *IEEE Transactions on Magnetics,* 27: 3055-3057, 1991.

45. C.P. Bean. Magnetization of Hard Superconductors. *Physical Review Letters,* 8: 250-253, 1962.

46. K.Wang, X. Gao and J.Lin. Calculation of the ground state of the one-dimensional two-impurity Anderson model. *Physical Review B,* 60: 15492, 1999.

47. M. Mehbod,W. Biberacher, A.G.M. Jansen and P.Wyder. Influence of Zn impurities on the superconducting Y-Ba-Cu-O compound. *Physical Review B,* 38: 11813-11815, 1988.

48. M. Mahtali, S. Chamekh, T. Boucherka and A. Bouabellou. Effects of Zn doping on YBaCuO superconductor. *Physica Status Solidi C,* 3: 3040-3043, 2006.

49. R.A. Serway. *Physics for Scientists and Engineers with Modern Physics,* International Edition Serway 3rd Edition, James Madison University, 1982.

50. F.B. Azzouz, M. Zouaoui, K.D. Mani, M. Annabi, G. V. Tendeloo and M. B. Salem. Structure, microstructure and transport properties of B-doped YBCO system. *Science Direct Physica C,* 442: 13-19, 2006.

51. Y.B. Kim, C.F. Hempstead and A.R. Strnad. Magnetization and Critical Supercurrents. *Physical Review*, 129:528, 1963.

52. P.W. Anderson and Y. B. Kim. Hard Superconductivity: Theory of the Motion of Abrikosov Flux Lines. *Review Modern Physics,* 36:39, 1964.

53. http://en.wikipedia.org/wiki/superconductors[retrieved 21 February 2015].

54. http://www.google.com.tr/search/superconductivity[retrieved 2 May 2015].

55. U. Kölemen, O. Uzun, M. A. Aksan, N. Güçlü and E. Yakıncı. An analysis of load-depth data in depth-sensing microindentation experiments for intermetallic MgB_2. *Journal Alloys and Compounds,* 415:294-299, 2006.

56. U. Kölemen, S. Çelebi, H. Karal, A. Öztürk, U. Çevik, S. Nezir and O. Görür. Superconducting and Vickers hardness properties of ZnO added YBCO bulk superconductors. *Physica Status Solidi B-Basic Solid State Physics,* 41:274-283, 2004.

57. Ph. Vanderbemden, A.D. Bradley, R.A. Doyle, W. Lo, D.M. Astill, D.A. Cardwell and A.M. Campbell. Superconducting properties of natural and artificial grain boundaries in bulk melt-textured YBCO. *Physica C*, 302:257-261, 1998.

58. D. Dimos, P. Chaudhari and J. Mannhart. Superconducting transport properties of grain boundaries in $YBa_2Cu_3O_7$ bicrystals. *Physical Review B,* 41:4038, 1990.

59. P.J. Gielisse, H. Niculescu, B. Roy, K.W. Jones, G. Larkin, and Z. Hu. Effect of Frequency on Sensitivity of HTS Sensors and Devices. *Superconductive Science and Technology*, 4: 416-418, 1991.

60. H. Niculescu and P. J. Gielisse. High temperature superconductor sensors for low field magnetometry. *Magnetics, IEEE Transactions on*, 28:809-812, 1992.

61. F. Perez, X. Obradors, J. Fontcuberta, X. Bozec, A. Fert. Intergranular flux penetration and creep in strongly connected $YBa_2Cu_3O_7$ ceramics. *Physica C: Superconductivity*, 235-240:2941-2942, 1994.

62. G. Ilonca, M. Mehbod, A. Lanckbeen and R. Deltour. Superconducting and normal-state transport properties in bulk YBaCuO, doped with Zn. *Journal Alloys and Compounds*, 195: 347-350, 1993.

63. T.Q. Yang, M. Abe, K. Horiguchi and K. Enpuku. Detection of magnetic nanoparticles with ac susceptibility measurement. *Science Direct Physica C,* 412-414:1496-1500, 2004.

64. A.Berenov, C. Farvacque, X. Qi, J.L. MacManus-Driscoll, D. Mac Phail and S. Foltyn. Ca doping of YBCO grain boundaries. *Physica C : Superconductivity,* 372-376 : 1059-1062, 2002.

65. C.H. Cheng and Y. Zhao. Repair of grain boundary by preferential-doping in $YBa_2Cu_3O_{7-y}$. *Physica C*, 463-465:174-177, 2007.

66. F. Alıkma, Master Thesis, *Marmara University*, 2012.

APPENDIX A: THE DEVICESOF THE MEASUREMENT SYSTEM

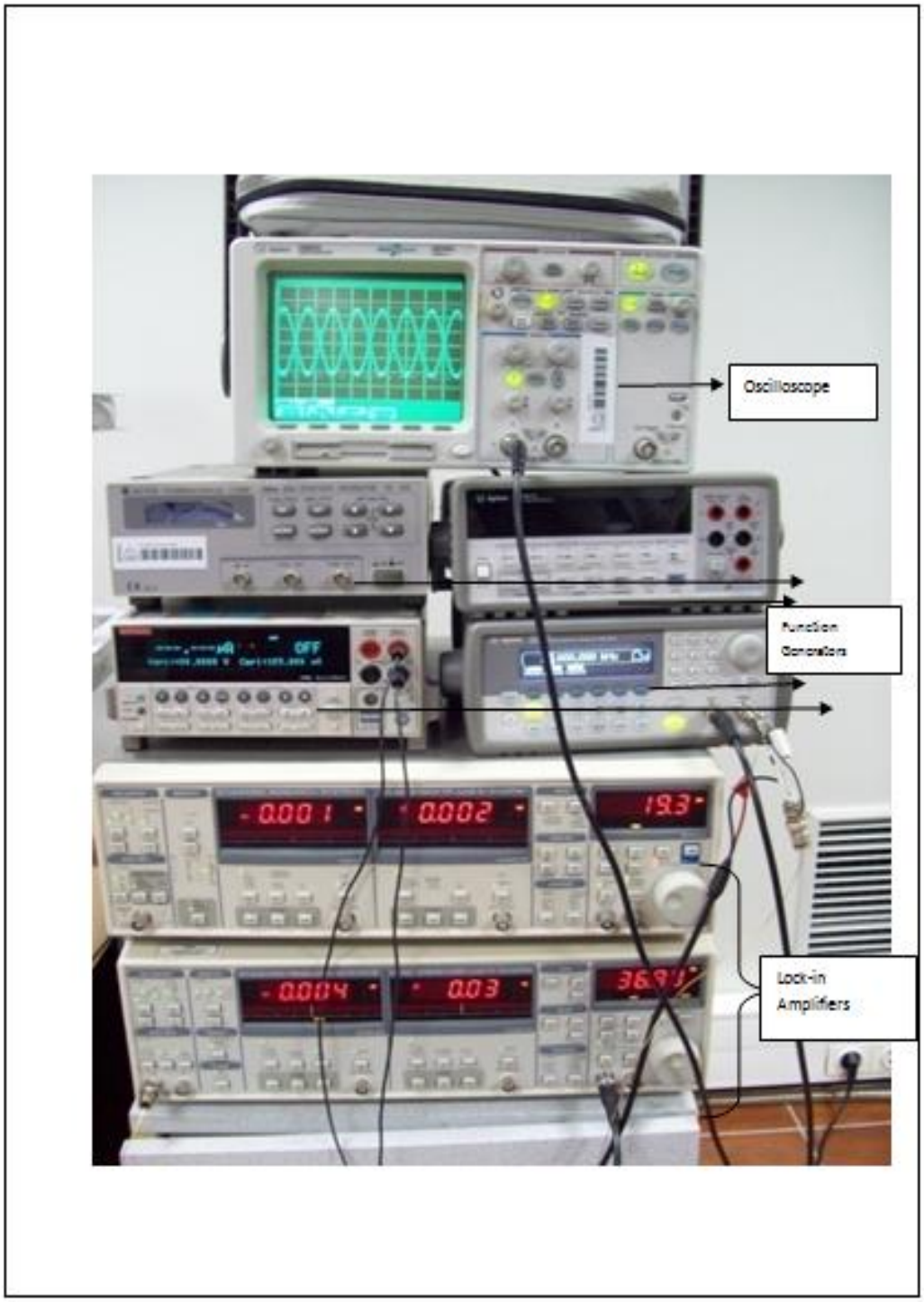

Figure A.1. Devices of the system.

APPENDIX B: ELECTRONIC FILTER DESIGN FOR THE MEASUREMENT OF THE 2nd HARMONIC SIGNALS

An AC field driven by a commercial function generator contains the harmonics of driven frequency f even if it has ultra low distortion as in the case of present study (SRS DS360 Ultralow distortion function generator). In order to realize 2nd harmonic measurements at low scales of the lock-in amplifier, the signal induced on the pick-up coil other than the frequency 2f must be filtered. With this reason, two different electronic filters were designed for different working frequencies. The filters are connected to the pick-up coil in series prior to the readout in lock-in amplifier.

For the frequency of 198 kHz:

The filter, which circuit was given in Figure B.1., allows the signals having frequency between 360 kHz and 400 kHz. Here notice that the driven frequency is 198 kHz. It has a quality factor of 10. Despite the frequency suppression was estimated to be higher than 1/1000, it was measured to be 1/200 due to the tolerances of circuit elements.

For the frequency of 49.9 kHz:

The filter whose circuit was given in Figure B.2, works at 99.8 kHz. It filters the signals other than 99.8 kHz with a high quality factor Q. The quality factor Q, central frequency and the gain is independent of each other and calculated from the following formulas.

$$f_0 = \frac{1}{2\pi C R_f}, Q = \frac{R_1}{R_Q}, G = \frac{R_1}{R_G}$$

In the circuit of the filter, NPO capacitors and metal film resistances with low frequency and temperature dependences have been used. The values of capacitors and resistances were measured by using HP 4294 Impedance Analyzer at 100 kHz.

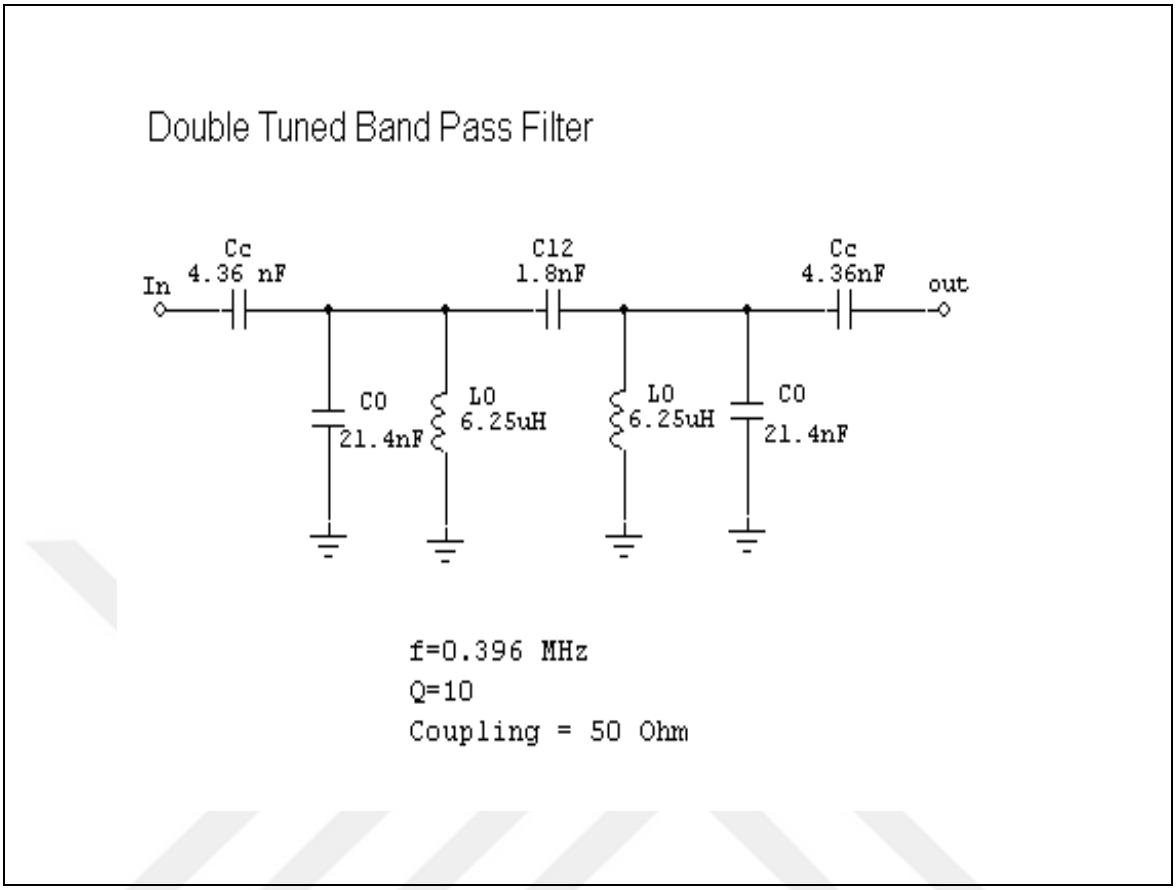

Figure B.1. Filter having frequency between 360 kHz- 400 kHz

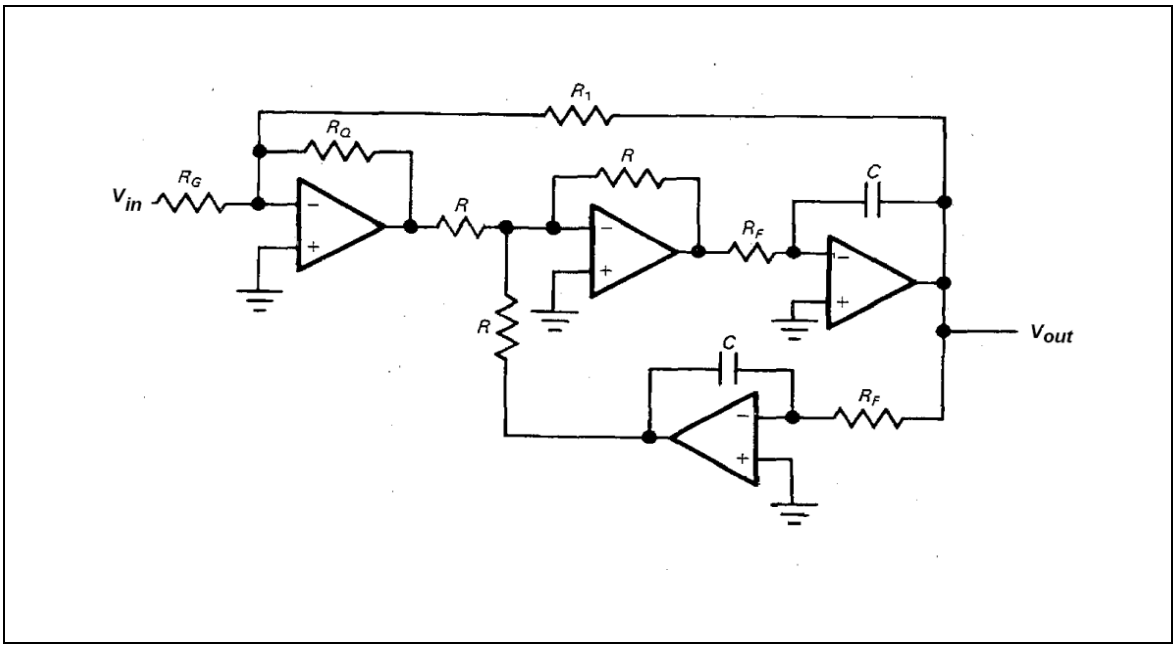

Figure B.2. Filter works at 99.8 kHz

APPENDIX C: SQUID (SUPERCONDUCTING QUANTUM INTERFERENCE DEVICE)

Figure C. 1 . MPMS-5 SQUID magnetometer from Quantum Design, Magnetic Laboratory at Tübitak-UME

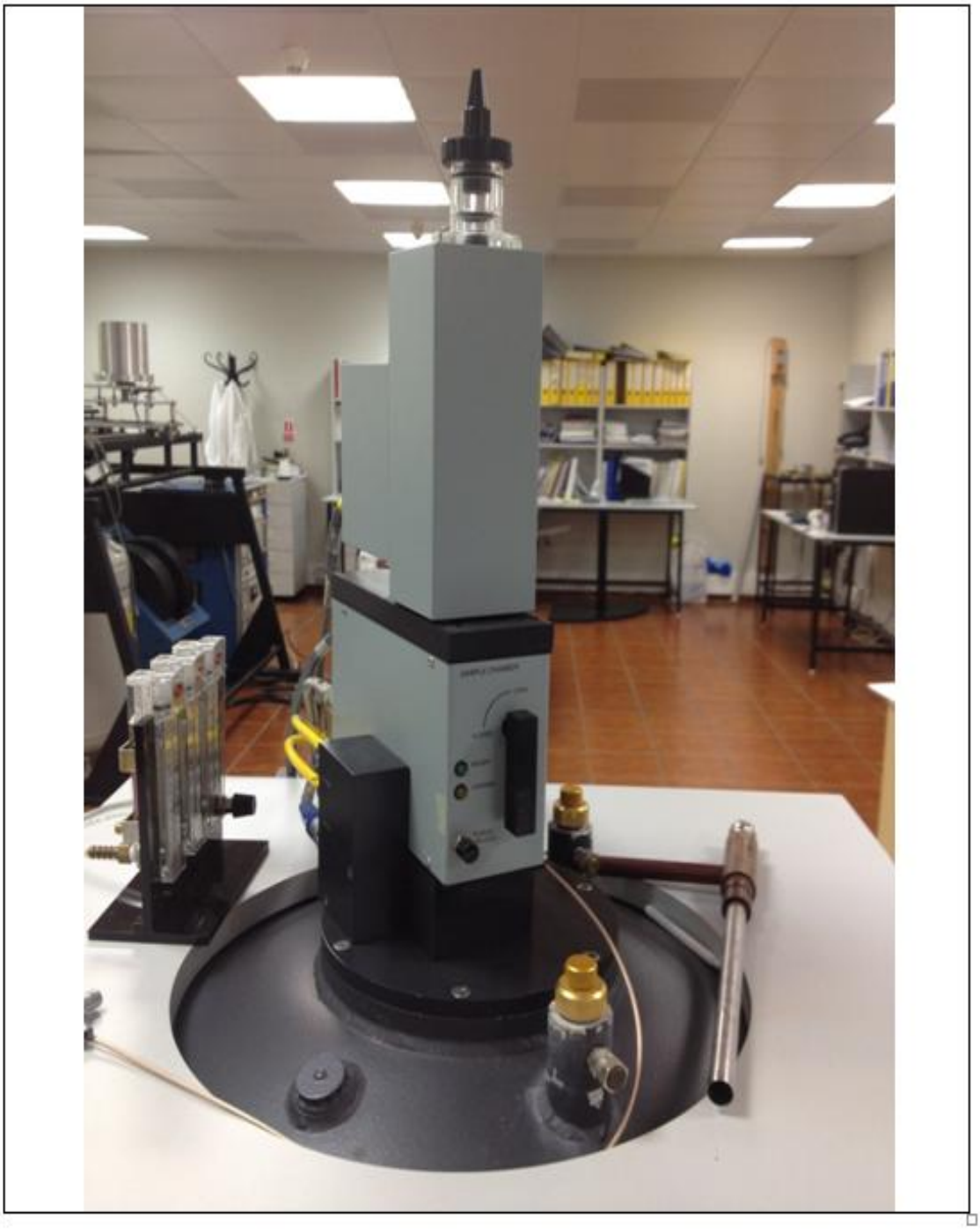

Figure C. 2. MPMS-5 SQUID magnetometer from Quantum Design, Magnetic Laboratory at Tübitak-UME.

Figure C. 3. MPMS-5 SQUID magnetometer from Quantum Design, Magnetic Laboratory at Tübitak-UME.

APPENDIX D: JOURNAL 1

J Supercond Nov Magn (2013) 26:1831–1835
DOI 10.1007/s10948-012-1887-4
ORIGINAL PAPER

Measuring DC Fields as Low as 0.5 nT by Using Bi-2223 Polycrystalline Superconductors

Ugur Topal · Fatma Alıkma · E. Gulce Coker

Received: 6 November 2012 / Accepted: 30 November 2012 / Published online: 14 December 2012

Abstract
In this study a novel type of magnetometer capable of direct measurement of DC fields as low as 0.5 nT was described. The second harmonic voltage generated by polycrystalline superconductors inserted in AC and DC fields was used as sensor signal. The experiments have shown that a 0.5 nT DC field can be detectable by using Bi-2223 superconductors as the core material. The Bi-2223 reveals better sensitivity compared to the other high-*T*c cuprates. Besides, the sensor works in a wide dynamical range (10^5 orders in magnitude), which increases its potential application areas.

Keywords
2^{nd} harmonic signal · High-T_C superconductor ·DC-magnetometer · Ultra-low DC field measurements ·Magnetic field sensor

APPENDIX E: JOURNAL 2

J Supercond Nov Magn
DOI 10.1007/s10948-012-1684-0
ORIGINAL PAPER

Improving the Sensitivity of Superconductor-Based DC Magnetometer

Fatma Alıkma · Cengiz Birlikseven · Gulay Gulmez · Enis Turhan · Eylem Gulce Coker · Ugur Topal

Received: 5 March 2012 / Accepted: 14 June 2012

Abstract
In this study we report on some critical factors affecting the sensitivity of a magnetic field sensor whose working principle is based on a linear DC field dependence of the second harmonic of the AC response in polycrystalline type-II superconductors. DC-fields down to 2 nT in magnitude could be detected by finding optimal conditions. The optimal sensor design was determined by studying superconductor cores having different geometries and coil configurations. The optimal AC-field frequency, which is required for excitation of the specimen, was found to be 50 kHz. The second harmonic signal changes quite linearly with the DC-field up to 0.1 Oe.

Keywords Second harmonic signal · High- *T*c superconductor · DC-magnetometer · Ultra-low DC field measurements · Magnetic field sensor

APPENDIX F: JOURNAL 3

J Supercond Nov Magn (2014) 27:133–141
DOI 10.1007/s10948-013-2280-7
ORIGINAL PAPER

The Role of Weak Links and Zn-Doping on Magnetic Parameters of High-*Tc* Superconductors

Ugur Topal · E. Gulce Coker · Fatma Alıkma · Ugur Kolemen · Orhan Uzun

Received: 13 May 2013 / Accepted: 5 June 2013 / Published online: 11 July 2013

Abstract
The second harmonic signal, which is generated by co-application of AC and DC fields to polycrystalline type-II superconductors, were analysed in terms of the weak links and the critical current density. With this aim the $YBa_2Cu_{3-x}Zn_xO_{7-y}$ (x = 0, 0.01, 0.02, 0.03, 0.05, and 0.1) samples were synthesized in order to adjust inter-granular couplings and thus the strength of weak links. The mechanical and magnetic measurements are in good agreement on that Zn doping reduces strength of the links between grains; however, contrary to the common expectations, it has no direct contribution to the 2nd harmonic signal strength.

Keywords

Superconductors · Superconductivity · Magnetometer · Magnetic properties

APPENDIX G: JOURNAL 4

J Supercond Nov Magn (2015) 28:513–518
DOI 10.1007/s10948-014-2767-x
ORIGINAL PAPER

Physical andMechanical Properties of B_2O_3 doped YBaCuO Superconductors: Applicability as a Low DC Magnetometer

E. Gulce Coker · U. Kolemen · U. Topal

Received: 10 June 2014 / Accepted: 1 September 2014 / Published online: 19 September 2014

Abstract
The effect of the inter-granular couplings on the second harmonic of the fundamental signal, which is generated by co-application of DC and AC fields to a magnetic material having nonlinear magnetization, was investigated on B_2O_3 doped YBaCuO superconductors. Physical and mechanical properties of B_2O_3 doped YBaCuO superconductors were also analysed to support electrical measurements.

Keywords
Mechanic measurements · Second harmonic signal · Micro hardness · Elastic modulus ·Depth-sensing indentation technique